BLIMP1 AND NR4A3 TRANSCRIPTION FACTORS RECIPROCALLY REGULATE ANTITUMOR CAR T-CELL STEMNESS AND EXHAUSTION

Inyoung Jung

A DISSERTATION

in

Cell and Molecular Biology

Presented to the Faculties of the University of Pennsylvania

in

Partial Fulfillment of the Requirements for the

Degree of Doctor of Philosophy

2022

Supervisor of Dissertation

Joseph A. Fraietta, Ph. D.

Assistant Professor of Microbiology

Graduate Group Chairperson

Daniel S. Kessler, Ph.D.

Associate Professor of Cell and Developmental Biology

Dissertation Committee

Daniel J. Powell Jr., Ph.D., Associate Professor of Pathology and Laboratory Medicine

Gerald P. Linette, M.D., Ph.D., Professor of Medicine

Xianxin Hua, M.D., Ph.D., Professor of Cancer Biology

Carl H. June, M.D., Professor of Pathology and Laboratory Medicine

ACKNOWLEDGMENTS

First and foremost, I would like to express my sincere thanks to my thesis advisor, Dr. Joseph A. Fraietta, for giving me the opportunity to conduct my thesis research in his laboratory. His enthusiasm, vision, and positive attitude deeply inspired me and made my 4 years of thesis so enjoyable. He always reminded me the reason why we are doing what we do to translate our science into medicine to benefit patients, which really helped me get through the hard moments. I greatly appreciate that he always supported my new ideas (even when they were not that great) and allowed me to explore new things, where looking back I learned the most during my thesis. He provided great collaboration opportunities with various research groups which I believe brought my thesis project to the next level. Outside the science, Joe also supported me to adapt to this country and new working environment and provided me the opportunity to solely focus on the science.

I would like to acknowledge our collaborators Dr. Shelley L. Berger and Sierra McDonald for conducting ATAC-seq analysis, which provided deeper insight on how *PRDM1* regulates T-cell exhaustion. The PSMA CAR T-cell trial conducted by Drs. Naomi B. Haas and Vivek Narayan was foundation of my thesis work and revealed unmet medical needs in prostate cancer. Dr. Andrew J. Rech helped with single cell RNA-seq analysis that profoundly improved the quality of our work. Dr. Gwanui Hong in Dr. Park F. Cho-Park's laboratory made a huge contribution to this work by conducting immunoblot experiments that confirmed CRISPR/Cas9-mediated gene deletions. Drs. Megan M. Davis, Gabriela Plesa and Donald Siegel generously provided precious patient

CAR T-cell infusion products for our single cell analysis and gave constructive feedback during our paper revision. Dr. Jun Xu performed translational correlative studies and flow cytometric analysis for the PSMA CAR T-cell trial. I acknowledge the CHOP sequencing core and Dr. Renata Pellegrino Da Silva for generating high-quality single cell RNA-seq data. I am deeply indebted to the Stem Cell and Xenograft Core. I extend a special thanks to Joshua Glover and Anthony Secreto for preparing and taking care of the mice in the facility. Yongu Lee helped me to learn all of the mouse handling and associated techniques. Thanks to Dr. Weimin Kong for helping with mouse work during the early years of my project. Dr. Marco Ruella and Carl H. June kindly provided B-cell leukemia, prostate, and pancreatic cancer cell lines for my *in vitro* and *in vivo* work. Also, I would like to give thanks to Lifeng Tian and Rong Xu for always keeping our flow cytometers in the best condition during my thesis years. I want to also acknowledge our lab members for always helping me get through daily tasks and challenges, from ordering reagents to all of the laboratory operational items. I have been lucky to have fun and talk about science with my fellow laboratory members. I acknowledge my thesis committee members, Drs. Daniel J. Powell Jr., Carl H. June, Gerald P. Linette, and Xianxin Hua for their support and guidance throughout my thesis work. Their scientific input and dedication to high-quality science significantly elevated the level of my work. Finally, I would like to thank my wife and families in Korea who have been supportive spiritually throughout life, helping me to get where I am today.

ABSTRACT

BLIMP1 AND NR4A3 TRANSCRIPTION FACTORS RECIPROCALLY REGULATE ANTITUMOR CAR T-CELL STEMNESS AND EXHAUSTION

Inyoung Jung

Joseph A. Fraietta

Chimeric antigen receptor (CAR) T-cells have not induced meaningful clinical responses in solid tumor indications. Loss of T-cell stemness, poor expansion capacity and exhaustion during prolonged tumor antigen exposure are major causes of CAR T-cell therapeutic resistance. scRNA-sequencing analysis of CAR T-cells from a first-in-human trial in metastatic prostate cancer identified two distinct and independently validated cell states associated with antitumor potency or lack of efficacy. Low levels of the *PRDM1* gene encoding the BLIMP1 transcription factor defined highly potent $TCF7^{+}CD8^{+}$ CAR T-cells, while enrichment of $TIM3^{+}CD8^{+}$ T-cells with elevated *PRDM1* expression predicted poor outcome. *PRDM1* single knockout promoted *TCF7*-dependent CAR T-cell stemness and proliferation resulting in marginally enhanced leukemia control. However, in the setting of *PRDM1* deficiency, a negative epigenetic feedback program of NFAT-driven T-cell dysfunction characterized by compensatory upregulation of *NR4A3* and multiple other genes encoding exhaustion-related transcription factors hampered effector function in solid tumors. *PRDM1* and *NR4A3* combined ablation skewed CAR T-cell phenotypes away from $TIM3^{+}CD8^{+}$ and toward $TCF7^{+}CD8^{+}$ to counter exhaustion of tumor-infiltrating CAR T-cells and improve *in vivo* antitumor responses, effects that were not achieved with BLIMP1 or NR4A3 single disruption alone. These data reveal a novel

molecular targeting strategy to enrich stem-like CAR T-cells resistant to exhaustion and underscore dual inhibition of *PRDM1*/*NR4A3* expression or activity as a promising approach to advance adoptive cell immuno-oncotherapy.

TABLE OF CONTENTS

LIST OF FIGURES

CHAPTER 1: Introduction

CHAPTER 2: *PRDM1* Upregulation is Associated with Reduction of $TCF7^{+}CD8$ and Enrichment of $TIM3^{+}CD8$ Populations within Infusion Products.

CHAPTER 3: *PRDM1* Knockout (KO) Increases *TCF7* Expression and Enhances Early Memory CAR T-cell Differentiation in a *TCF7*-Dependent Manner

CHAPTER 4: Combinatorial *PRDM1* and *NR4A3* KO Renders CAR T-cells Resistant to Exhaustion.

CHAPTER 5: Discussion

CHAPTER 1: INTRODUCTION

Parts of this chapter were previously published in:

Vivek Narayan, Julie S. Barber-Rotenberg, **In-Young Jung**, Simon F. Lacey, Andrew J. Rech, Megan M. Davis, Wei-Ting Hwang, Priti Lal, Erica L. Carpenter, Shannon L. Maude, Gabriela Plesa, Neha Vapiwala, Anne Chew, Michael Moniak, Ronnie A. Sebro, Michael D. Farwell, Amy Marshall, Joan Gilmore, Lester Lledo, Karen Dengel, Sarah E. Church, Tyler D. Hether, Jun Xu, Mercy Gohil, Thomas H. Buckingham, Stephanie S. Yee, Vanessa E. Gonzalez, Irina Kulikovskaya, Fang Chen, Lifeng Tian, Kyle Tien, Whitney Gladney, Christopher L. Nobles, Hayley E. Raymond, Prostate Cancer Cellular Therapy Program Investigators, Elizabeth O. Hexner, Donald L. Siegel, Frederic D. Bushman, Carl H. June, Joseph A. Fraietta and Naomi B. Haas (2022) PSMA-targeting TGFβ-insensitive armored CAR T-cells in metastatic castration-resistant prostate cancer: a phase 1 trial, *Nat. Med.*. 28, 724-734

CAR T-Cell Therapy for Cancer Treatment

Chimeric antigen receptors (CARs) are synthetic receptors engineered to redirect T-cells to target tumor-associated or tumor-specific surface antigens. Since the first CAR development in 1989, tremendous efforts have been made to bolster CAR T-cell proliferation and effector function[1]. First generation CARs, composed of extracellular binding domains fused to the CD3-zeta endodomain failed to initiate sufficient CAR-T expansion and displayed limited anti-tumor activity in patients (**Figure1.1**)[2,3]. Subsequently, second generation CARs incorporating costimulatory domains from CD28

or 4-1BB molecules successfully addressed the limitations of first-generation CARs and facilitated optimal clonal expansion and persistence of T-cells (**Figure 1.1**)[4].

The second-generation CAR T-cell therapies demonstrated unprecedented high rates of complete remission in hematological malignancies. In the pivotal ELIANA trial with relapsed or refractory B-cell acute lymphoblastic leukemia (B-ALL), the complete response rate (CR) of CD19-directed CAR T-cell therapy was 81% at 3 months, and event-free survival and overall survival rate at 12 months were 50% and 76%, respectively[5]. In large B-cell lymphoma (LBCL), the overall response rate and CR rates were 82% and 58%, respectively, with a progression free survival rate of 44% at 12 months [6]. Since the first U.S. Food and Drug administration (FDA) approval of a CD19-directed CAR-T therapy, Tisagenlecleucel, for treatment of relapsed or refractory B-ALL, six CAR T-cell products received FDA approval, including the most recent B-cell maturation antigen (BCMA)-directed CAR T-cell therapies for multiple myeloma.

Barriers to Effective CAR T-cell Therapies for Cancer

Despite these successes, a sizable portion of patients with B-cell leukemia, lymphoma and myeloma poorly respond to CAR T-cell therapy due to primary resistance[7-10]. Moreover, only a small subset of patients who initially experienced remission achieve durable CRs[11-15]. For example, in B-cell non-Hodgkin lymphoma (B-NHL) and lymphoblastic leukemia (B-CLL), the CR rate is lower than that in B-ALL, although remissions were durable in the majority of patients[16,17]. On the contrary, in B-

ALL, 83% to 93% of patients underwent short-term CR, but only 50% achieved relapse-free survival due to relapse associated with target antigen loss and lack of CAR-T persistence[18,19]. A series of recent studies demonstrated that the lack of durable CRs in B-cell malignancies are associated with low frequency of early memory T-cells and enrichment of exhausted CD8 T-cells in apheresis and CAR T-cell infusion products[10,20,21].

The therapeutic potency of CAR T-cell therapies has been even more limited against solid tumor indication, which comprise the majority of cancers[22-24]. Solid cancers pose unique challenges to CAR T-cell therapies compared to hematologic malignancies. First, CAR T-cells must traffic to solid tumor sites and infiltrate into the tumor bed. Key factors preventing CAR T-cell trafficking and infiltration include mismatches between CAR T-cell chemokine receptors and chemokines produced by tumors, deposition of stromal cells and extracellular matrix and aberrant vasculature[23,25]. Even if CAR T-cells successfully infiltrate into tumors, they often become dysfunctional due to immunosuppressive factors operative within the TME, such as immunosuppressive cytokines, inhibitory receptors, and a hostile metabolic landscape[23-25]. Further, the effector functions and self-renewal capacity of CAR T-cells can be further suppressed due to exhaustion and terminal differentiation induced by chronic tumor antigen exposure (**Figure 1.2**)[26,27].

Among the barriers illustrated above, attrition of T-cell memory differentiation and stemness as well as induction of exhaustion pose significant challenges to CAR T-cell therapies in both hematopoietic and nonhematopoietic malignancies. In this thesis,

we examined how early memory differentiation and exhaustion profiles in CAR T-cell infusion products affect clinical response and developed an engineering strategy to enhance the therapeutic potency of CAR T-cells.

T-cell Stemness and Early Memory

T-cells undergoes clonal expansion and differentiation in response to interactions between the endogenous T-cell receptor and the antigen-major histocompatibility complex (MHC) complex, which is supported by other environmental signals within the tissue microenvironment. Upon elimination of antigen, short-lived effector T-cells (SLECs) undergo apoptosis during the contraction phase of the response and long-lived memory precursor cells (MPECs) give rise to a heterogeneous pool of memory CD8 T-cells (**Figure 1.3**)[28,29]. Unlike terminal effector or effector memory T-cells, early memory T-cells, such as stem-like memory and central memory T-cells, express high levels of costimulatory receptors and homeostatic cytokine receptors, such as CD27, CD28, and IL7R which are required for T-cell survival and long-term persistance[30,31]. In addition, upregulation of CCR7 and CD62L promotes homing of early memory T-cells to secondary lymphoid organs, while effector cells express high levels of adhesion molecules and chemokine receptors for peripheral tissue localization[32-34]. EOMES, TCF1, BCL6, ID3, and STAT3 are transcription factors known to facilitate early memory differentiation and counteract effector pathways[35-38]. On the other hand, transcription factors promoting terminal effector differentiation include T-bet, BLIMP1, ID2, and STAT4 (**Figure 1.4**)[37-41].

T-cell stemness is characterized by a high degree of self-renewal capacity, enhanced polyfunctionality, reduced terminal effector differentiation, and the persistence of proliferative potential[42]. Transcription factors, such TCF1, FOXO1, STAT3, ID3, and MYB play a central role in preserving T-cell stemness and early memory differentiation[28,43]. *Tcf7* deficient mice lack CD8 memory precursor development and exhibit impaired memory recall responses in a Lymphocytic choriomeningitis virus (LCMV) Armstrong infection model, demonstrating the essential role of TCF1 in early memory differentiation and functionality[44]. Stem-like T-cell populations are also found in exhausted T-cells. In a murine model of chronic LCMV infection, a small subset of stem-like exhausted T-cells exhibit self-renewal capacity and persistence and give rise to terminal exhausted T-cells following antigen encounter[45]. Stem-like exhausted T-cells were recently found in tumors as well. Tumor-reactive $TCF7^{+}PD1^{+}$ stem-like CD8 T-cells were detected in melanoma patients, and this CD8 population mediates a proliferative burst in response to vaccination and immune checkpoint blockade therapies[46,47]. Further, the frequency of this stem-like CD8 T-cell population is highly correlated with durable anti-tumor activity of cellular immunotherapies, both in animal models and human trials[10,20,21,48,49].

Preserving T-cell memory and stemness is crucial for efficacious CAR T-cell therapy. In chronic lymphocytic leukemia (CLL) patients for example, T-cells show a gradual impairment of memory and enrichment terminal effector differentiation, which are associated with poor *ex vivo* CAR T-cell expansion and unfavorable clinical responses in patients[8,50,51]. Furthermore, CAR T-cells lose stemness and memory due to

bead-based activation during *ex vivo* manufacturing or in response to tonic CAR signaling, which have a negative impact on CAR T-cell antitumor potency[27,52-54].

T-cell Exhaustion

T-cell exhaustion was first characterized in chronic LCMV infection, in which LCMV-specific $CD8^+$ T-cells lose effector function and proliferative potential[55,56]. Exhausted T-cells also exhibit distinct inhibitory receptor expression profiles and an epigenetic landscape that are distinguished from effector or memory T-cells[7,57-59].

Loss of effector function and proliferative capacity

One of the key features that characterizes exhausted T-cells is progressive loss of effector function[60,61]. Following chronic LCMV infection, $CD8^+$ T-cells lose the ability to produce TNFα and IL-2 at day 8 post-infection, while maintaining IFNγ production until day 30[57], indicating that there is hierarchical impairment of T-cell function. However, although cytotoxicity of T-cells is compromised, exhausted T-cells often sustain the capacity to degranulate, as denoted by expression of the degranulation marker, CD107a[57], and retain robust granzyme B (GZMB) expression as well as cytotoxic capacity[62].

In contrast to memory T-cells which undergo antigen-independent proliferation via IL-7 and IL-15 signaling thereby maintaining long-term persistence, terminally exhausted T-cells are incapable of IL-7/15-mediated homeostatic proliferation due to downregulation of the IL-7Rα[63]. However, a small subset of this exhausted population known as progenitor exhausted T-cells, can expand robustly and give rise to a large pool

of terminally differentiated exhausted T-cells. However, despite a high degree of proliferative capacity, progenitor exhausted T-cells often express lower levels of Ki-67 expression (i.e., a nuclear protein necessary for cellular proliferation) and incorporate less BrdU *in vivo*, compared to the terminally exhausted T-cells which have undergone massive *in vivo* expansion[64,65]. Furthermore, this progenitor population of exhausted T-cells is more resistant to apoptosis as it up-regulates the anti-apoptotic BCL2 protein via the TCF1/c-Myb axis[65]. Accordingly, when adoptively transferred into chronic LCMV and tumor mouse models, progenitor exhausted T-cells successfully differentiate into terminal exhausted T-cells and exhibit long-term persistence, while terminally exhausted T-cells fail to expand and persist[19,65,66].

Expression of multiple inhibitory receptors

Exhausted T-cells are characterized by co-expression of multiple inhibitory receptors such as PD1, TIM3, LAG3, TIGIT, 2B4 and CTLA4[64,65,67-70]. These inhibitory receptors contain distinct intracellular motifs, including ITIM and ITSM, which further activate downstream immunosuppressive regulator such as SHP1 and SHP2. In acute infection, effector T-cells transiently upregulate inhibitory receptors, preventing the development of immunopathology. Once the antigen is cleared, effector populations differentiate into memory T-cells and downregulate inhibitory receptors. On the contrary, in various chronic infections and cancers where T-cells are continuously exposed to antigens, high levels of inhibitory checkpoints are sustained. This co-expression of multiple inhibitory receptors renders T-cells dysfunctional, although the effector function

of early exhausted T-cells can be reinvigorated, at least partially, by immune checkpoint blockade[58,64].

Distinct epigenetic and transcriptional landscapes

Mechanistically, chronic T-cell activation in the absence of sufficient costimulatory signals initiates transcriptional and epigenetic reprogramming. Cytoplasmic component 1 (NFAT) is one of the most upstream transcription factors that governs T-cell exhaustion. The NFAT family is activated by calcineurin which is downstream of T-cell receptor (TCR) signaling, and chronic T-cell activation suppresses the activating NFAT:AP1 complex and instead upregulates a monomeric NFAT complex[71,72]. The monomeric NFAT directly binds to transcription start sites and induces exhaustion-related transcription factors such as TOX and NR4A families (**Figure 1.5**)[59,73,74]. Once induced, TOX and NR4A genes trigger upregulation of multiple inhibitory receptors and dampen CD8 T-cell effector function, which are hallmarks of T-cell exhaustion. TOX and NR4A families epigenetically reprogram T-cells toward exhaustion states by regulating chromatin accessibility of effector and exhaustion-related genes and by promoting acetylation of histone 3 at lysin 27 (H3K27ac); this leads to upregulation of tolerance-related genes[59,74,75]. T-cell exhaustion imposes a pivotal barrier for efficacious immunotherapies. CAR T-cell exhaustion is known to be influenced by the quality of lukapheresed T-cell that go into the cellular manufacturing process, non-antigen-specific spontaneous CAR activation, and chronic antigen stimulation[4,27,76,77]. Recent studies demonstrated that CAR T-cell exhaustion can be partially ameliorated by inhibition of tonic CAR signaling, intermittent CAR-T rest, disruption of NR4A, IRF4,

and BATF, and optimal regulation of cell-surface CAR expression levels as well as signal strength[27,74,76-79].

Role of *PRDM1* in T-cell memory and exhaustion

BLIMP1 encoded by *PRDM1* is a zinc-finger motif-containing transcriptional repressor which plays a critical role in T-cell homeostasis, differentiation, and exhaustion. *Prdm1* expression facilitates the development of short-lived effector cells ($KLRG1^{high}CD127^{low}$), while suppressing development of long-lived memory precursor effector cells ($KLRG1^{low}CD127^{high}$)[40]. In acute LCMV infection, *Prdm1* restricts the proliferative capacity of virus-specific CD8 T-cells by facilitating short-lived effector cell differentiation[40]. *Prdm1* directly represses the transcription of "stemness-related genes" such as *Tcf7* and *Bcl6*, suggesting that *Prdm1* limits the self-renewal capability of CD8 T-cells[80]. In addition, *Prdm1* plays a central role in the development of terminal exhausted T-cells in a chronic model of LCMV infection[81]. *Prdm1* ablation significantly reduces expression levels of inhibitory receptors in CD8 T-cells during chronic antigen stimulation. However, *Prdm1* KO CD8 T-cells exhibit substantially impaired cytolytic activity, suggesting that *Prdm1* is essential for maintaining residual cytotoxicity in exhaustion conditions[81]. Mechanistically, BLIMP1 has been shown to epigenetically regulate T-cell memory by directly binding to DNA and recruiting histone modifying enzymes such as G9a and HDAC2[82]. *Prdm1* disruption increases H3-acetylation and decreases H3K9-trimethylation of *Il2ra* and *Cd27* genes, thereby allowing sustained expression of CD25 and CD27 to support persistent cytokine responsiveness as well as

co-stimulation required for T-cell survival (**Figure 1.6**)[82]. However, the precise epigenetic underpinnings of BLIMP1/*PRDM1*-mediated regulation of T-cell exhaustion and effector function remain elusive.

Early memory and exhaustion profiles of CAR T-cell infusion products and clinical efficacy

CD19 or BCMA-directed CAR T-cells have shown promising clinical efficacy, but a substantial portion of patients fail to respond to these therapies and the safety of this approach largely varies among patients who received CAR-T therapies. This disparity in clinical outcome is presumably due to a combination of multiple host or disease-related factors such as functional defects of T-cells, baseline tumor burden, impaired death receptor signaling, and the intestinal microbiome[10,20,21,83-85]. Recent studies identified cellular and molecular features of apheresed T-cells and CAR T-cell infusion products associated with clinical response and safety[10,20,21]. We previously found that durable complete remissions in response to CD19 CAR T-cell therapy (CTL019) in CLL were associated with a high level of peak CAR T-cell expansion following infusion and long-term persistence[9]. Cell products from complete responders showed superior tumor control and expansion capacity in a leukemic mouse model and exhibited high levels of *ex vivo* proliferative capacity during manufacturing, suggesting that the intrinsic potency of CAR T-cell products are deterministic of clinical efficacy. Transcriptional profiling of CAR-T products revealed that favorable clinical responses directly correlate with early memory T-cell and IL-6/STAT3 signatures, while infusion products from non-responders were

enriched with gene expression profiles associated with terminal differentiation, glycolysis, and T-cell exhaustion pathways[22]. In addition, an increased frequency of $CD27^{+}CD45RO^{-}CD8^{+}$ memory-like T-cells in CLL patient apheresis products were associated with durable remission in CLL. Similarly, LBCL patients treated with axicabtagene ciloleucel who achieved long-term remission had high frequencies of memory $CD8^{+}$ T-cells in CAR T-cell infusion products, whereas gene signatures related to T-cell exhaustion correlated with early treatment failure[86]. More recently, single-cell analysis of apheresed T-cells of patients with B-cell malignancies who received CD19-directed CAR T-cell therapy demonstrated that the *TCF7* signaling pathway is enriched in naïve and early memory pre-manufactured T-cells, which are positively associated with long-term CAR T-cell persistence in the clinic[20]. In contrast, an *IRF7*-driven chronic interferon signature was highly upregulated in baseline apheresed T-cell from patient who showed poor CAR-T persistence[20].

Importantly, it may be possible to overcome the above intrinsic CAR T-cell dysfunctions by using highly proliferative, 'optimally programmed' CAR T-cells. However, the cellular and molecular basis for CAR T-cell-intrinsic resistance in failed therapy of solid tumors has not yet been elucidated. Thus, engineering approaches to generate CAR T-cells with optimal potency and other aforementioned desirable features informed by correlative analyses have been scant to date.

TGFβ-insensitive armored anti-PSMA CAR T-cells in metastatic castration-resistant prostate cancer.

Prostate cancer is the second leading cause of cancer death in males. Initially, prostate cancer is androgen-dependent and androgen deprivation therapy has shown to control prostate cancer at early stages[87]. However, the majority of the patients eventually become resistant to this therapy as they progress to the later stage of the disease known as metastatic castration-resistant prostate cancer (mCRPC)[88,89]. Currently, second-generation anti-androgen therapies such as abiraterone and enzalutamide chemotherapies are often used for mCRPC, showing improved overall survival, prostate-specific antigen (PSA) response, and progression-free survival[90-92]. However, 20 to 40% of patients demonstrate primary resistance to these chemotherapies, and patients who initially respond eventually become non-responsive[93]. In recent years, numerous immunotherapeutic approaches have been tested in mCRPC. Sipuleucel-T, an FDA-approved prostate cancer vaccine, demonstrated a 4.1-month survival improvement and a 16.1-month improvement in overall survival when combined with androgen receptor-targeting agents, as compared to standard-of-care therapies[94,95]. However, Sipuleucel-T failed to reduce PSA levels in patients and is currently not actively used in the clinic[87,96].

In the KEYNOTE-028 trial, a small subset of PD-L1-positive castration-resistant prostate cancer patients treated with anti-PD1 therapy showed durable objective response[96]. However, the vast majority of CRPC patients remain resistant to this checkpoint therapy presumably due to poor T-cell infiltration and low tumor mutation burden[96].

CAR T-cell therapies have shown promising therapeutic potency in blood cancers, however, the clinical efficacy in solid tumors has been limited[22-24,97]. Identification of prostate tumor associated antigens including PSMA, PSA, PAP, PSCA enabled development of CAR T-cells for prostate cancer[88]. Few preclinical or clinical studies examining CAR-T-cell potency in mCRPC are currently ongoing (**Figure 1.7**)[88]. Recently we evaluated safety and feasibility of PSMA-redirected CAR T-cells in a phase I trial (NCT03089203)[97]. Since high levels of TGFβ present in prostate tumors are associated with poor prognosis, angiogenesis, tumor invasion, metastasis, and T-cell dysfunction, the PSMA CAR T-cells were armored with a dnTGFbRII to endow resistance to the immunosuppressive effects of TGFβ[98]. Thirteen mCRPC patients were treated with CAR T-cells across two CAR-T dose levels with or without lymphodepletion. Five patients who received CAR T-cell therapy developed grade 2 or higher cytokine-release syndrome (CRS), including one patient who experienced grade 4 CRS and concurrent sepsis. The high-grade CRS was associated with an acute increase in serum levels of effector cytokines such as IL-8, IFN-γ and IL2. Four subjects experienced a decrease in PSA level greater than 30%, although no partial response was observed according to standard response evaluation criteria for solid tumors. CAR T-cells were detected in metastatic lesions in seven out of nine subjects, demonstrating CAR T-cell trafficking capability to tumor sites (**Figure 1.8**). Notably, the patients who achieved PSA responses exhibited robust peripheral blood CAR T-cell expansion (**Figure 1.9**). In particular, a patient who exhibited >98% decline in PSA showed the highest level of clonal CAR T-cell expansion. The enhanced peripheral blood CAR T-cell expansion and persistence were associated with the use of cyclophosphamide and fludarabine

lymphodepletion and administration of high doses of CAR T-cells. Interestingly, consistent with previous findings in CAR T-cell trials in B-cell malignancies, a higher frequency of early memory CD8 PSMA CAR T-cells in infusion products was significantly associated with superior peripheral blood CAR T-cell expansion capacity (**Figure 1.10**). The limited CAR T-cell responses observed in this study were accompanied by a marked increase in the expression of inhibitory molecules in the TME, including T-cell immunoglobulin and mucin domain-3 (Tim-3), programmed death-ligand 2 (PD-L2), V-domain Ig suppressor of T-cell activation (VISTA) and B7-H3/CD276, suggesting that there may be adaptive T-cell dysfunction following CAR T-cell infusion (**Figure 1.11**). Overall, our translational and correlative studies suggest that enhancement of CAR T-cell memory and prevention of CAR T-cell exhaustion could improve the antitumor efficacy of PSMA-directed CAR T-cells.

In this thesis, through single-cell RNA-seq analysis of CAR T-cell infusion products from mCRPC patients enrolled in NCT03089203, we aimed to identify the cellular and molecular features associated with favorable and unfavorable CAR T-cell potency and antitumor response. Then, we developed a novel engineering strategy to enrich desirable and reduce undesirable CAR T-cell subsets to improve therapeutic efficacy.

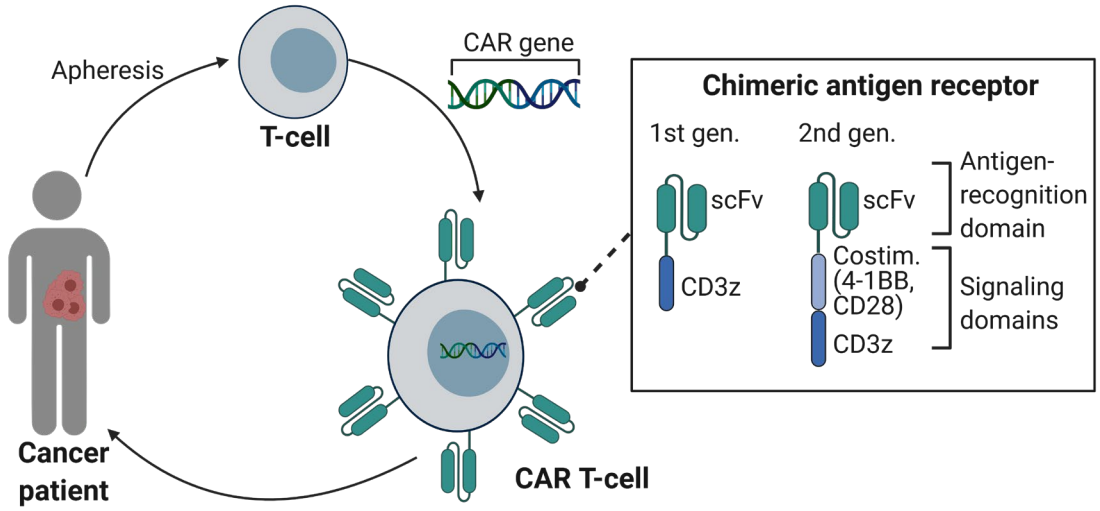

Figure 1.1 Schematic diagram of CAR T-cell manufacturing process and CAR structure

For autologous CAR T-cell manufacturing, T-cells are collected from patients and engineered to express chimeric antigen receptors (CARs) using insertional viruses (e.g., lentiviruses, retroviruses), transposons, or CRISPR/Cas9-mediated editing, followed by donor DNA cassette integration. First generation CARs are typically composed of an extracellular single-chain variable fragment (scFv) binding motif and an intracellular CD3 T-cell activation domain. Second generation CARs contain additional costimulatory domains such as 4-1BB or CD28, which improve clonal T-cell expansion, persistence, and effector function.

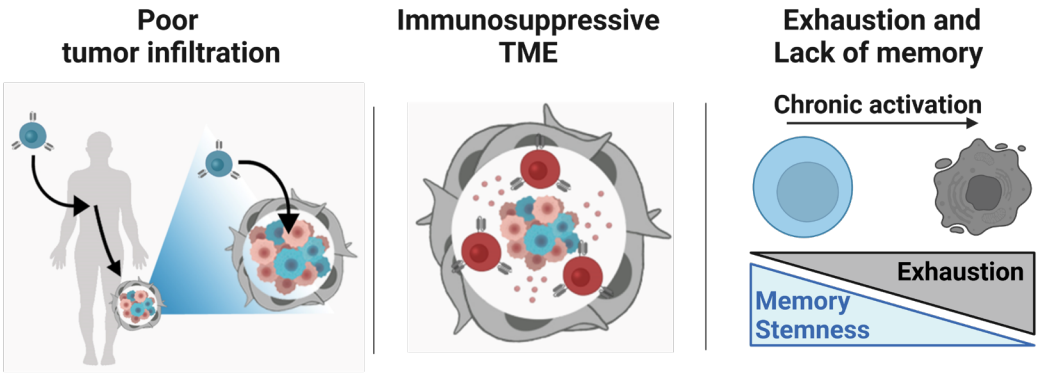

Figure 1.2 Barriers to effective CAR T-cell therapy for solid tumors

In solid tumors, CAR T-cells need to migrate to tumor sites and penetrate tumor tissue through the vascular endothelium. Factors that prevent CAR T-cell infiltration include a lack of appropriate chemokine receptors, deposition of immunosuppressive stromal cells and extracellular matrix, high levels of TGFβ, and dysregulated vasculature. Although CAR T-cells successfully penetrate tumor tissue, the antitumor activity of tumor-infiltrating CAR T-cells can be compromised by various extrinsic immunosuppressive factors, such as inhibitory checkpoints and additional immunosuppressive soluble factors. Also, CAR T-cells are continuously activated due to the high antigen-load present in the TME. This can lead to induction of exhaustion and attrition of memory differentiation and stemness, which are associated with poor antitumor responses in the clinic.

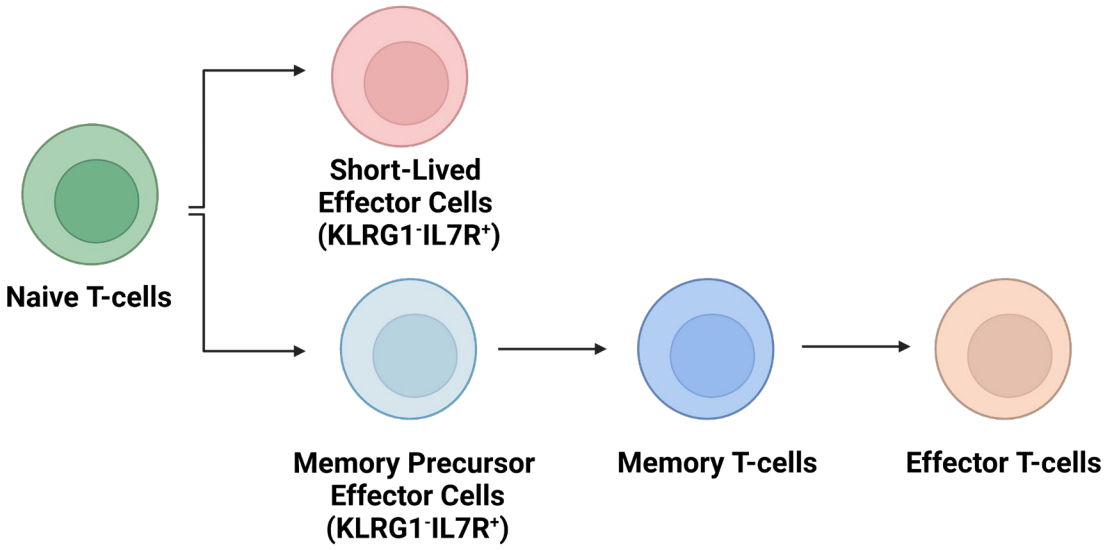

Figure 1.3 Lineage differentiation of memory T-cells.

After encountering antigens, naïve T-cells can give rise to two distinct effector cell populations: short-lived effector cells (SLECs) and memory precursor effector cells (MPECs). While SLECs undergo apoptosis during the contraction phase of the T-cell-mediated immune response, MPECs differentiate into long-lived and protective memory T-cells. Secondary challenges with the same or similar antigens induce rapid expansion of effector cells from memory T-cell pools.

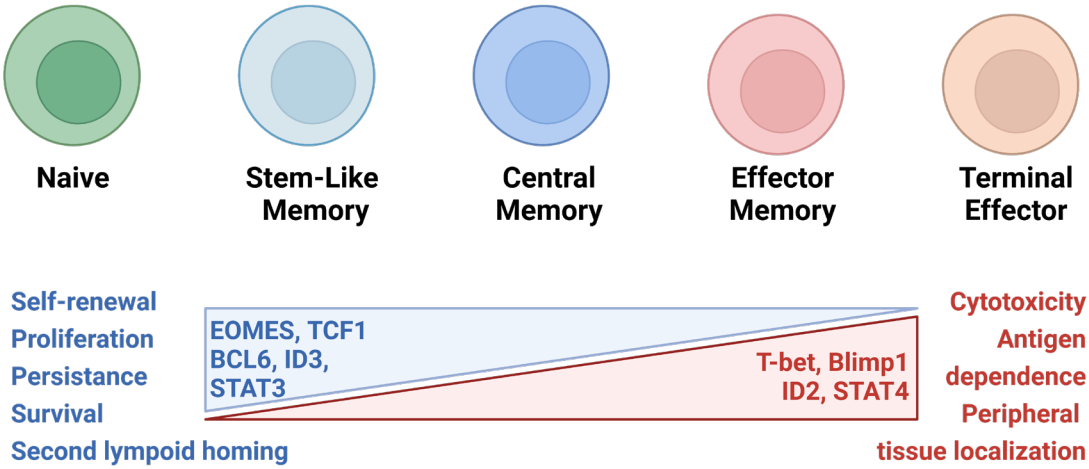

Figure 1.4 Heterogeneity of the memory T-cell compartment.

During progressive differentiation from naïve T-cells to terminal effector cells, T-cells gradually lose self-renewal capacity, proliferative potential, persistence, survival, and homing capacity to secondary lymphoid organs. Instead, effector cells acquire effector function and the ability to traffic and penetrate peripheral tissue by upregulating adhesion proteins and chemokine receptors such as CX3CR1. Key transcription factors involved in early memory and terminal effector differentiation are indicated in the above diagram.

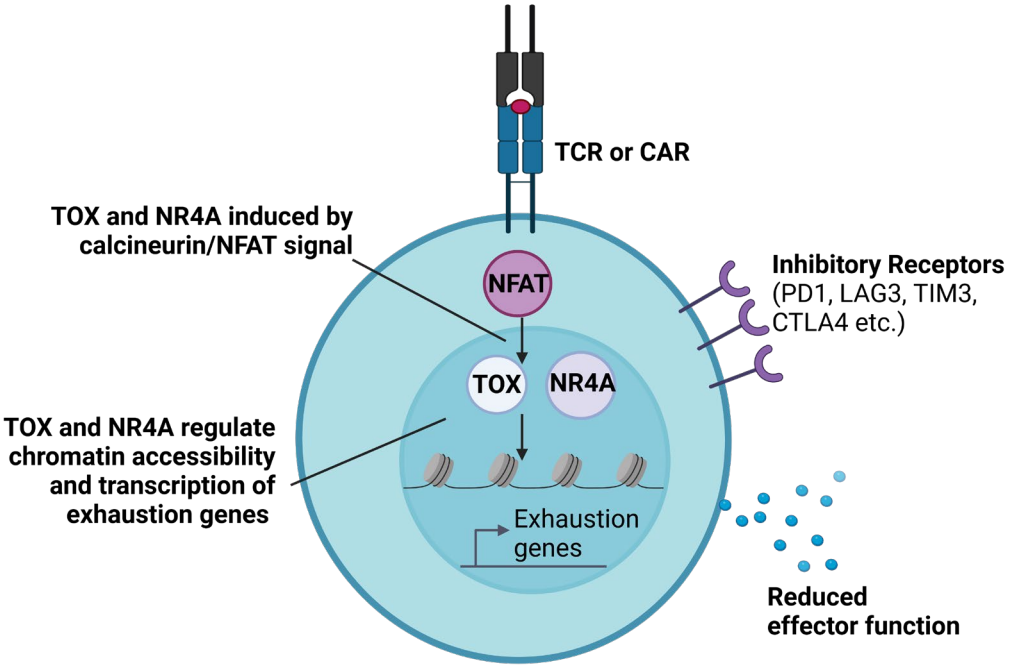

Figure 1.5 Mechanisms of T-cell exhaustion

Chronic TCR or CAR stimulation induces calcineurin/NFAT signaling, which is necessary and sufficient for induction of T-cell exhaustion. Monomeric NFAT induces expression of downstream TOX and NR4A transcription factors. TOX and NR4A families modulate global chromatin accessibility and directly bind to exhaustion-related gene loci to regulate gene expression.

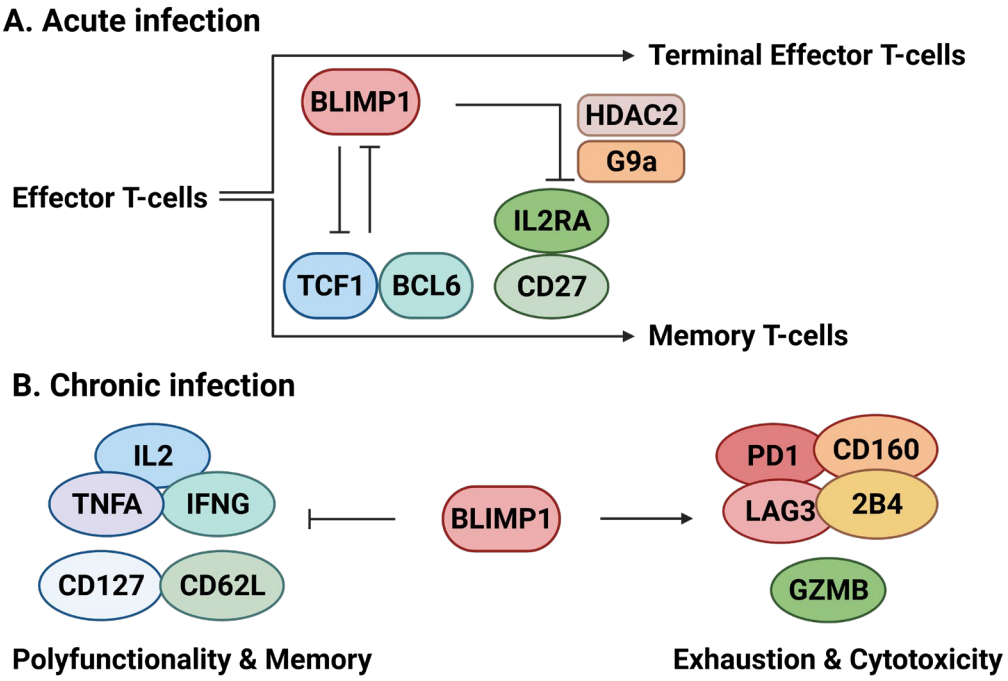

Figure 1.6 Role of BLIMP1 in CD8 T-cell differentiation

A schematic illustrating how BLIMP1 regulates CD8 T-cell differentiation during acute and chronic viral infection. (**A**) In acutely LCMV-infected mice, BLIMP1 promotes differentiation of short-lived effector cell differentiation by repression of key memory/stemness transcription factors such as Tcf7 and Bcl6. Also, BLIMP1 restrains survival of CD8 T-cells by suppressing the expression of Il2ra and Cd27 through recruitment of the histone modification enzymes, HDAC2 and G9a, to Il2ra and Cd27 loci. (**B**) In chronic LCMV infection, BLIMP1 inhibits CD8 T-cell polyfunctionality and memory-related gene expression. Concurrently, BLIMP1 promotes T-cell exhaustion and increased expression of multiple inhibitory receptors. Furthermore, BLIMP1 sustains

cytolytic activity and viral control capacity of LCMV-specific CD8 T-cells by facilitating expression of Granzyme B and CD107.

Publication	Publication year	Institution	Stage	CAR-T cell	Generation	Costimulation
Vivek et al.	2022	Uiversity of Pennsylvania	Pahse1 (NCT03089203)	TGFbRII-armored Anti PSMA CAR-T cells	Second generation	4-1BB
Slovin et al	2017	Memorial Sloan-Kettering Cancer Center	Phase I (NCT01140373)	Anti PSMA CAR-T cells	Second generation	CD28
Gade et al.	2005	Memorial Sloan-Kettering Cancer Center	Preclinical	Anti PSMA CAR-T cells	First generation	NA
Maher et al.	2002	Memorial Sloan-Kettering Cancer Center	Preclinical	Anti PSMA CAR-T cells	Second generation	CD28
Zuccolotto et al.	2014	University of Padua	Preclinical	Anti PSMA CAR-T cells	Second generation	CD28
Ma et al.	2014	Roger Williams Med Center	Preclinical	Anti PSMA CAR-T cells	Second generation	CD28
Zhang et al.	2018	Oxford University	Preclinical	TGFbRII-armored Anti PSMA CAR-T cells	Second generation	4-1BB
Hassani et al.	2019	Tehran Univ Med Science	Preclinical	Anti PSMA CAR-T cells	Second generation	CD28
Priceman et al	2017	City of Hope	Preclinical	Anti PSCA CAR-T cell	Second generation	4-1BB
Hillerdal et al.	2014	Uppsala University		Anti PSCA CAR-T cell	Third generation	CD28 OX-40
Kloss et al.	2012	Memorial Sloan-Kettering Cancer Center	Preclinical	Anti PSCA/Anti PSMA CAR-T cell	Third generation	CD28 OX-40
Feldman et al.	2017	Institute of radiopharmaceutical Cancer Research, Dresden	Preclinical	Anti PSCA/Anti PSMA CAR-T cell	Second generation	CD28
Tanya et al.	2019	City of Hope, Duarte	Pahse1 (NCT03873805)	Anti PSCA CAR-T cell	Second generation	4-1BB

Figure 1.7 CAR T-cell development in prostate cancer[87]

Abbreviations: CAR: chimeric antigen receptor, PSMA: prostate-specific membrane antigen, TGFβ: transforming growth factor β, PSCA: prostate stem cell antigen.

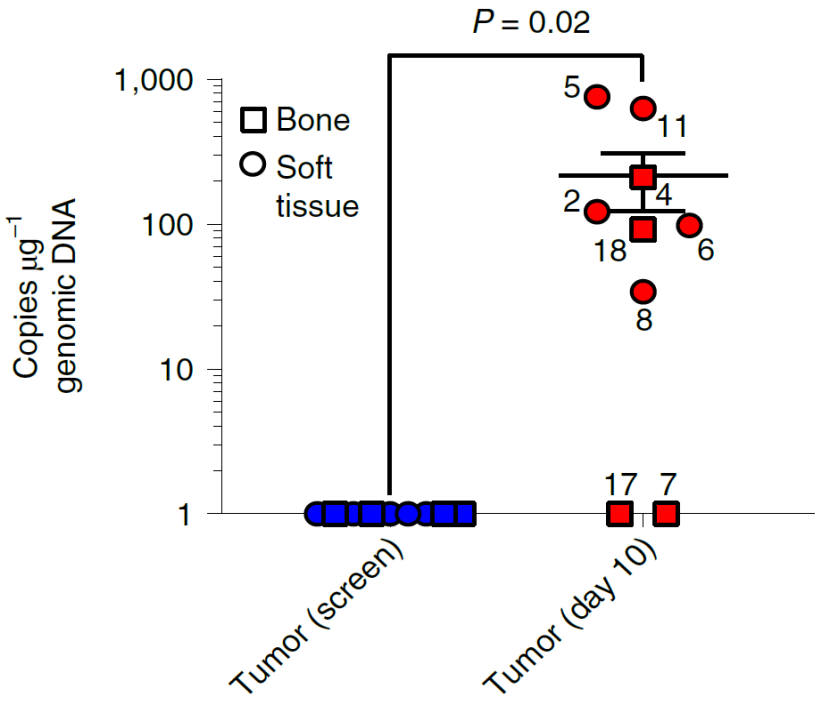

Figure 1.8 dnTGFbRII-armored PSMA CAR T-cell trafficking to tumors[97].

dnTGFbRII-armored PSMA CAR T-cell trafficking to metastatic tumor sites was quantified using qPCR measurements of the CAR transgene in tumor biopsies at baseline relative to day 10 post-CAR T-cell infusion. Biopsy type and subject identification numbers are indicated in the figure. Mean ± s.e.m.; paired two-sided Wilcoxon signed-rank test. *$P < 0.05$, *$P < 0.01$, ***$P < 0.001$, n.s.: not significant.

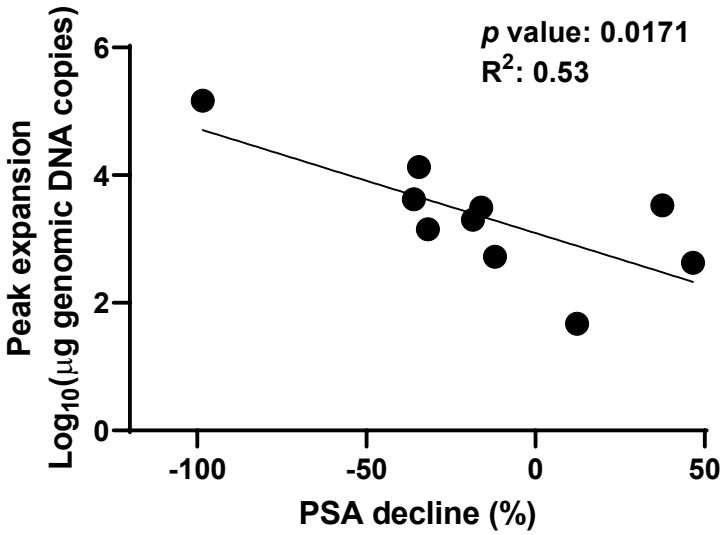

Figure 1.9 Correlation between peak peripheral blood CAR T-cell expansion and PSA response.

Linear regression between peak peripheral blood CAR T-cell expansion and the PSA decline level in mCRPC patients treated with dnTGFbRII-armored PSMA CAR T-cells. *p* value and R^2 are indicated.

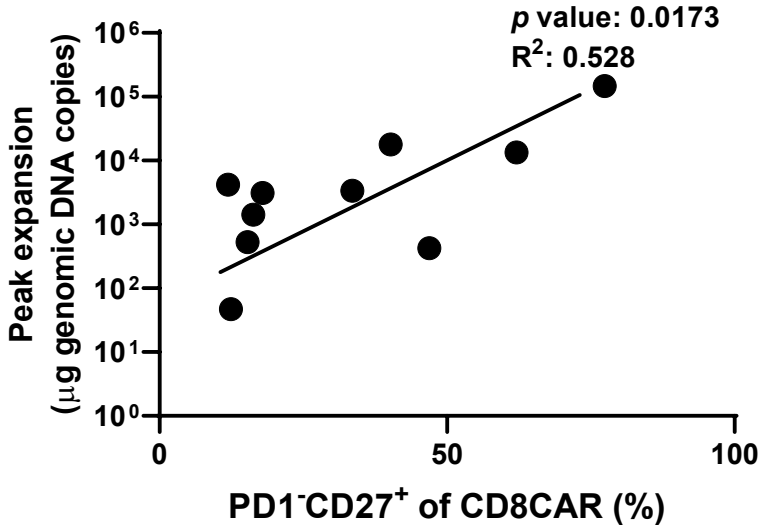

Figure 1.10 Correlation between peak peripheral blood CAR T-cell expansion and frequency of early memory CD8 CAR T-cells in infusion products.

Linear regression between peak peripheral blood CAR T-cell expansion and the frequency of $PD1^{-}CD27^{+}$ CD8 CAR T-cells in patient infusion products. *p* value and R^2 are indicated.

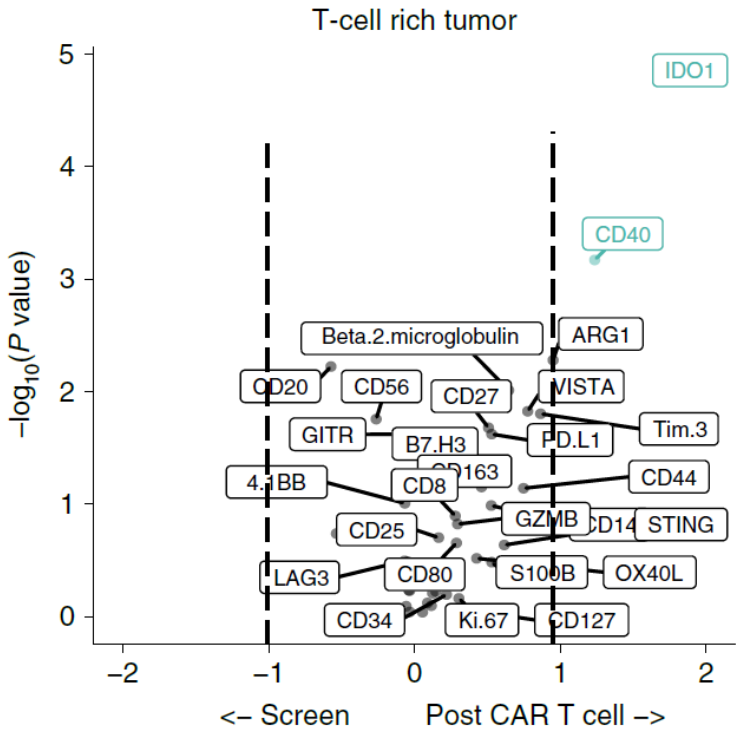

Figure 1.11 Immunophenotyping of T-cells in the tumor using digital spatial profiling[97].

A volcano plot demonstrating protein expression levels in T-cell-rich tumor regions at pre- versus post-CAR T-cell infusion time points. Protein names labeled in green indicate markers with a false discovery rate less than 0.05.

CHAPTER 2: *PRDM1* Upregulation is Associated with Reduction of TCF7^{+}CD8 and Enrichment of TIM3^{+}CD8 Populations in Infusion Products.

Parts of this chapter were previously published in:

In-Young Jung, Vivek Narayan, Sierra McDonald, Andrew J. Rech, Robert Bartoszek, Gwanui Hong, Megan M. Davis, Jun Xu, Alina C. Boesteanu, Julie S. Barber-Rotenberg, Gabriela Plesa, Simon F. Lacey, Julie K. Jadlowsky, Donald L. Siegel, Dana M. Hammill, Prostate Cancer Cellular Therapy Program Investigators, Park F. Cho-Park, Shelley L. Berger, Naomi B. Haas, and Joseph A. Fraietta (2022) BLIMP1 and NR4A3 Transcription Factors Reciprocally Regulate Antitumor CAR T-cell Stemness and Exhaustion *Sci. Transl. Med.* (*In Revision*).

Abstract

Autologous CAR T-cell therapies have induced promising clinical responses in hematological malignancies, yet there is appreciable variation in therapeutic efficacy. A series of recent studies demonstrated that the cellular and molecular heterogeneity of infusion products contributes to the clinical effectiveness of CAR T-cells in B-cell malignancies[10,20,21]. However, characteristics of CAR T-cell products associated with antitumor efficacy and clinical response are poorly investigated in solid tumor indications. Here we characterized CAR T-cell infusion products from a first-in-human trial in metastatic prostate cancer (NCT03089203) using single cell RNA-sequencing

(scRNA-seq) and identified four CD8 T-cell clusters with unique molecular features[97]. $TCF7^+$ CD8 T-cells were significantly enriched with stem-like memory T-cell gene signatures, while $TIM3^+$ CD8 T-cells upregulated genes related to T-cell exhaustion. Enrichment of TCF7 $CD8^+$ T-cells was associated with enhanced CAR T-cell expansion and prostate-specific antigen (PSA) response, whereas a low TIM3 $CD8^+$ signature score correlated with poor CAR T-cell expansion and antitumor activity in patients. Interestingly, low levels of the *PRDM1* defined favorable $TCF7^+CD8^+$ CAR T-cell populations, and unfavorable $TIM3^+CD8^+$ T-cells exhibited elevated *PRDM1* expression. Based on these results, we hypothesized that *PRDM1* mediates CAR T-cell exhaustion and attrition of stemness, and CRISPR/Cas9 (clustered regularly interspaced short palindromic repeats and CRISPR-associated protein 9)-mediated *PRDM1* disruption may ameliorate T-cell exhaustion and preserve early memory differentiation states.

Introduction

Prostate cancer is the most common malignancy among men, with an estimated 268,490 cases in 2022 alone. In addition, prostate cancer is the second-leading cause of cancer-related mortality among men, accounting for an estimated 10% of annual male cancer deaths. Advanced prostate cancer commonly progresses within two years following the initiation of androgen-ablative therapy, often with osseous and visceral metastases. Unfortunately, metastatic castration-resistant prostate cancer (mCRPC) remains an incurable malignancy. For this reason, mCRPC is a major unresolved therapeutic challenge and there is high interest in the development and clinical testing of T-cell–redirecting therapies, such as CAR T-cells.

The ability to control T-cell specificity through introduction of cloned T-cell receptors (TCR) or CARs into T-cells has produced a flexible therapeutic platform capable of harnessing the immense cytotoxic potential of the T-cell to eliminate cancer. CAR T-cells directed toward the B cell antigen CD19 have shown impressive clinical results in hematologic malignancies, which recently culminated in the FDA approval of anti-CD19 CAR T-cells for acute lymphoblastic leukemia (ALL) and diffuse large B cell lymphoma (DLBCL). Despite these successes, the efficacy of CAR T-cell therapy in solid tumor indications is limited in large part by lack of therapeutic levels of CAR T-cell expansion, the failure of these cells to persist durably, antigen heterogeneity/loss, diminished anti-tumor function in the immunosuppressive tumor microenvironment (TME) and/or treatment-related toxicities. Thus, advancing these therapies will require further innovation in cellular engineering and manufacturing to enhance the survival,

proliferation and function of CAR T-cells following adoptive transfer. This is particularly evident in the setting of prostate cancer, where CAR T-cell therapy approaches have failed [99].

T-cell-intrinsic negative regulatory mechanisms, such as upregulation of cognate inhibitory receptors (e.g. PD-1 and CTLA-4) [10,100,101], a reduction in stem cell memory/central memory functions [10,22,52,102,103], and immune senescence [101] are major barriers to the success of CAR T-cell therapy. CAR T-cells derived from naïve and early memory subsets have been shown to robustly expand *in vivo* and are long-lived with a self-renewal capacity [48,60,67]. We and others have demonstrated that naïve or stem-like early memory T-cells genetically redirected with CARs have more durable engraftment and antitumor effector function compared to highly differentiated cells [10,68]. However, persistent tumor antigen stimulation in the setting of hematopoietic and non-hematopoietic cancers often leads to exhaustion. T-cell exhaustion is characterized by upregulation of multiple inhibitory receptors [67-70], the inability to respond to homeostatic cytokines, loss of effector function [60,61] and reduced survival [19]. CAR T-cell exhaustion can also be facilitated by antigen-independent tonic signaling through the synthetic antigen receptor during *ex vivo* cell expansion, following infusion and/or infiltration into the toxic TME [52,104]. Importantly, it may be possible to overcome many of the above issues by using a combination of novel cellular engineering and genome-editing strategies to generate highly proliferative, 'optimally programmed' CAR T-cells.

Here, we analyzed five TGFβ receptor-armored PSMA CAR T-cell infusion products from the mCRPC patients and identified CAR T-cell populations that are

associated with favorable antitumor activity and PSA response. Moreover, to identify targets for CAR T-cell engineering in subsequent studies, we performed differential gene expression analysis and identified transcription factors that define desirable and undesirable CD8 CAR T-cell populations.

Results

Single-cell RNA-seq study design and CD8 T-cell clustering of dnTGFbRII-armored PSMA CAR T-cell infusion products.

We retrospectively performed scRNA-seq analysis on five autologous PSMA CAR T-cell infusion products administered to mCRPC cancer patients (**Figure 2.1A**). These products were selected based on sample availability and to represent a range of clinical outcomes including *in vivo* CAR T-cell expansion and prostate-specific antigen (PSA) response[97]. CAR-positive T-cells were isolated using magnetic bead-based sorting for subsequent single-cell analysis. 20,702 cells were obtained after eliminating low-quality cells, consisting mostly of T-cells and rare B-cells (**Figure 2.1A-C**). To identify transcriptional features associated with CAR T-cell therapeutic potency, we first focused on $CD8^+$ T-cells. Initial sub-clustering identified four distinct $CD8^+$ T-cell populations: $TCF7^+CD8^+$, $CCR7^+CD8^+$, $GZMA^+CD8^+$, and $TIM3^+CD8^+$ T-cells (**Figure 2.1D, E**). $TCF7^+CD8^+$ and $CCR7^+CD8^+$ T-cells express high levels of early memory-related genes such as IL7R, while $GZMA^+CD8^+$ and $TIM3^+CD8^+$ T-cells showed effector-like gene expression profile with elevated expression levels of GZMB, ID2 (**Figure 2.2A**).

$TCF7^+$ CD8 T-cells enrich stem-like memory T-cell signatures while $TIM3^+$ CD8 T-cells express high levels of exhaustion-related genes.

Notably, a $TCF7^+CD8^+$ subset was the only cell population that expressed a high-level of a stemness transcription factor gene, *TCF7* **(Figure 2.1E**). In accordance with

this *TCF7* expression profile, $TCF7^+CD8^+$ T-cells were significantly enriched in $TCF7^+$ stem cell-like T-cell signatures that are associated with robust antiviral responses in mouse models of acute and chronic lymphocytic choriomeningitis virus (LCMV) infection (**Figure 2.3A**) [45,105,106]. In contrast, a $TIM3^+CD8^+$ cluster was markedly enriched in murine antigen-specific T-cell and human CAR T-cell exhaustion signatures, whereas memory-like $CCR7^+CD8^+$ and $TCF7^+CD8^+$ populations possessed low exhaustion scores (**Figure 2.3B, C**). Consistent with this analysis, the $TIM3^+CD8^+$ T-cell population exhibited upregulation of multiple inhibitory molecule transcripts, including HAVCR2, LAG3, CTLA4, and MAF, compared to stem cell-like $TCF7^+CD8^+$ cells (**Figure 2.2A, B**).

A recent study that characterized leukapheresed T-cells of pediatric ALL patients demonstrated that enrichment of an interferon (IFN) response signature is associated with poor CAR T-cell persistence[107]. We thus queried the $CD8^+$ T-cell clusters identified in our analysis for this battery of genes and found that $TIM3^+CD8^+$ T-cells in mCRPC patient infusion products had significantly higher IFN response signature scores compared to the other populations (**Figure 2.3D**). The $TIM3^+CD8^+$ state is associated with short CD19 CAR T-cell persistence in ALL, which often prognosticates poor outcome (**Figure 2.3E**).

$TCF7^+$ CD8 T-cells and $TIM3^+$ CD8 T-cells are associated with favorable and unfavorable clinical response, respectively.

We then scored PSMA CAR T-cell infusion products for the TCF7 and TIM3 signatures and analyzed how these signature scores correlate with PSA decline in mCRPC patients following CAR T-cell transfer. In accordance with our recently reported clinical findings[97], there is a clear dose- and lymphodepletion-dependent relationship with peripheral blood CAR T-cell expansion and early antitumor effects, as determined by serum PSA decrease (**Figure 2.4B**). Patients 2 and 5 were treated in the cohort that received the lowest dose of CAR T-cells in this trial, without lymphodepleting preconditioning prior to cell infusion. It is intriguing that independently of conditioning and cell dose, Patient 2 pre-infusion CAR T-cells with a highly enriched TCF7 signature and a low TIM3 score exhibited superior *in vivo* expansion and PSA response induction, compared to the infusion product of patient 5 with lower TCF7 and elevated TIM3 population scores (**Figure 2.4A, B**).

To determine the generalizable nature of our initial findings, we next sought to investigate $CD8^+$ clusters associated with response to CAR T-cell therapy in LBCL [86]. Intriguingly, the $TCF7^+CD8^+$ population highly expressed a gene set enriched in anti-CD19 CAR T-cell infusion products derived from complete responder (CR) patients, whereas the $TIM3^+CD8^+$ T-cell population exhibited the highest scores for a gene set that characterizes non-responder (NR) anti-CD19 CAR T-cells (**Figure 2.4C**).

These results suggest that increasing $TCF7^+CD8^+$ populations and decrease $TIM3^+CD8^+$ populations in CAR T-cell infusion products may enhance CAR T-cell efficacy.

TCF7$^+$ CD8 T-cells are defined by low level of *PRDM1* expression while TIM3$^+$ CD8 T-cells upregulate PRDM1 express low level of *TCF7*.

To identify transcription factors that define desirable and undesirable CD8 CAR T-cell populations, we conducted differential gene expression analysis between TCF7$^+$CD8 and TIM3$^+$CD8 T-cells (**Figure 2.5A**). Among the transcription factors that are upregulated in the TIM3$^+$CD8$^+$ population, we focused on BLIMP1 (encoded by *PRDM1*). *PRDM1* is known to play a central role in driving T-cell exhaustion and terminal differentiation[108-110]. In addition, high expression of *PRDM1* is associated with loss of T-cell stemness and self-renewal capacity through reciprocal repression of *TCF7*[111]. Consistent with these results, TIM3$^+$CD8$^+$ cells displayed the highest expression level of *PRDM1*, whereas TCF7$^+$CD8$^+$ T-cells exhibited low levels of *PRDM1* expression among the CD8$^+$ clusters (**Figure 2.5B**).

We also examined whether similar BLIMP1 expression profiles are observed in CD4 compartment. The CD4 and CD8 compositions of each clinical CAR T-cell product are presented in **Figure 2.6A**. A scRNA-seq analysis of the CD4$^+$ compartment in clinical CAR T-cell products is shown in **Figure 2.6B**. Clustering all CD4$^+$ T-cells revealed four major cell states: TCF7$^+$CD4$^+$, CCR7$^+$CD4$^+$, MKI67$^+$CD4$^+$, and CTLA4$^+$CD4$^+$ clusters. CTLA4$^+$CD4$^+$ cells displayed the highest expression level of *PRDM1* whereas TCF7$^+$CD4$^+$ T-cells exhibited low levels of *PRDM1* expression among the CD4$^+$ clusters **Figure 2.6C, D**.

To further validate these findings, we compared *PRDM1* and *TCF7* expression in cohorts of chronic lymphocytic leukemia (CLL) patients treated with autologous CD19 CAR T-cells. As expected, pre-infusion CAR T-cells from CR and very good partially responding (PR_{TD}) subjects exhibited significantly lower levels of *PRDM1* and elevated *TCF7* expression, compared to poorly functional products from non-responders (NR) or conventional partial responders (PR) (**Figure 2.5C**). We therefore originally hypothesized that *PRDM1* mediates CAR T-cell exhaustion and attrition of stemness, and thus, *PRDM1* KO may mitigate T-cell exhaustion and improve CAR T-cell expansion, persistence and antitumor efficacy.

Discussion

The full therapeutic potential of CAR T-cell therapies in cancer is often hindered by poor expansion, persistence, and lack of durable effector function of the transferred cellular product. Unfortunately, to date, efficacy in solid tumors has been limited in particular[22-24], and the underpinnings of CAR T-cell intrinsic antitumor potency in these indications have not been elucidated. Our results suggest for the first time that-cellular and molecular diversity of infused CAR T-cells is a major factor contributing to the variability in antitumor efficacy among solid tumor patients with advanced metastatic disease.

A central finding from our study is that the presence of stem cell-like $TCF7^{+}CD8^{+}$ and absence of $TIM3^{+}CD8^{+}$ exhausted T-cells are indicative of CAR T-cell expansion and antitumor activity in both non-hematopoietic and hematopoietic cancers, suggesting that the intrinsic fitness of the engineered T-cells, in addition to absolute T-cell number and spatial distribution within a patient's tumor is crucial for induction of effective tumor immunity. $TCF7^{+}CD8^{+}$ T-cells are a distinct CD8 population that expands and generates cytotoxic progenitors which are critical for elicitation of robust antitumor function in response to checkpoint blockade therapies[45,46,70]. Additionally, the TCF7 regulon not only associates with a favorable naive T-cell state but is maintained in effectors among patients with long-term CAR T-cell persistence who experience durable remission[107]. This is concordant with a previous report suggesting that TCF7 mediates persistence of $CD8^{+}$ effector T-cells as well as their differentiation toward a central memory phenotype[112]. Similar cell populations were identified in the CD4 compartment, and

$CD4^+$ CAR T-cells may be critical for maintaining long-term persistence and antitumor function[113]. Examination of larger patient cohorts is needed to validate and build on these molecular determinants of CAR T-cell activity and outcome.

In contrast to $TCF7^+CD8^+$ T-cells, we found poorly functional cells expressing exhausted or dysfunctional transcriptomic programs associated with lack of *in vivo* PSMA CAR T-cell proliferative potency and PSA responses in mCRPC. $TIM3^+CD8^+$ T-cells upregulated pathways associated with exhaustion, the interferon response, lack of persistence, and poor CAR T-cell clinical efficacy and expressed a low level of *TCF7*, which is predictive of negative outcome in checkpoint inhibitor-treated patients[47]. Notably, we discovered that unlike $TCF7^+CD8^+$ T-cells, $TIM3^+CD8^+$ T-cells express a high level of *PRDM1* that has been reported to negatively regulate *TCF7* and mediate terminal T-cell differentiation and exhaustion[108,109]. Altogether, our scRNA-seq results suggest that disruption of *PRDM1* KO has potential of enriching favorable and decreasing unfavorable CAR T-cell populations in infusion product by alleviating T-cell exhaustion and improving *TCF7*-mediated T-cell stemness.

Materials and Methods

Primary human samples

Infusion product samples were acquired from patients with mCRPC who enrolled in a completed clinical trial of single-agent PSMA CAR T-cell therapy, which was approved by the Institutional Review Board (IRB) of the University of Pennsylvania. All ethical regulations were followed. This study is registered at ClinicalTrials.gov (NCT03089203) [97]. Correlative analyses presented in this report are exploratory, given the post-hoc nature of the investigation.

Correlative assays and response assessments

Correlative assays conducted on patient samples (e.g., qPCR for CAR T-cell quantification) were carried out according to our previously published methods [22]. Antitumor responses, as measured by maximum decline in PSA from baseline for the patients whose CAR T-cell infusion products were analyzed in this study, are reported [97].

Single-cell RNA-seq

PSMA CAR T-cell infusion products from 5 different patients were thawed in a 37°C water bath and dead cells were eliminated using the Dead Cell Removal Kit (Miltenyi Biotec). PSMA CAR-positive T-cells were enriched by magnetic cell separation using a Biotin-goat anti-mouse IgG F(ab)2 fragment (Jackson ImmunoResearch #115-065-072) and anti-biotin kits (Miltenyi Biotech). scRNA-seq

libraries were prepared using Chromium Single Cell 3' v3.1 Reagent Kits (10X Genomics) following the manufacturer's instructions. Isolated CAR T-cells were washed and resuspended in PBS containing 0.04% BSA and ~20,000 cells were loaded per reaction to capture ~10,000 cells. Sequencing was performed on a Novaseq 6000 (Illumina) at a depth of > 20,000 reads per cell.

Reads were aligned to the human reference genome (GRCh38) using Cell Ranger version 6.0.0. Subsequent quality control and downstream analyses were performed using Seurat 4.0. Cells were filtered based on the following criteria to eliminate low-quality cells: 1) a minimum of 1000 genes and a maximum of 6000 genes detected per cell; and 2) less than 15% of mitochondrial gene counts. After quality control, 20,702 cells remained. Gene-cell matrices from five CAR T-cell products were then integrated using SelectIntegrationFeatures, PrepSCTIntegration, FindIntegrationAnchors, and IntegrateData functions in Seurat. CD4-positive and CD8-positive cells were clustered using FindNeighbors/FindClusters, followed by differential gene expression analysis using the FindClusters command. Module scores were then calculated using AddModuleScore to assess the enrichment of gene signatures in CD4 and CD8 subclusters.

Statistical analyses

Statistical analyses were conducted using Shapiro-Wilk test and D'Agostino & Pearson tests for normality. For nonparametric comparisons of three or more groups, the

Kruskal-Wallis test with a post-hoc Dunn's multiple comparison test were used. Statistical tests were performed in Prism 9 (GraphPad Software) and *P* values <0.05 were considered significant.

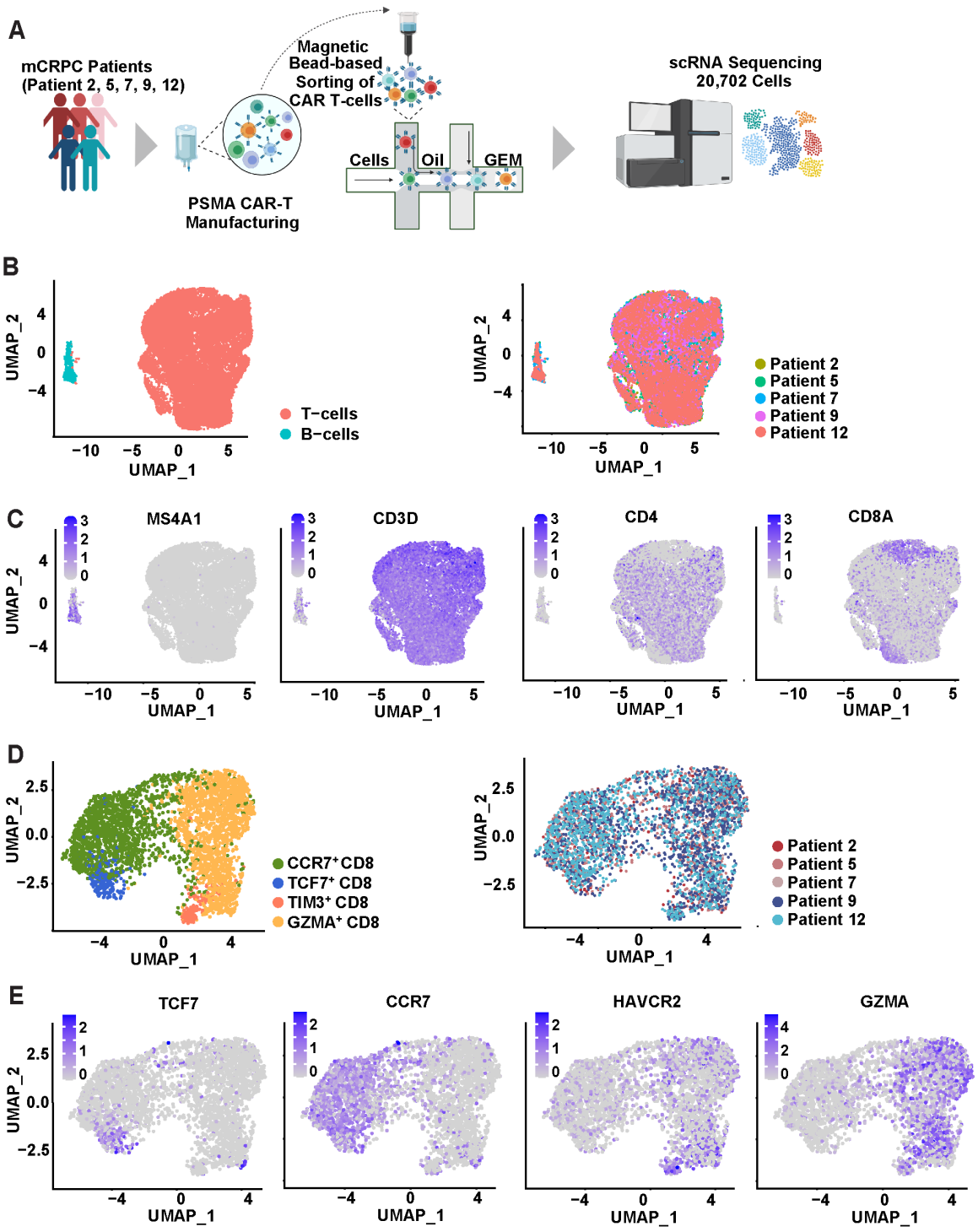
A
mCRPC Patients
(Patient 2, 5, 7, 9, 12)
PSMA CAR-T
Manufacturing
Magnetic
Bead-based
Sorting of
CAR T-cells
Cells
Oil
GEM
scRNA Sequencing
20,702 Cells
B
UMAP_2
UMAP_1
T−cells
B−cells
Patient 2
Patient 5
Patient 7
Patient 9
Patient 12
C
MS4A1
CD3D
CD4
CD8A
D
CCR7⁺CD8
TCF7⁺ CD8
TIM3⁺ CD8
GZMA⁺ CD8
E
TCF7
CCR7
HAVCR2
GZMA

Figure 2.1 Single-cell RNA-seq study design and CD8 T-cell clustering of dnTGFbRII-armored PSMA CAR T-cell infusion products.

(**A**) A schematic of study design and sample processing for scRNA-seq analysis of mCRPC patient PSMA CAR T-cell infusion products. (**B**) Infusion products analyzed by scRNA-seq using integrated data from five patients (total 20,702 cells that passed QC). Clusters are labeled with cell types (left) and patient origin (right). (**C**) UMAP plot displaying mRNA transcripts for selected genes (*MS4A1*, *CD3D*, *CD4*, and *CD8A*) expressed in CAR T-cell infusion products. (**D**) Uniform manifold approximation and projection (UMAP) plot showing sub-clustering of $CD8^+$ T-cells from mCRPC patient CAR T-cell infusion products. Cells are labeled according to marker gene expression and patient origin. (**E**) UMAP plot showing CD8 T-cell cluster-defining marker expressions.

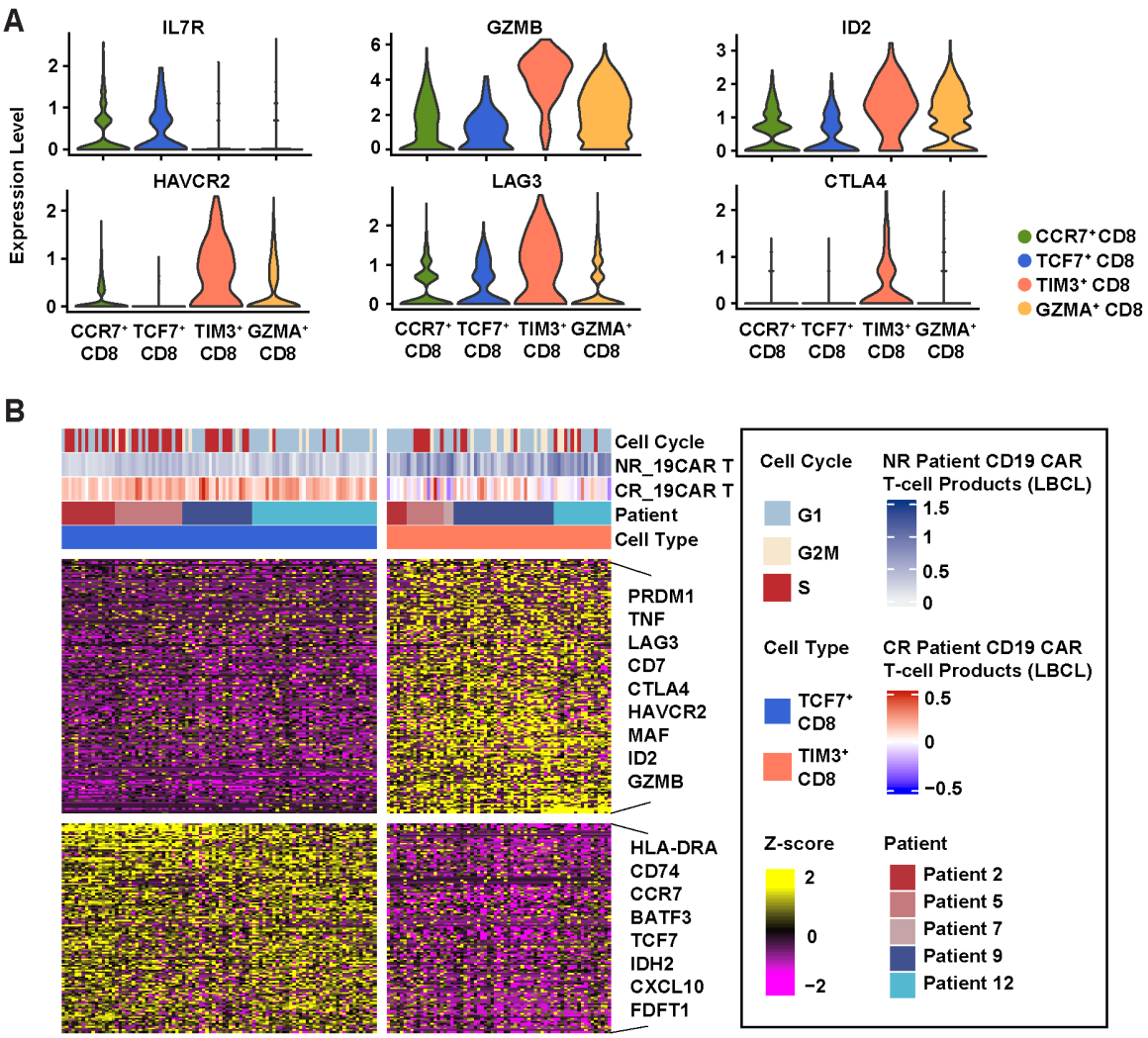

Figure 2.2 Differential gene expression analysis of CD8 CAR T-cells.

(**A**) Violin plot showing expression levels of markers associated with $CD8^+$ T-cell early memory differentiation, cytotoxicity, and exhaustion. (**B**) Differentially expressed genes compared between $TCF7^+CD8^+$ and $TIM3^+CD8^+$ clusters. Top bars indicate cell clusters, patient origin, CD19 CAR T-cell response score (GSE151511), and cell cycle.

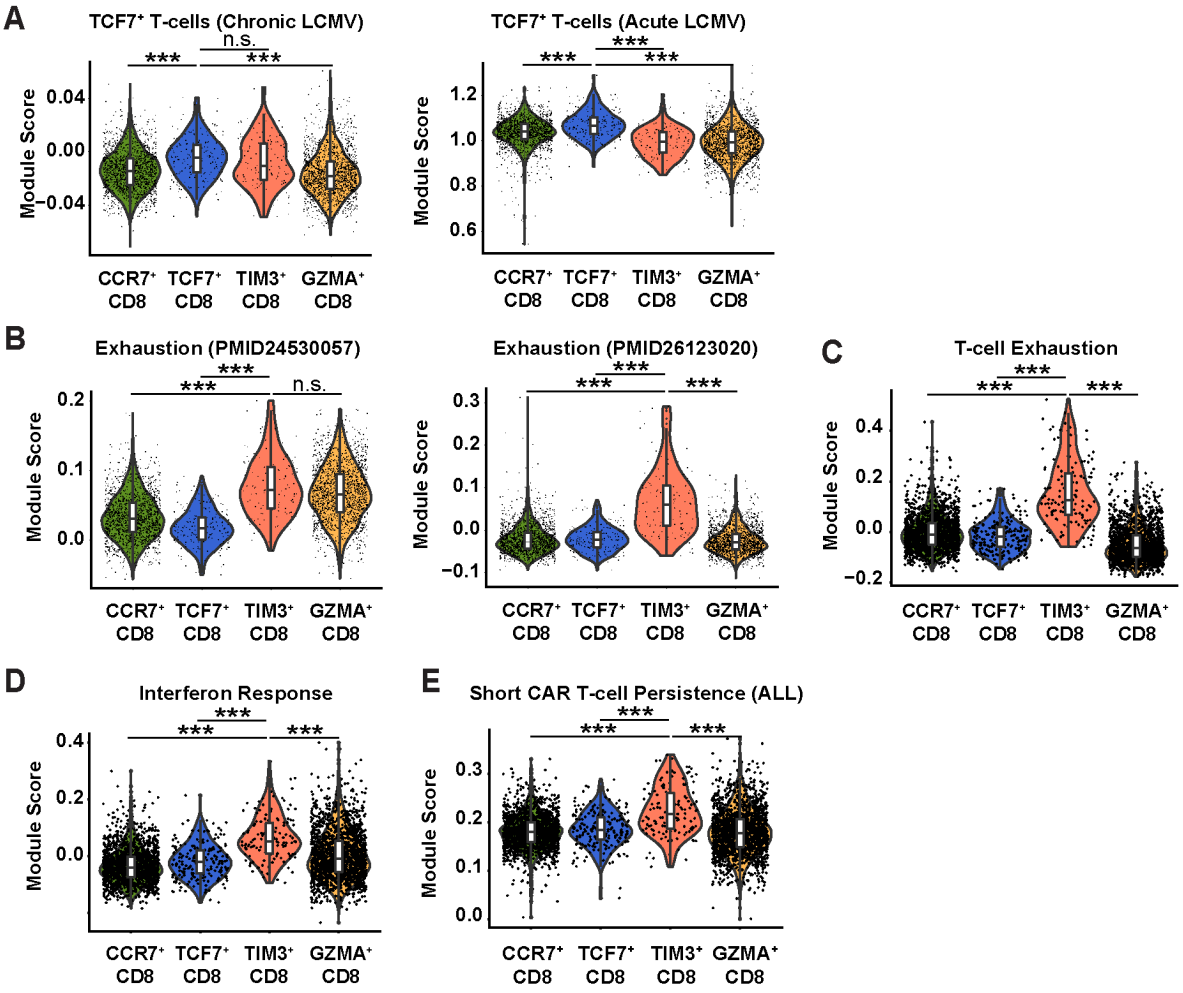

Figure 2.3 TCF7+ CD8 T-cells enrich stem-like memory T-cell signatures while TIM3+ CD8 T-cells express high levels of exhaustion and interferon response pathways.

(**A-C**) Scores of gene signatures enriched in (**A**) TCF7^{+} T-cells in LCMV clone 13 (GSE83978; left) and LCMV Armstrong infection (GSE83978; right), (**B**) mouse exhausted T-cells (PMID24530057, PMID26123020), (**C**) human exhausted T-cells (PMID31802004), and (**D**) interferon (IFN) response genes (PMID33820778). (**E**) Gene signature score enriched in premanufacture T-cells from ALL patients with poor CD19

CAR T-cell persistence (PMID33820778). *$P < 0.05$, *$P < 0.01$, ***$P < 0.001$, n.s.: not significant (Kruskal-Wallis test with a post hoc Dunn's multiple comparison test).

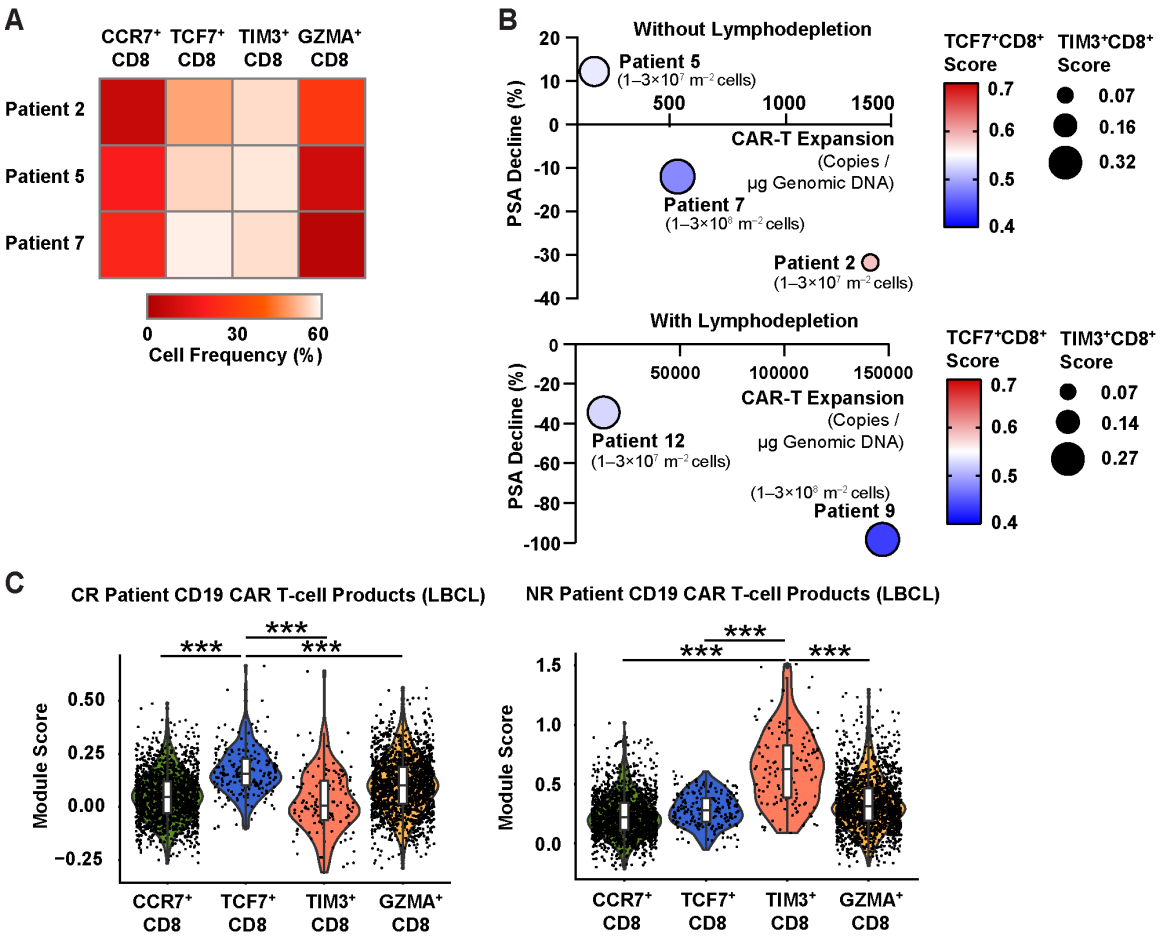

Figure 2.4 TCF7+ CD8 T-cells and TIM3+ CD8 T-cells are associated with favorable and unfavorable clinical response, respectively.

(**A**) Frequencies of CCR7^{+}CD8^{+}, TCF7^{+}CD8^{+}, TIM3^{+}CD8^{+}, and GZMA^{+}CD8^{+} clusters in each CAR T-cell infusion product. (**B**) Bubble plot showing the association between mCRPC patient CAR T-cell infusion product TCF7^{+}CD8^{+} and TIM3^{+}CD8^{+} signature scores, PSA response and peripheral blood (PB) CAR T-cell expansion. CAR T-cell doses and lymphodepletion conditions for each patient are indicated. (**C**) Gene signature score enriched in anti-CD19 CAR T-cell infusion products of complete responder (CR) (GSE151511; left) and non-responder LBCL patients (GSE151511; right). *$P < 0.05$, *P

< 0.01, $***P < 0.001$, n.s.: not significant (Kruskal-Wallis test with a post hoc Dunn's multiple comparison test).

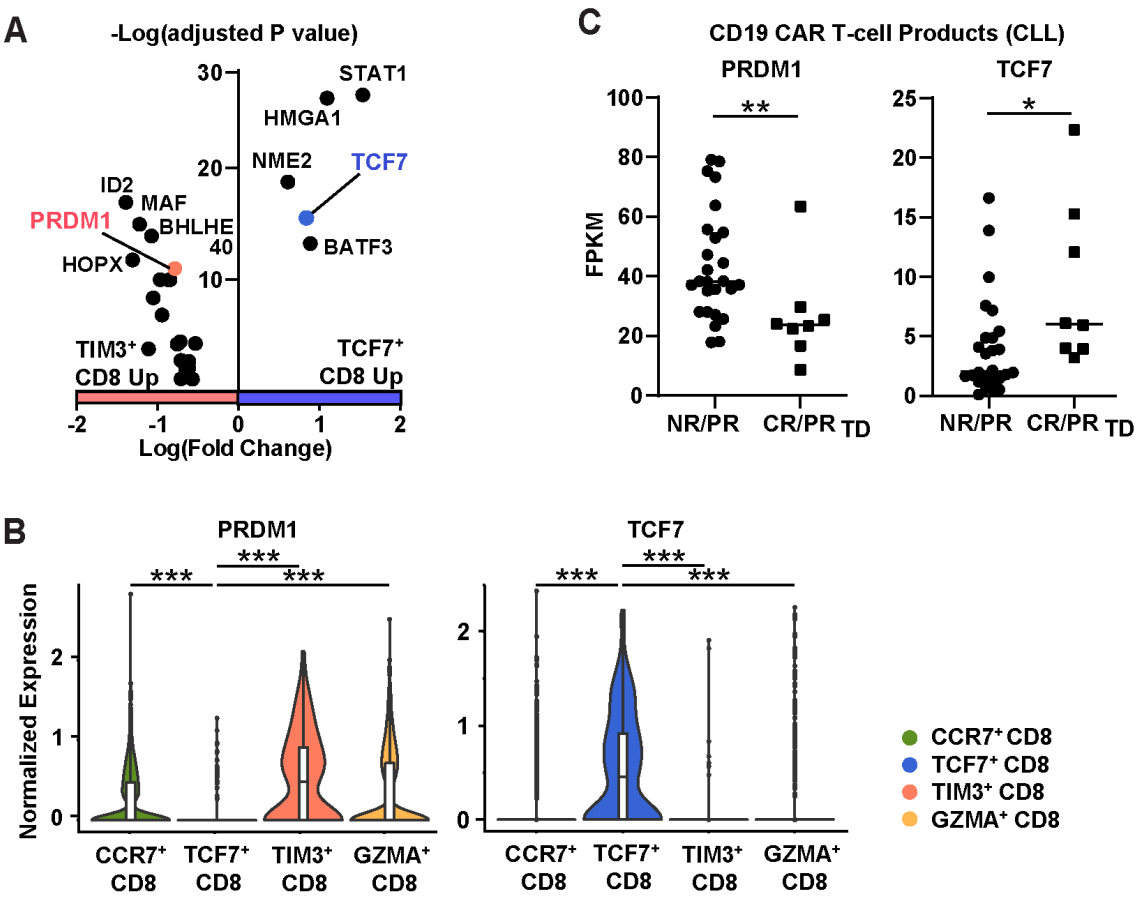

Figure 2.5 TCF7+ CD8 T-cells are defined by low level of PRDM1 expression, while TIM3+ CD8 T-cells upregulate PRDM1 and express low levels of TCF7.

(**A**) Differential expression of transcription factors between $TCF7^{+}CD8^{+}$ and $TIM3^{+}CD8^{+}$ clusters. (**B**) Expression levels of *PRDM1* and *TCF7* in $CD8^{+}$ subclusters. (**C**) *PRDM1* and *TCF7* expression levels in CD19 CAR T infusion products from chronic lymphocytic leukemia patients (CR: complete response; PR_{TD}: very good partial response; PR: partial response; NR: no response); (FPKM: Fragments per kilo base of transcript per million mapped fragments). $*P < 0.05$, $*P < 0.01$, $***P < 0.001$, n.s.: not significant (Kruskal-Wallis test with a post hoc Dunn's multiple comparison test).

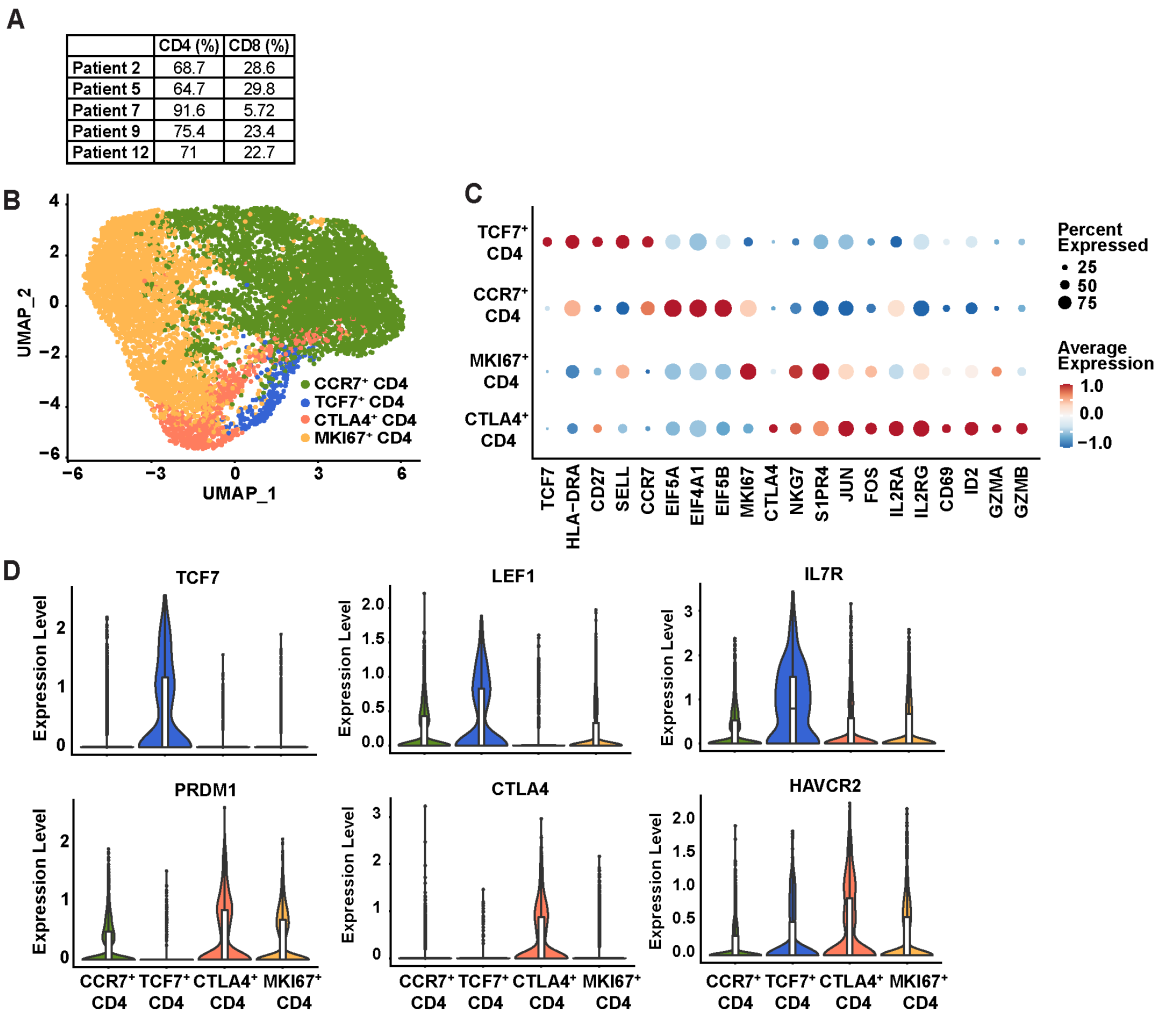

	CD4 (%)	CD8 (%)
Patient 2	68.7	28.6
Patient 5	64.7	29.8
Patient 7	91.6	5.72
Patient 9	75.4	23.4
Patient 12	71	22.7

Figure 2.6 TCF7+ CD4 T-cells exhibit low level of PRDM1 expression while CTLA4+ CD4 T-cells upregulate PRDM1 express low level of TCF7.

(**A**) Frequencies of $CD4^+$ and $CD8^+$ T-cells in mCRPC patient CAR T-cell infusion products. (**B**) UMAP plot displaying sub-clustering of infusion product $CD4^+$ T-cells. (**C, D**) Cluster-defining marker gene expression profiles of $CD4^+$ subclusters.

CHAPTER 3: *PRDM1* Knockout (KO) Enhances Early Memory CAR T-cell Differentiation in a TCF7-Dependent Manner

Parts of this chapter were previously published in:

In-Young Jung, Vivek Narayan, Sierra McDonald, Andrew J. Rech, Robert Bartoszek, Gwanui Hong, Megan M. Davis, Jun Xu, Alina C. Boesteanu, Julie S. Barber-Rotenberg, Gabriela Plesa, Simon F. Lacey, Julie K. Jadlowsky, Donald L. Siegel, Dana M. Hammill, Prostate Cancer Cellular Therapy Program Investigators, Park F. Cho-Park, Shelley L. Berger, Naomi B. Haas, and Joseph A. Fraietta (2022) BLIMP1 and NR4A3 Transcription Factors Reciprocally Regulate Antitumor CAR T-cell Stemness and Exhaustion *Sci. Transl. Med.* (*In Revision*).

Abstract

scRNA-seq analysis identified heterogeneity in the cellular and molecular features of CAR T-cells that contribute to variation in therapeutic product potency across multiple CAR T-cell trials[21,97]. PR/SET domain 1 (*PRDM1*) gene encoding the BLIMP1 transcription factor was upregulated in poorly functional $TIM3^{+}CD8^{+}$ T-cells and downregulated in highly potent $TCF7^{+}$ CD8 T-cells. Based on these findings, we hypothesized that deletion of *PRDM1* may potentiate CAR T-cell stemness and anti-tumor function. CRISPR/Cas9-mediated *PRDM1* disruption profoundly enhanced CAR T-cell expansion capacity and early memory differentiation. Bulk RNA-sequencing demonstrated that *PRDM1* deficient CAR T-cells increased mitotic cell cycle, fatty acid oxidation, and oxidative phosphorylation pathway, while downregulating a gene signature associated with terminal CD8 T-cell differentiation. Moreover, *PRDM1*

disruption increased the expression level of stemness-related transcription factor TCF1 and significantly enriched a $TCF7^{+}CD8^{+}$ T-cell signature associated with favorable antitumor product potency in mCRPC and B-cell lymphoma trials[21,97]. *TCF7* disruption compromised CAR-T expansion, early memory differentiation, and polyfunctionality of PRDM1 KO CAR T-cells, suggesting that *TCF7* plays central role in preserving T-cell stemness and early memory. Lastly, *PRDM1* ablation substantially improved CAR T-cell expansion, persistence, and memory differentiation in a prostate cancer xenograft mouse model, although *PRDM1* KO CAR T-cells showed marginal improvement in tumor control capability.

Introduction

Single cell analysis of PSMA CAR T-cell infusion products revealed that enrichment of a $TCF7^{+}CD8^{+}$ signature was associated with enhanced CAR T-cell expansion and PSA response, while CAR T-cell products with elevated $TIM3^{+}CD8^{+}$ exhausted T-cells showed poor expansion and clinical efficacy in our mCRPC trial. These results are concordant with those presented in previous studies, in which an increased early memory gene signatures and *TCF7* regulon present in CAR T-cell products and pre-manufacture T-cells are associated with long-term CAR-T persistence and durable antitumor responses in B-cell leukemia and lymphoma trials[20,21]. Despite these findings, engineering strategies to enrich highly functional stem-like memory products and diminish exhausted T-cell populations have yet been developed. We identified that $TIM3^{+}CD8^{+}$ T-cells are defined by high levels of *PRDM1* expression, which negatively correlates with a *TCF7* expression profile. These results suggest that *PRDM1* may be associated with T-cell exhaustion and attrition of stemness in prostate cancer. Our findings are also in line with previous studies showing that *PRDM1* transcripts and binding motifs are enriched in terminal effector or exhausted CD8 CAR T-cells from poor responders in non-Hodgkin's lymphoma and B-cell leukemia, suggesting that *PRDM1* may play a critical role in CAR T-cell dysfunction in blood cancer as well[20,114]. Based on these results, we postulated that *PRDM1* suppresses *TCF7*-driven T-cell stemness and facilitates CAR T-cell exhaustion and that *PRDM1* disruption using CRISPR/Cas9 will enhance CAR T-cell expansion, persistence, and antitumor potency by preserving T-cell stemness and mitigating T-cell exhaustion.

Results

PRDM1 knockout in human CAR T-cells using CRISPR/Cas9.

To examine how BLIMP1 deficiency affects CAR T-cell fate, we knocked out *PRDM1* in PSMA CAR T-cells using CRISPR/Cas9 technology. Because the dominant negative TGFβ receptor component used in our recently published clinical study can potentially confound findings[97], this was not included in the tested constructs. CAR T-cells with KO at the *AAVS1* safe harbor locus were used as a negative control for gene editing in subsequent *in vitro* and *in vivo* functional studies[115]. Electroporation of Cas9 and gRNA on day 3 post T-cell activation led to 80-95% of indel (insertion and/or deletion mutations) in PSMA CAR T-cells generated from 4 different donors (**Figure 3.1A**). Targeted amplicon sequencing revealed that the majority of indels introduced by CRISPR/Cas9 were out-of-frame mutants (**Figure 3.1B**), which coincides with substantial reduction in BLIMP1 protein level in *PRDM1* KO CAR T-cells (**Figure 3.1C**). PSMA CAR expression levels were comparable between control *AAVS1* KO and *PRDM1* KO CAR T-cells, suggesting that the knockout process doesn't affect CAR expression levels (**Figure 3.1D**).

PRDM1 KO potentiates early memory differentiation of PSMA CAR T-cells.

Next, we characterized the phenotype and function of *PRDM1* KO CAR T-cells during an *in vitro* 'stress test' involving repetitive PSMA stimulation through the CAR (**Figure 3.2A**). Briefly, PSMA CAR-positive *AAVS1* KO and *PRDM1* KO PSMA CAR

T-cells were isolated and challenged with PC3 cell line expressing PSMA (PC3-PSMA). After 4-5 days, *PRDM1* KO CAR T-cells were replated and rechallenged with PC3-PSMA, and this restimulation process continued until CAR T-cell proliferation become arrested (typically after 5-6 stimulation). *PRDM1* KO CAR T-cells initially showed increased effector cytokine production compared to control CAR T-cells 24-hours after the first restimulation (**Figure 3.2B**). In addition, we found that while the expansion capacity of *AAVS1* KO CAR T-cells gradually declined following repetitive stimulation, *PRDM1* KO CAR T-cells sustained high proliferative capacity even after multiple rounds of stimulation and concomitantly upregulated cell cycle-related gene signatures (**Figure 3.2C-E**).

This enhanced expansion capacity of *PRDM1* KO CAR T-cells is likely attributed to increased memory formation. Accordingly, *PRDM1* KO increased the frequency of $CD45RO^{+}CCR7^{+}$ and $CD45RO^{+}CD62L^{+}CD8^{+}$ central memory CAR T-cells (**Figure 3.3A**). Consistent with this observations, *PRDM1* KO CAR T-cells displayed increased expression of *CD62L*, *CCR7*, *MYB*, *ID3*, and *TCF7*, while downregulating effector-related genes including *KLRG1*, *PRF1*, and *GZMA* (**Figure 3.3B**). Gene set enrichment analysis (GSEA) demonstrated that *PRDM1* KO CAR T-cells enriched transcriptomic signatures of memory precursor effector cells, fatty acid oxidation, and the tricarboxylic acid cycle, indicating that *PRDM1* KO CAR T-cells are skewed toward an early memory fate (**Figure 3.3C-E**).

***PRDM1* KO increases TCF1 expression and TCF7^{+}CD8^{+} stem-like memory signature.**

We next sought to investigate whether *PRDM1* KO derepresses TCF1 expression. *PRDM1* KO not only profoundly increased expression of TCF1, but also upregulated genes encoding other transcription factors that are crucial for maintaining T-cell stemness, such as *MYB*, *BCL6* and *ID3* (**Figure 3.4A, B**)[116-118]. Moreover, *PRDM1* KO CAR T-cells were significantly enriched in Tcf7^{+} stem cell-like T-cell signatures observed in acute and chronic LCMV mouse models[45,106], suggesting that *PRDM1* inhibits *TCF7*-mediated stemness (**Figure 3.4C**). Notably, consistent with our hypothesis, *PRDM1* KO CAR T-cells exhibited decreased TIM3^{+}CD8^{+} gene signatures and transcriptionally resembled TCF7^{+}CD8^{+} T-cells observed in the PSMA CAR T-cell infusion products, implying that *PRDM1* KO reprogram toward clinically favorable T-cell state (**Figure 3.4D**).

***TCF7* preserves T-cell stemness and early memory differentiation of *PRDM1* KO CAR T-cells.**

To examine whether TCF1 upregulation is required for the maintenance of early memory differentiation and robust CAR T-cell proliferative potential as observed in **Figure 3.2**, we knocked out *TCF7* (**Figure 3.5A**) and subsequently assessed CAR T-cell expansion in a restimulation assay. We found that *TCF7* depletion significantly counteracted the effect of *PRDM1* KO by reducing proliferative capacity, which was

accompanied by decreased frequencies of CCR7 and CD62L expressing memory CAR T-cells (**Figure 3.5B-D**). Because lack of polyfunctionality is a hallmark of terminal differentiation and T-cell dysfunction [118], we next stimulated *PRDM1* and *TCF7* single or double KO CAR T-cells and measured expression of IL-2, IFNγ and TNFα. *PRDM1* ablation increased frequencies of polyfunctional CAR T-cells compared to *AAVS1* KO control CAR T-cells (**Figure 3.5E**), which coincides with the previously observed increased early memory differentiation of *PRDM1* KO CAR T-cells. Conversely, TCF7 depletion decreased the frequency of polyfunctional *PRDM1* KO CAR T-cell populations (**Figure 3.5E**), suggesting that *PRDM1* deficiency enhances CAR T-cell polyfunctionality, at least in part, via *TCF7* upregulation. Taken together, these data imply that *PRDM1* knockout enhances CAR T-cell early memory differentiation in a *TCF7*-dependent manner.

PRDM1 KO marginally enhances tumor control despite profound increases in CAR T-cell memory, persistence, and proliferative capacity.

Based on the above results, we next assessed the *in vivo* antitumor activity of *PRDM1* KO CAR T-cells in xenogeneic mouse models (**Figure 3.6A**). When tested against a relatively low burden of flank- engrafted PC3 prostate tumor cells, *PRDM1* KO PSMA CAR T-cells exhibited a modest enhancement of tumor control compared to control CAR T-cells (**Figure 3.6B**). Similarly, and consistent with a very recent report [119], *PRDM1* KO anti-CD19 CAR T-cells better suppressed cancer growth compared to

control CAR T-cells in a B-cell acute lymphoblastic leukemia (ALL) model (NALM-6), although these CAR T-cells eventually failed to eradicate tumors (**Figure 3.6 C-E**). In an *in vivo* 'stress test' in which tumor burden is escalated to reveal CAR T-cell functional limits (**Figure 3.7A**), *PRDM1* KO CAR T-cells showed comparable antitumor activity compared to *AAVS1* KO CAR T-cells (**Figure 3.7B**). Despite lack of improved tumor control over *AAVS1* KO CAR T-cells, *PRDM1* KO CAR T-cells exhibited enhanced *in vivo* expansion and persistence (**Figure 3.6C, D**). Additionally, consistent with our *in vitro* studies, *PRDM1* KO CAR T-cells maintained a higher fraction of central memory T-cells (**Figure 3.6F, 3.7E**), indicating that *PRDM1* deficiency improves CAR-T expansion and persistence by preserving early memory pools. Together, these results suggest that despite significant improvements in expansion and persistence, *PRDM1* knockout alone is not sufficient to potentiate robust and sustained CAR T-cell antitumor efficacy in aggressive tumor models.

Discussion

Here we demonstrated that *PRDM1* deletion significantly improves expansion capacity and persistence of human CAR T-cells. This enhancement is attributed, at least in part, to increases early memory T-cell differentiation as revealed by RNA-seq and flow cytometric analyses. The early memory phenotype is sustained by the increased level of TCF1 as *TCF7* knockout counteracts the effect of *PRDM1* disruption. Our finding is consistent with previous mouse LCMV studies in which BLIMP1 facilitates development of short-lived effector T-cells and suppresses development of memory precursors by induction of effector-related genes such as *Klrg1* and *GzmB* and repression of memory-related genes such as *CD127*, *CCR7*, and *CD62L*[40,82]. Furthermore, $CXCR5^{-}TCF1^{low}$ terminally exhausted T-cells exhibit higher *Prdm1* expression levels compared to $CXCR5^{+}TCF1^{high}$ stem-like exhausted T-cells[120]. Blimp1-ablated T-cells were more skewed to $CXCR5^{+}$ T-cells in LCMV, implying that BLIMP1 negatively regulates TCF1-driven stemness[120].

Despite the substantial increase in CAR T-cell expansion and persistence, *PRDM1* KO CAR T-cells displayed only a marginal improvement in antitumor activity in low tumor burden prostate cancer and B-ALL xenograft models. Furthermore, in a more aggressive high tumor-burden prostate cancer model, *PRDM1* KO failed to improve tumor control compared to control *AAVS1* KO CAR T-cells. Yoshikawa et al. recently showed that *PRDM1* ablation potentiates CAR T-cell potency in B-ALL blood cancer models by increasing CAR T-cell expansion and the memory recall response. However, the therapeutic potential of *PRDM1* KO CAR T-cells in aggressive solid tumor models

has not been thoroughly assessed[121]. Our results imply that enhanced early memory and expansion capacity are not sufficient for CAR T-cells to exert anti-tumor activity in aggressive solid tumor models and additional engineering is thus required for further improvement.

Materials and Methods

Primary human samples

Peripheral blood mononuclear cells (PBMC) were collected for small-scale CAR T-cell production via leukapheresis from healthy subjects. Study participants provided written informed consent according to the Declaration of Helsinki and the International Conference on Harmonization Guidelines for Good Clinical Practice.

Cell lines

PC3, PSMA-expressing PC3, and NALM-6 cells engineered to express click beetle green luciferase and green fluorescent protein (CBG-GFP), were kindly provided by Carl H. June and Marco Ruella (University of Pennsylvania), respectively. PC3 and PC3-PSMA cells were cultured in Dulbecco's Modified Eagle Medium (DMEM) supplemented with 10% fetus bovine serum (FBS) and streptomycin/penicillin. NALM-6 cells were maintained in Roswell Park Memorial Institute (RPMI) 1640 media supplemented with 10% fetus bovine serum (FBS) and streptomycin/penicillin (R10 media). HEK 293T-cells, used for lentivirus production, were obtained from ATCC and cultured in R10 media. Low-passage banks of cells were tested for mycoplasma with a MycoAlert kit (Lonza), according to the manufacturer's instructions. Authentication of cell lines was carried out by the University of Arizona Genetics Core, based on criteria established by the International Cell Line Authentication Committee. Short-tandem-repeat profiling revealed that these cell lines were above the 80% match threshold.

Mycoplasma testing and authentication were routinely performed before and after molecular engineering.

Lentivirus production

Vector construction and lentiviral production were conducted as previously described[122]. In brief, CARs comprised of anti-PSMA[122] and anti-CD19[123] single-chain variable fragments (scFv) fused to 4-1BB and CD3ζ stimulatory endodomains were subcloned into the pTRPE vector. Lentivirus supernatant was collected from 293T-cells transfected with the pTRPE transfer vector and packaging plasmids using Lipofectamine 2000 (Thermo Fisher Scientific) and concentrated using ultracentrifugation.

Lentiviral transduction and T-cell culture

Healthy donor T-cells were isolated from peripheral blood mononuclear cells (PBMC) using the Pan T-cell Isolation Kit according to the manufacturer's instructions (Miltenyi Biotec). T-cells were activated with anti-CD3/CD28 antibody coated Dynabeads (Thermo Fisher Scientific) at 3:1 bead:cell ratio in T-cell media (OpTmizer CTS SFM media (Gibco) supplemented with 5% human AB serum and 100u/mL human IL-2). Following a 24-hour incubation, lentivirus encoding the PSMA CAR was added to the culture at a multiplicity of infection (MOI) of 2.5. CAR T-cell expansion was carried out as previously described[122].

CRISPR/Cas9-mediated gene editing

Following T-cell activation as described above, beads were removed using a magnet on day 3 and electroporation was carried out with a P3 primary cell 4D-nucleofector kit (Lonza). 2×10^6 CAR T-cells were transfected with 12 μg TrueCut™ S. pyogenes Cas9 (Invitrogen) and 0.2nmol of chemically-modified tracrRNA and crRNA (Integrated DNA Technologies). Following electroporation, CAR T-cells were cultured in T-cell media. The crRNA sequences used in this study were: AAVS1: 5'-CCATCGTAAGCAAACCTTAG-3', PRDM1: 5'-CATCAGCACCAGAATCCCAG-3', TCF7: 5'-TCAGGGAGTAGAAGCCAGAG-3'. The frequency of targeted mutations generated by double strand break were determined by Sanger sequencing and subsequent TIDE (tracking of indels by decomposition) analysis. Primers used for targeted amplification were: PRDM1-F1: tctcagaaggagccacaggaacgg, PRDM1-R1: cacccaccctatgctgcaagttgc. Western blot and flow cytometric analysis were conducted to confirm KO at the protein level.

Western blot analysis

T-cells (1×10^6 cells) were suspended in a low-salt lysis buffer (10 mM HEPES, pH 7.9, 10 mM KCl, 0.1 mM EDTA, 0.1 mM EGTA, 1 mM DTT, 0.5 mM PMSF, 2 μg/ml aprotinin, 2 μg/ml leupeptin) and allowed to swell on ice for 30 minutes. After centrifugation (1000 × g), supernatants obtained from cells lysates (30 μg) were analyzed by 10% SDS-polyacrylamide gel electrophoresis and electrophoretically transferred to PVDF membranes (Millipore). The membranes were washed with PBS containing 0.1%

Tween 20 (PBST), and then blocked for 1-hour in 5% skim milk in PBST. After washing with PBST, membranes were incubated overnight with one of the following antibodies: Mouse monoclonal anti-β-Tubulin (Sigma-Aldrich #T8318; 1:100) or rabbit monoclonal anti-Blimp1 (Cell Signaling #9115; 1:100). Membranes were washed with PBST and treated with 1:1000 diluted horseradish peroxidase-coupled goat anti-mouse or anti-rabbit secondary antibodies (Thermo Fisher Scientific) in PBST for 1-hour. After washing, the membranes were incubated in Pierce™ ECL western blotting substrate (Thermo Fisher Scientific) and visualized on X-ray film.

Flow cytometry

Cell surface anti-human antibodies were diluted in FACS buffer (PBS + 2% FBS). PSMA CAR expression was measured using an allophycocyanin (APC)-conjugated recombinant human PSMA protein (Sino Biological). T-cell immunophenotyping was carried out using the following antibodies: PD1-BV421 (Biolegend #329920), CD45-BV570 (Biolegend #304226), CD8-BV650 (Biolegend #301042), CD8-APC-H7 (BD Biosciences #560179), CD4-BV785 (Biolegend #317442), TIM3-PE (Biolegend #345006), CCR7-PE-CF594 (BD Biosciences #562381), CD62L-PE-Cy5 (Biolegend #304808), LAG3-PE-Cy7(eBioscience #25-2239-42), hCD45-APC (BD Biosciences #340943), murine CD45-PerCP-Cy5.5 (Biolegend #103132), CD127-BV570 (Biolegend #351307), HLA-DR-Alexa Fluor700 (Biolegend #307625), CD25-APC (ebioscience #17-0259-42). For intracellular staining, cells were first permeabilized and washed using the FoxP3 Transcription Factor Staining Buffer Kit (eBioscience) and

subsequently stained with following antibodies: IL2-PE-CF594 (BD Biosciences #562384), IFNγ-BV570 (Biolegend #502534), TNFα- Alexa Fluor700 (Biolegend #502928), Perforin-BV421 (Biolegend # 353307), Perforin-APC (Biolegend #308112), GZMB-PE-Cy5.5 (Invitrogen #GRB18), TCF1- Alexa Fluor488 (Cell Signaling Technology #6444S), TOX-APC (Miltenyi Biotech #130-107-785), NFATC1-PE (Biolegend #649606) according to our previously published methods [22]. Samples were then analyzed using an LSRFortessa (BD Biosciences), FlowJo software (FlowJo, LLC) and/or FCS Express (De Novo Software).

CAR T-cell restimulation assay

CAR T-cell expansion capacity and effector function were assessed using a restimulation assay, as previously described[22,122,124]. Briefly, AAVS1 KO, PRDM1 KO, TCF7 KO, NR4A3 KO, and PRDM1 + TCF7 dKO PSMA CAR-positive T-cells were isolated using a Biotin-goat anti-mouse IgG F(ab)2 fragment (Jackson ImmunoResearch #115-065-072) and anti-biotin kits (Miltenyi Biotech). Following isolation, CAR T-cell purity was confirmed by flow cytometric analysis and CAR T-cells were then serially exposed (i.e., every 2-5 days) to irradiated PC3-PSMA cells at an effector-to-target (E:T) ratio of 3:1 or 1:1. Restimulation assays were carried out for 25-30 days, since cell counts become largely unreliable beyond the fifth and sixth rounds of stimulation due to senescent proliferative arrest and a marked decrease in the viability of chronically stimulated CAR T-cells. Supernatants were collected 24-hours post-tumor challenge for cytokine analysis using the LEGENDplex™ human CD8 panel (Biolegend), and absolute

numbers of T-cells in culture were monitored using a Luna automated cell counter (Logos Biosystems) during the assay.

Mouse xenograft studies

Mouse studies were performed with 6- to 8-week-old male NOD/SCID/IL-2Rγ-null (NSG) mice in compliance with a University of Pennsylvania Institutional Animal Care and Use Committee approved protocol. For the subcutaneous PC3-PSMA model, 10^6 or 5×10^6 PC3-PSMA-CBG-GFP tumor cells were premixed with Matrigel (Corning) and injected into the flanks of NSG mice. When the average tumor size reached 150-200 mm^3 or 500 mm^3, 3.5×10^5 PSMA CAR T-cells were injected intravenously. Tumor growth weekly monitored weekly by taking caliper measurements (tumor volume = (length × $width^2$)/2). Animals were sacrificed when tumor volume exceeded 1500 mm^3 or 2 cm in diameter. For the intraosseous PC3-PSMA model, male NSG mice were intrafemorally transplanted with 2×10^5 PC3-PSMA cells. On day 27, 1-2 $\times 10^5$ PSMA CAR T-cells were infused intravenously, and tumor burden was measured by bioluminescent imaging. To characterize CAR T-cell phenotype and function, peripheral blood and tumor tissues were isolated from mice. Blood samples were obtained at peak CAR T-cell expansion via cheek bleeding.

For the B-cell acute lymphoblastic leukemia model, NSG mice were intravenously injected with 1×10^6 NALM-6-CBG cells. On day 7 post-tumor injection,

3×10^5 CD19 CAR T-cells were intravenously infused, and tumor growth was assessed twice weekly using bioluminescent imaging[22].

Bulk RNA-seq

On days 0, 5 and 20 of the CAR T-cell restimulation assay, before stimulation and after the first and fourth tumor challenge respectively, $CD8^+$ CAR T-cells were isolated using CD8 microbeads (Miltenyi Biotec) and total mRNA was extracted with RNA Clean & Concentrator™ kits (Zymo Research). Bulk RNA-seq was conducted by Novogene using the Novaseq6000 system (paired-end 150bp) at 40×10^6 reads per sample. Reads were pseudoaligned to the human genome (GRCh38) transcriptomes using kallisto v0.46.0.

Differential expression analyses between *AAVS1* KO PSMA CAR T-cells and *PRDM1* KO PSMA CAR T-cells were performed using the edgeR v3.34.0 and limma v3.48.0 packages. Briefly, expression data were normalized using a trimmed mean of log expression ratios method and transformed into log2(counts per million). Linear models were used to assess differential expression, and *P* values were adjusted using the Benjamini and Hochberg method. Gene set enrichment analysis was conducted using GSEABase v1.54.0, clusterProfiler v4.0.2, and msigdbr v7.4.1.

Statistical analyses

Statistical analyses were conducted using Shapiro-Wilk test and D'Agostino & Pearson tests for normality. Pairwise comparisons were performed using the Mann Whitney U test and Student's t-test as appropriate. For nonparametric comparisons of three or more groups, the Kruskal-Wallis test with a post-hoc Dunn's multiple comparison test were used. Mouse survival was assessed using the Gehan-Breslow-Wilcoxon test. Statistical tests were performed in Prism 9 (GraphPad Software) and *P* values <0.05 were considered significant.

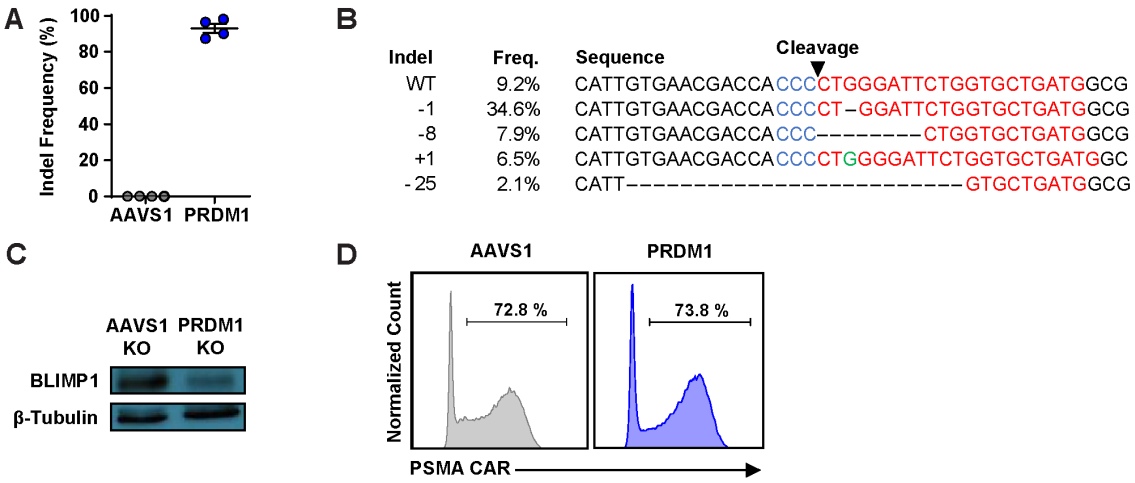

Figure 3.1 PRDM1 knockout in human CAR T-cells using CRISPR/Cas9.

(**A**) *PRDM1* editing efficiency measured by Sanger sequencing and subsequent TIDE (Tracking of Indels by Decomposition) analysis. (**B**) Amplicon sequencing of *PRDM1* indel variants generated by CRISPR/Cas9-mediated gene editing. (**C**) Representative Western blot analysis for BLIMP1 expression.

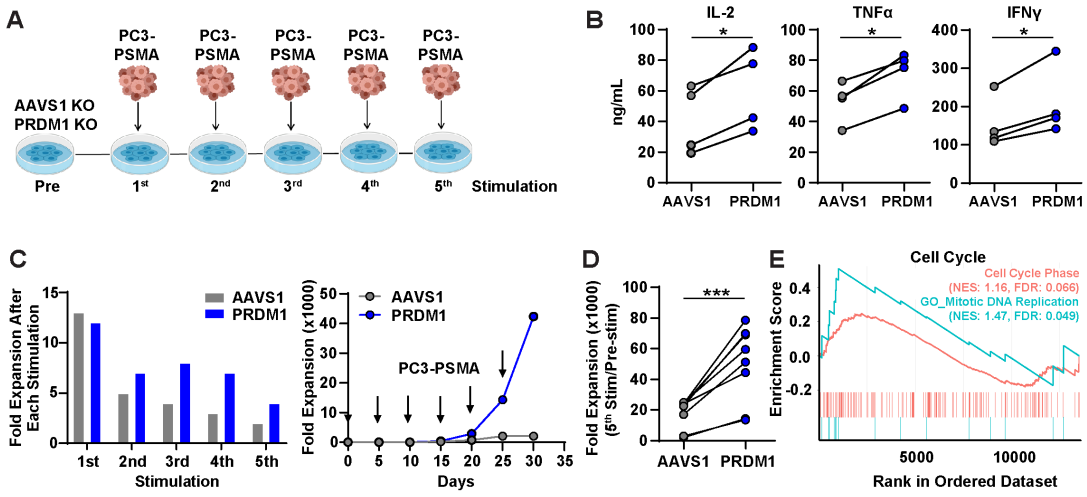

Figure 3.2 PRDM1 disruption enhances effector cytokine production and CAR T-cell proliferation.

(**A**) Schematic of the restimulation assay used to 'stress test' *PRDM1* KO PSMA CAR T-cells. CAR T-cells were challenged with PSMA-expressing PC3 prostate tumor targets every 4-5 days at an effector to target (E:T) ratio of 3:1. (**B**) Effector cytokines produced by CAR T-cells after initial tumor cell challenge. (**C**) Representative CAR T- cell expansion kinetics during restimulation assay from one donor. Left: CAR T-cell expansion after each stimulation, Right: Cumulative CAR T-cell expansion. Arrow indicates the timing of PC3-PSMA challenge. (**D**) Summary of the expansion capacity of *AAVS1* and *PRDM1* KO CAR T-cells during the restimulation assay with four different donors. (**E**) Gene set enrichment analysis (GSEA) of *PRDM1* KO versus *AAVS1* KO CAR T-cells comparing gene signatures related to the cell cycle and mitotic DNA replication. CAR-T samples were harvested on day 5 following the first tumor challenge. NES: normalized enrichment score, FDR: false discovery rate. All knockout and restimulation experiments were conducted with CAR T-cells manufactured from 4

different healthy donors. RNA-seq experiments were conducted with CAR T-cells manufactured from 2 different healthy subjects, each with replicates generated from two independent experiments. *$P < 0.05$, *$P < 0.01$, ***$P < 0.001$, n.s.: not significant (paired *t*-test).

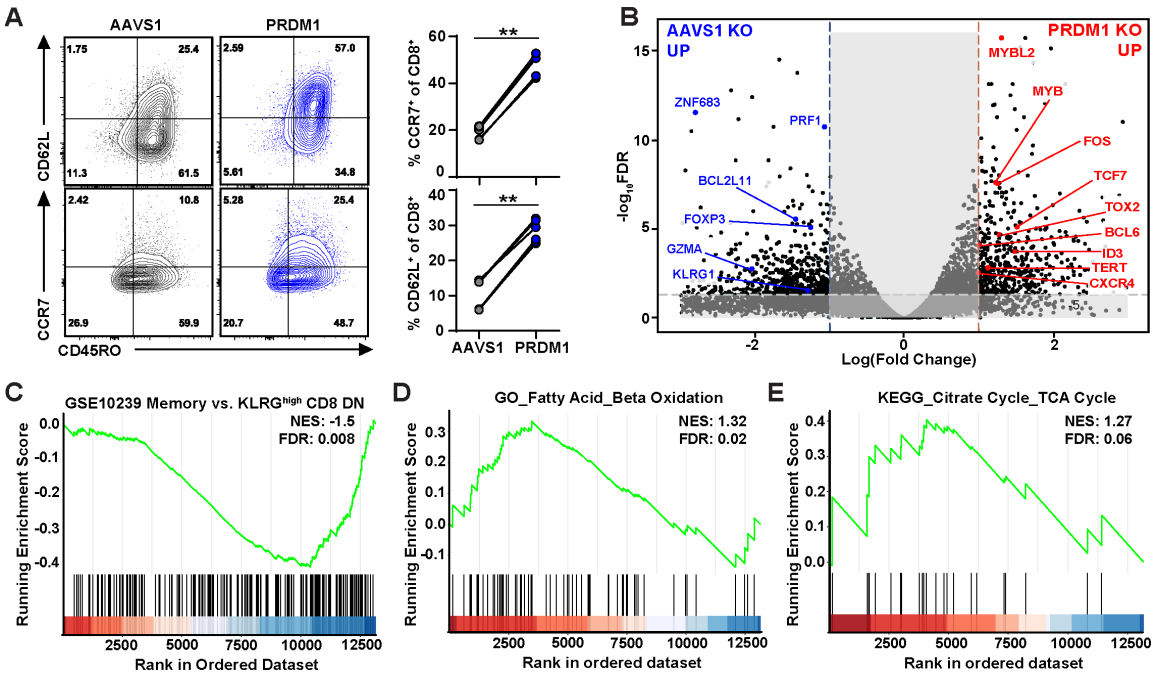

Figure 3.3 PRDM1 disruption enhances early memory differentiation of CAR T-cells.

CAR T-cells were challenged with PSMA-expressing PC3 prostate tumor targets every 4-5 days at an effector to target (E:T) ratio of 3:1. (**A**) Early memory marker expression measured by flow cytometry after two consecutive tumor challenges. (**B**) Volcano plot displaying the results of differential gene expression analysis when comparing *PRDM1* KO to control *AAVS1* KO CAR T-cells. (**C-E**) GSEA of *PRDM1* KO versus *AAVS1* KO CAR T-cells comparing gene sets associated with (**C**) memory T-cells (GSE10239), (**D**) GO_Fatty acid_Beta oxidation, and (**E**) KEGG_TCA cycle. NES: normalized enrichment score, FDR: false discovery rate. All knockout and restimulation experiments were conducted with CAR T-cells manufactured from 4 different healthy donors. RNA-seq experiments were conducted with CAR T-cells manufactured from 2 different healthy

subjects, each with replicates generated from two independent experiments. *$P < 0.05$, *$P < 0.01$, ***$P < 0.001$, n.s.: not significant (paired *t*-test).

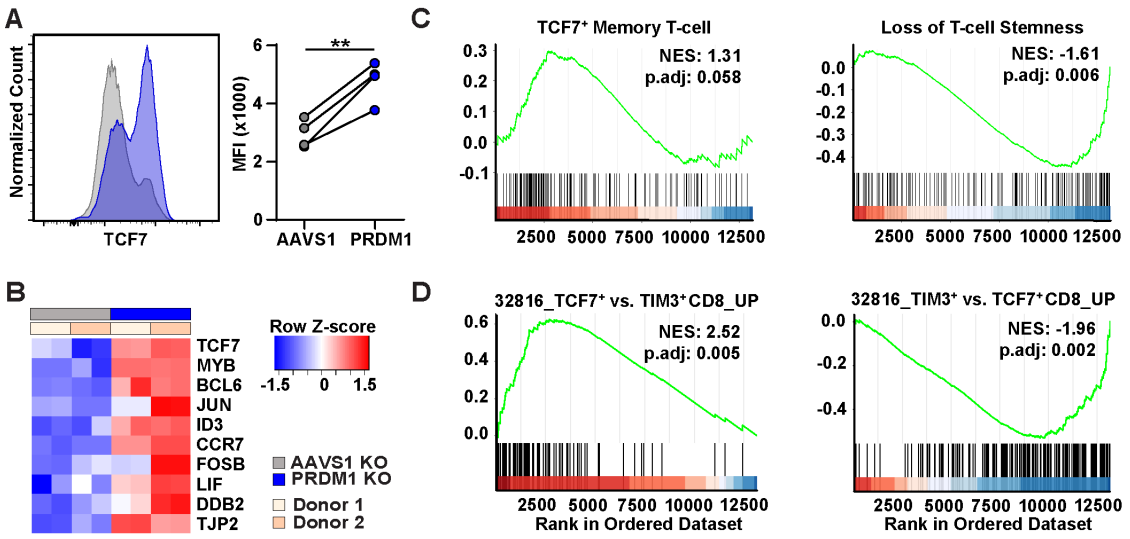

Figure 3.4 PRDM1 KO increases TCF7 expression and a TCF7+CD8+ T-cell stem-like memory signature.

(**A**) TCF7 expression level measured by flow cytometric analysis of *PRDM1* KO versus *AAVS1* KO CAR T-cells PSMA CAR T-cells derived from $n = 4$ different healthy subjects (two-tailed *t*-test). (**B**) Analysis of CAR T-cells for transcripts enriched in $TCF7^+$ stem cell-like T-cells observed in LCMV mouse models. (**C**) GSEA of *PRDM1* KO relative to *AAVS1* KO CAR T-cells comparing gene sets associated with a $TCF7^+$ T-cell memory state (GSE83978) and loss of stemness (GSE84105). NES: normalized enrichment score, FDR: false discovery rate. (**D**) GSEA of *PRDM1* KO versus *AAVS1* KO CAR T-cells evaluating gene sets enriched in $TCF7^+CD8^+$ (left) and $TIM3^+CD8^+$ clusters (right) observed in mCRPC patient CAR T-cell infusion products. NES: normalized enrichment score, FDR: false discovery rate. $*P < 0.05$, $*P < 0.01$, $***P < 0.001$, n.s.: not significant.

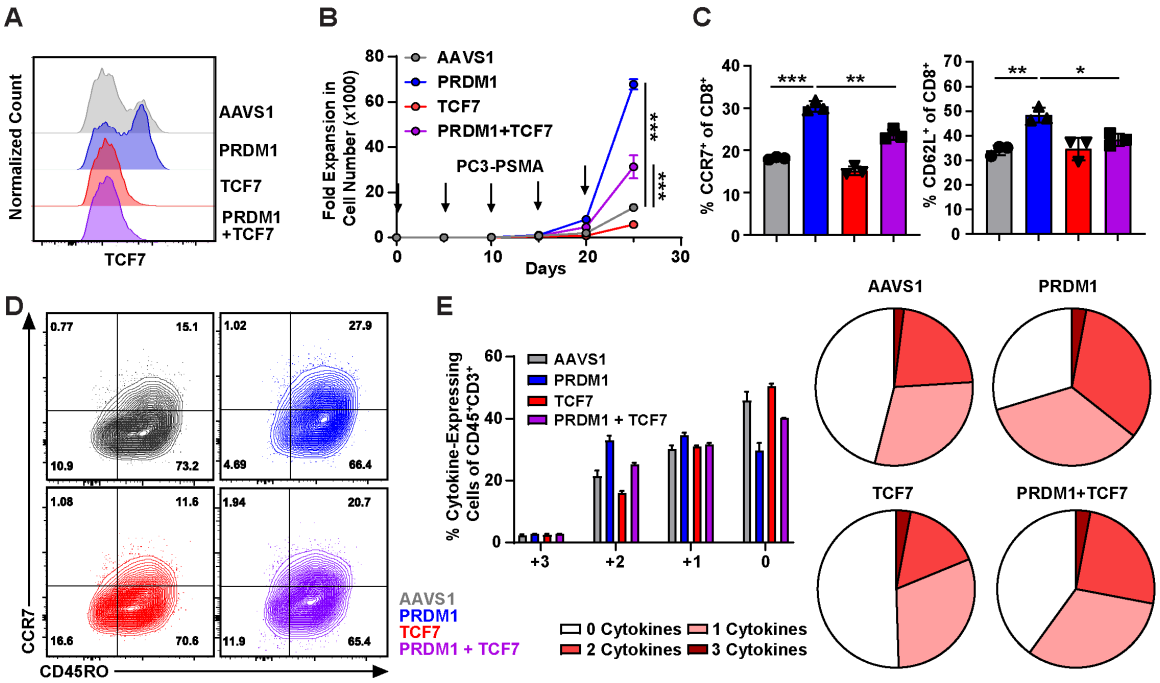

Figure 3.5 TCF7 preserves T-cell stemness and early memory differentiation of PRDM1 KO CAR T-cells.

(**A**) Representative histogram of flow cytometric TCF7 expression in *PRDM1* and *TCF7* KO variants. (**B**) Expansion kinetics during a restimulation assay of gene-edited CAR T-cells. CAR T-cells were challenged with PC3-PSMA target-cells every 5 days at an E:T of 3:1. Arrow indicates the timing of PC3-PSMA challenge. Data represent the mean ± S.D. (n = 3 independent experiments). (**C, D**) CCR7 and CD62L expression following the first *in vitro* tumor cell challenge. Data indicate mean ± S.D. from n = 3 independent experiments. (**E**) CAR T-cell polyfunctionality (IL-2, IFNγ and TNFα expression) evaluated after a 15-hour co-culture with PC3-PSMA cells. Data show mean ± S.D. from n = 3 independent experiments. *P < 0.05, *P < 0.01, ***P < 0.001, n.s.: not significant (**B, C:** two-tailed t-test).

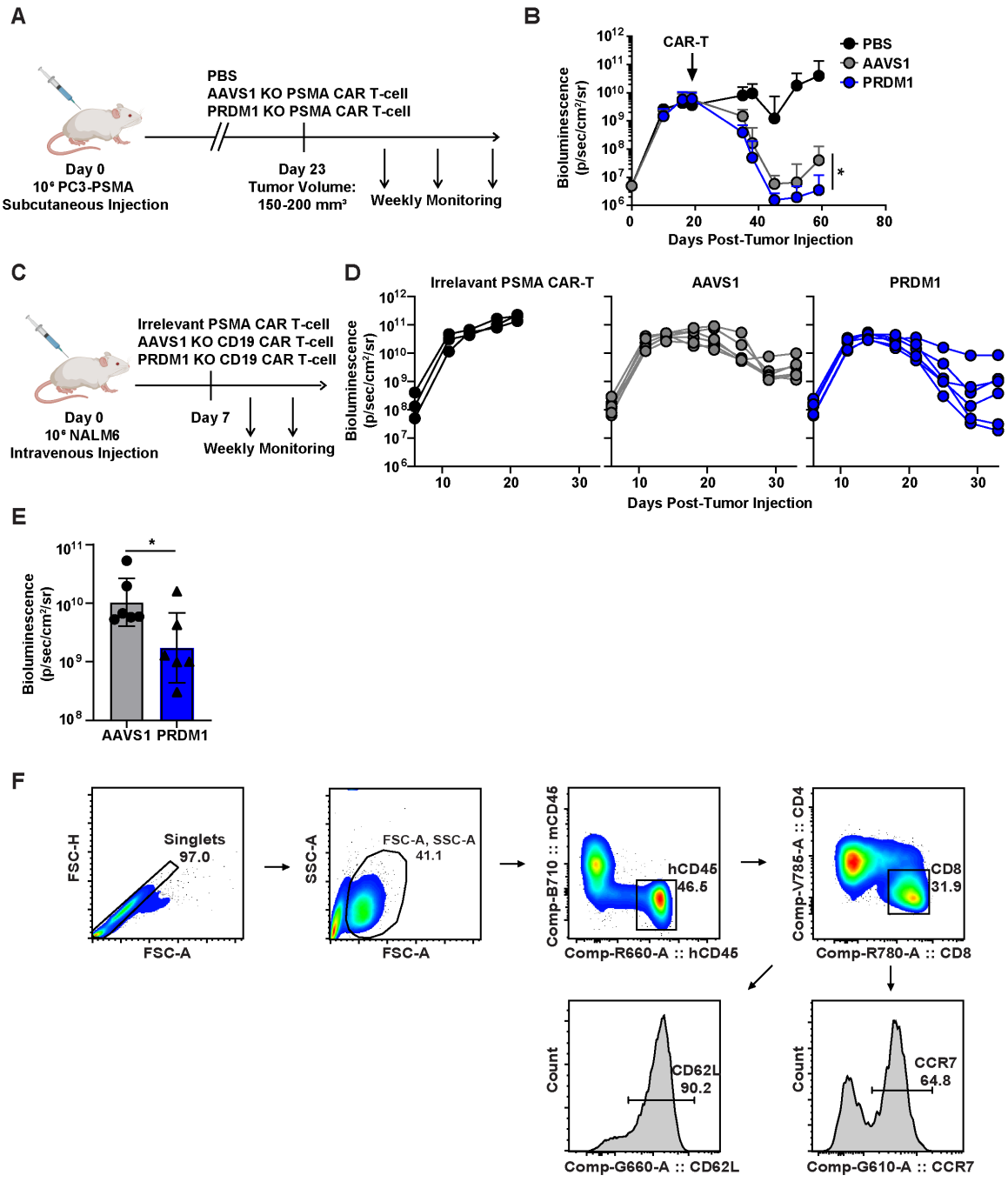
A
PBS
AAVS1 KO PSMA CAR T-cell
PRDM1 KO PSMA CAR T-cell
Day 0
10⁶ PC3-PSMA
Subcutaneous Injection
Day 23
Tumor Volume:
150-200 mm³
Weekly Monitoring
B
CAR-T
PBS
AAVS1
PRDM1
Bioluminescence (p/sec/cm²/sr)
Days Post-Tumor Injection
C
Irrelevant PSMA CAR T-cell
AAVS1 KO CD19 CAR T-cell
PRDM1 KO CD19 CAR T-cell
Day 0
10⁶ NALM6
Intravenous Injection
Day 7
Weekly Monitoring
D
Irrelavant PSMA CAR-T
AAVS1
PRDM1
Bioluminescence (p/sec/cm²/sr)
Days Post-Tumor Injection
E
Bioluminescence (p/sec/cm²/sr)
AAVS1 PRDM1
F
FSC-H
FSC-A
Singlets
97.0
SSC-A
FSC-A, SSC-A
41.1
Comp-B710 :: mCD45
Comp-R660-A :: hCD45
hCD45
46.5
Comp-V785-A :: CD4
Comp-R780-A :: CD8
CD8
31.9
Count
Comp-G660-A :: CD62L
CD62L
90.2
Comp-G610-A :: CCR7
CCR7
64.8

Figure 3.6 In vivo studies using prostate cancer and B-ALL xenogeneic mouse models to examine the antitumor potency of PRDM1 KO CAR T-cells.

(**A**) A schematic of the low tumor burden PC3-PSMA xenograft mouse model is shown. (**B**) Tumor burden monitored by bioluminescent imaging. Data depict geometric mean ± S.D.; $n = 6$, representative of two independent experiments. (**C**) A schematic of the NALM-6 xenograft model. Briefly, NSG mice were intravenously injected with 1×10^6 NALM6-CBG cells. 1×10^5 CD19 CAR T-cells and negative control, PSMA CAR T-cells, were treated 7 days post-tumor injection ($n = 6$) (**D**) NALM-6 B-ALL growth monitored by bioluminescent imaging. (**E**) Tumor burden on day 16 post CAR T-cell injection is shown. Data indicate the geometric mean ± S.D.; $n = 6$ (Mann Whitney U test). (**F**) Representative flow cytometry plots showing a gating strategy to characterize the immunophenotype of CAR T-cells in the peripheral blood. *$P < 0.05$, *$P < 0.01$, ***$P < 0.001$, n.s.: not significant.

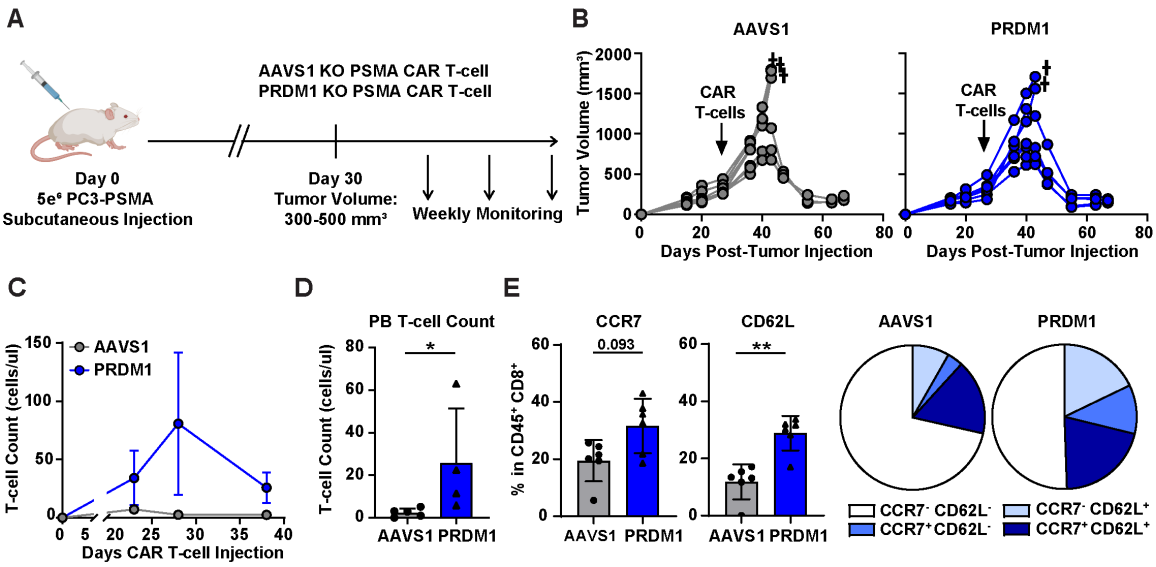

Figure 3.7 PRDM1 KO fails to improve solid tumor control despite significant increases in CAR T-cell proliferative capacity and persistence.

(**A**) A schematic of high tumor burden PC3-PSMA xenograft mouse model. Male NSG mice were subcutaneously transplanted with 5×10^6 PC3-PSMA cells, and 3.5×10^5 PSMA CAR T-cells were given intravenously when tumor volume reached ~500 mm3. (**B**) Tumor growth monitored by caliper measurements. † = death. (**C**) CAR-T expansion kinetics in the peripheral blood. (**D**) Absolute numbers of human T-cells in the peripheral blood on day 38 post-CAR T-cell injection. (**E**) Frequencies of peripheral blood CAR T-cells expressing CCR7 and CD62L, as measured by flow cytometry. Data are mean ± S.D.; n = 6 for figure B and E and n = 4-5 for figure C and D. *P < 0.05, *P < 0.01, ***P < 0.001, n.s.: not significant (Mann Whitney U test).

CHAPTER 4: Combinatorial *PRDM1* and *NR4A3* KO Renders CAR T-cells Resistant to Exhaustion.

Parts of this chapter were previously published in:

In-Young Jung, Vivek Narayan, Sierra McDonald, Andrew J. Rech, Robert Bartoszek, Gwanui Hong, Megan M. Davis, Jun Xu, Alina C. Boesteanu, Julie S. Barber-Rotenberg, Gabriela Plesa, Simon F. Lacey, Julie K. Jadlowsky, Donald L. Siegel, Dana M. Hammill, Prostate Cancer Cellular Therapy Program Investigators, Park F. Cho-Park, Shelley L. Berger, Naomi B. Haas, and Joseph A. Fraietta (2022) BLIMP1 and NR4A3 Transcription Factors Reciprocally Regulate Antitumor CAR T-cell Stemness and Exhaustion *Sci. Transl. Med.* (*In Revision*).

Abstract

PRDM1 single knockout CAR T-cells exhibited enrichment of the $TCF7^{+}CD8^{+}$ phenotype in association with significantly improved CAR T-cell persistence and expansion. However, genetic deletion of *PRDM1* alone resulted in only marginal enhancement of CAR T-cell efficacy against B-cell leukemia and completely failed to rescue the tumor control capacity of CAR T-cells in a high tumor burden solid tumor model. We found that during prolonged tumor antigen exposure, several exhaustion-related transcription factors, including Nuclear Receptor Subfamily 4 Group A Member 3 (*NR4A3*), were reciprocally upregulated in *PRDM1*-deficient CAR T-cells and drove epigenetically programmed T-cell dysfunction in an NFAT-dependent manner. *PRDM1* and *NR4A3* dual-ablation counteracted the development of T-cell exhaustion, which was

not observed with single KO of either gene. This strategy also led to a marked increase in the survival and expansion of TILs; increased the capacity of the CAR TILs to produce effector cytokines after stimulation; and reduced expression of cell-surface inhibitory receptors. In immunodeficient mice bearing soft tissue or bone engrafted prostate cancer cells, pancreatic cancer, and aggressive B-cell leukemia, a single intravenous infusion of *PRDM1*/*NR4A3* dual KO CAR T-cells resulted in higher antitumor efficacy, T-cell durability and overall prolongation of survival compared to conventional CAR T-cell treatment. Our identification of the reciprocal nature of BLIMP1 and NR4A3 activity as a novel mechanism regulating the balance of T-cell differentiation and exhaustion represents an actionable and therapeutically effective strategy for achieving desired therapeutic outcomes.

Introduction

T-cell exhaustion is a major barrier to effective CAR T-cell therapy. T-cell exhaustion induced by chronic CAR activation leads to upregulation of inhibitory receptors, poor polyfunctionality, effector function, and proliferation, which negatively affect anti-tumor activity of CAR T-cells in various cancers [4,27,76,77].

We previously demonstrated that *PRDM1* single knockout enriched stem-like $TCF7^{+}CD8^{+}$ CAR T-cells and enhanced CAR T-cell expansion and persistence. However, *PRDM1* KO CAR T-cells showed only marginal improvement in tumor control capacity in low tumor burden prostate cancer as well as B-cell leukemia xenograft models and a comparable level of antitumor efficacy against a high tumor burden *in vivo*. Together, these results suggest that despite significant improvements in expansion and persistence, *PRDM1* knockout alone is not sufficient to potentiate robust CAR T-cell antitumor efficacy in aggressive tumor models and that effector function of *PRDM1* KO CAR T-cells may not be optimally sustained during chronic activation in the TME.

Here we found that *PRDM1* KO CAR T-cells failed to maintain effector cytokine secretion and impair cytolytic activity during continuous tumor challenge. Mechanistically, deletion of *PRDM1* upregulates exhaustion-related transcription factors, including NR4A3, by increasing calcineurin-NFAT signaling and chromatin accessibility of *TOX* and *NR4A* families. Simultaneous disruption of *PRDM1* and *NR4A3* sustained substantially improved antitumor efficacy by reinvigorating the effector function of tumor-infiltrating CAR T-cells in multiple solid cancer models. Furthermore, *PRDM1*/*NR4A3* KO enhanced the memory recall response and induced durable antitumor

efficacy in blood cancer models. Altogether, these results indicate that BLIMP1 and NR4A3 reciprocally regulate CAR T-cell exhaustion and that *PRDM1*/*NR4A3* dual knockout is an actionable engineering strategy to achieve long-term CAR T-cell-mediated antitumor potency.

Results

PRDM1 KO hampers CAR T-cell effector function during chronic CAR stimulation.

To evaluate the effector functions of *PRDM1* KO CAR T-cells in the setting of repetitive antigen exposure, we first assessed cytokine levels 24-hours after the first and fifth rounds of *in vitro* PC3-PSMA tumor cell stimulation. *PRDM1* KO initially increased effector cytokine production as shown in **Figure 3.2B** and **Figure 4.1A**. However, after multiple tumor antigen challenges, *PRDM1* KO CAR T-cells exhibited impaired effector cytokine production (**Figure 4.1A**), despite inhibitory receptor downregulation (**Figure 4.1B**). Indeed, PRDM1 KO CAR T-cells dramatically reduced cytokine production to a similar degree as control CAR T-cells, indicating that regulation of inhibitory receptor expression is decoupled from effector cytokine elaboration during chronic stimulation (**Figure 4.1A**). Further, after five consecutive tumor challenges, the cytolytic activity of PRDM1 KO CAR T-cells was impaired compared to that of control CAR T-cells (**Figure 4.1C**). This result is consistent with a previous study in which PRDM1 deficiency profoundly compromised the cytotoxic activity of antigen-specific $CD8^+$ T-cells during chronic viral infection (32).

PRDM1 KO CAR T-cells fail to maintain high effector function due to upregulation of exhaustion-related transcription factors.

To elucidate the mechanism by which PRDM1 KO CAR T-cells fail to maintain effector function following chronic antigen stimulation, we performed bulk RNA-seq on CAR T-cells harvested after several rounds of tumor challenge. We observed that

PRDM1 KO increased the expression of early memory-related genes, including MYB, LEF, CCR7, IL7R, and CD28, even after multiple stimulations (**Figure 4.2A**). Intriguingly, together with these early memory-related genes, PRDM1 KO resulted in upregulation of genes encoding multiple exhaustion-related TFs such as the NR4A family of TFs, TOX, TOX2, and IRF4 (**Figure 4.2B**, **left**). To rule out potential model-dependent effects, we took advantage of a publicly available RNA sequencing expression dataset of CD8+ TILs from B16F10 (melanoma) tumor-bearing PRDM1 conditional knockout (cKO) syngeneic mice. Concordant with our findings in CAR T-cells, PRDM1 cKO CD8+ TILs exhibited upregulated expression of NR4A3, NR4A1, and IRF4 compared to wild type counterparts (**Figure 4.2B**, **right**).

Combinatorial *PRDM1* and *NR4A3* KO sustains the effector function of chronically stimulated CAR T-cells.

We hypothesized that the observed compensatory upregulation of exhaustion-associated TF genes can limit the effector function of *PRDM1* KO CAR T-cells during chronic stimulation and that deletion of these exhaustion factors will render *PRDM1* KO CAR T-cells capable of maintaining antitumor effector function. Because *NR4A3* was the most significantly upregulated exhaustion-related TF gene examined in *PRDM1* KO CAR T-cells after multiple episodes of antigen stimulation (**Figure 4.2B, left**) and *NR4A3* is significantly elevated in hypofunctional NR/PR CLL patient CD19 CAR T-cells (**Figure 4.2C**), we next knocked out both *NR4A3* and *PRDM1* (**Figure 4.3A**) and functionally characterized the gene-edited CAR T-cells. We observed that while *NR4A3* single KO CAR T-cells exhibited a similar expansion level as control CAR T-cells,

PRDM1/*NR4A3* dual knockout CAR T-cells exhibited the highest level of antigen-induced proliferative capacity (**Figure 4.3B**). *PRDM1*/*NR4A3* KO CAR T-cells exhibited increased frequencies of CCR7, CD62L, and TCF1 (encoded by *TCF7*) expressing CD8 T-cells compared to *PRDM1* single KO CAR T-cells (**Figure 4.4A, B**). Because $CD4^+$ CAR T-cells are important to antitumor efficacy [125,126], we also determined the impact of the various knockouts on $CD4^+$ CAR T-cells with respect to differentiation phenotypes, as well as cytotoxic molecule expression during the aforementioned *in vitro* stress tests. Similar to $CD8^+$ CAR T-cells, *PRDM1* KO increased frequencies of $CD4^+$ CAR T-cells expressing early memory markers such as CCR7 and TCF1 (**Figure 4.4C**).

Next, we assessed effector functions in the context of *PRDM1*/*NR4A3* KO and found that *PRDM1*/*NR4A3* KO CAR T-cells maintained elevated levels of effector cytokine production after multiple tumor challenges, whereas *PRDM1* and *NR4A3* single KO CAR T-cells showed similar IL-2 and TNFα secretion levels as control CAR T-cells (**Figure 4.3C, D**). This potency enhancement conferred by *PRDM1* and *NR4A3* dual KO was consistent in the context of both high and low PSMA expression (**Figure 4.5A, B**). Furthermore, unlike *PRDM1* single KO CAR T-cells which lost cytotoxic function following serial stimulation, *PRDM1*/*NR4A3* KO CAR T-cells displayed sustained killing activity over time (**Figure 4.3E, F**). This partially restored cytotoxic function of *PRDM1/NR4A3* KO CAR T-cells is attributed to increased expression levels of perforin and granzyme in both CD4+ and $CD8^+CAR^+$ T-cells (**Figure 4.3G and Figure 4.4D**).

To determine whether *PRDM1*/*NR4A3* KO CAR T-cells exhibit aberrant growth patterns, potential indicative of transformation, we tested whether there is antigen-independent growth in *PRDM1/NR4A3* KO CAR T-cells using PC3 cells with and

without PSMA expression as stimuli. Notably, we observed that *PRDM1/NR4A3* KO CAR T-cells fail to expand, accompanied by a reduction in viability when co-cultured with PSMA-negative PC3 cells, suggesting that-cell expansion and survival are antigen-dependent (**Figure 4.3H**).

Upregulation of exhaustion-related TFs in *PRDM1* KO CAR T-cells is attributed to increased chromatin accessibility and calcineurin-NFAT signaling.

We next sought to investigate the mechanism of exhaustion-associated TF upregulation in *PRDM1* KO CAR T-cells. Emerging evidence indicates that *PRDM1* epigenetically regulates transcription of memory-related genes by directly binding to their promoter regions and recruiting histone modifiers[127]. We therefore investigated whether *PRDM1* KO affects the chromatin accessibility of exhaustion-related TF genes by performing ATAC-seq on control and *PRDM1* KO CAR T-cells. *PRDM1* KO significantly increased global chromatin accessibility (**Figure 4.6A**). Transcription motif enrichment analysis revealed that a *PRDM1* motif was one of the most significantly enriched TF binding sites in *PRDM1* KO CAR T-cells (**Figure 4.6B-C**), suggesting that *PRDM1* can act as an epigenetic repressor. Consistent with previous chromatin immunoprecipitation sequencing (ChIP-seq) results[127], *PRDM1* KO increased chromatin accessibility at loci corresponding to early memory and stemness genes such as *TCF7*, *CD28*, *CCR7*, *SELL*, and *MYB* (**Figure 4.7**). Notably, we found that even before tumor challenge, *PRDM1* KO significantly increased chromatin accessibility at exhaustion-related TF regions, including *TOX*, *TOX2*, and *NR4A3*, and that a subset of these open

regions colocalized with the above *PRDM1* motif (**Figure 4.6D**). These observations indicate that *PRDM1* contributes to epigenetic repression of a battery of exhaustion-associated TFs, and that *PRDM1* KO CAR T-cells are predisposed to upregulate exhaustion-associated TFs.

Given that CAR T-cell dysfunction can be induced by prolonged exposure to cancer cells due to low cytotoxic activity[128], we investigated how the impaired cytotoxicity of *PRDM1* KO CAR T-cells affects regulation of exhaustion-associated TFs. *PRDM1* KO CAR T-cells downregulated Granzyme B and Perforin levels (**Figure 4.8A**). This decrease in cytotoxic proteins led to delayed tumor clearance, which caused *PRDM1* KO CAR T-cells to be exposed to target cancer cells twice as long as control CAR T-cells (**Figure 4.8B, C**). Due to prolonged exposure to cancer cells, *PRDM1* KO increased expression of NFAT2 (**Figure 4.8D**). As TOX and NR4A TF families are induced by calcineurin-NFAT signaling, we used the FK506 calcineurin inhibitor to examine the involvement of NFAT in exhaustion-related TF upregulation in *PRDM1* KO CAR T-cells [129,130]. FK506 treatment either completely or partially counteracted *PRDM1* KO-mediated upregulation of TOX, NR4A2, and NR4A3 during restimulation, suggesting that *PRDM1* KO may induce upregulation of exhaustion-associated TFs via increased NFAT signaling (**Figure 4.8E-G**).

***PRDM1*/*NR4A3* dual KO enhances in vivo CAR T-cell antitumor activity by preserving TCF1$^+$ CD8 T-cells and increasing effector function.**

Based on the observation that *PRDM1/NR4A3* dual KO sustains the proliferative ability, effector functions and early memory phenotype of CAR T-cells, we next examined whether *PRDM1/NR4A3* KO CAR T-cells would elicit enhanced antitumor activity *in vivo*. While *AAVS1*, *PRDM1*, and *NR4A3* single KO CAR T-cells controlled tumor growth in ~50% of mice in the high-burden PC3-PSMA cell xenograft model, *PRDM1/NR4A3* double KO CAR T-cells successfully suppressed tumor growth in all treated mice, in association with overall prolongation of survival (**Figure 4.9A, B**). Because advanced prostate cancer commonly progresses within two years following the initiation of androgen-ablative therapy often with osseous in addition to visceral metastases, we also tested our approach in an intraosseous PC3-PSMA prostate tumor model. Bioluminescent tumor burden was also significantly decreased by a single infusion of *PRDM1/NR4A3* KO PSMA CAR T-cells compared to *PRDM1* and *NR4A3* single KO as well as *AAVS1* KO CAR T-cells in mice bearing intraosseous tumors generated by PC3-PSMA cell engraftment (**Figure 4.9C**). We subsequently collected tumor and blood samples to characterize the immunophenotype of CAR T-cells. We found that both *PRDM1* single KO and *PRDM1/NR4A3* double KO significantly increased the absolute numbers of CAR T-cells in the tumor and peripheral blood (**Figure 4.10A**). This increased T-cell number may be due in part to the elevated frequencies of early memory T-cells with optimal proliferative potential observed with *PRDM1* KO (**Figure 4.10B**), which is consistent with our previous results. To investigate how *PRDM1* and *NR4A3* depletion affect T-cell dysfunction, we first evaluated the frequencies of inhibitory receptor-expressing CAR T-cells. While *PRDM1* single KO CAR T-cells demonstrated reduced PD-1, TIM-3 and LAG-3 expression in the peripheral

blood, their inhibitory receptor expression was comparable to *AAVS1* KO CAR T-cells in the tumor where CAR T-cells receive persistent antigen stimulation (**Figure 4.10C-E**). In contrast, *PRDM1/NR4A3* KO CAR T-cells demonstrated a significant reduction in the proportion of $PD1^{+}TIM3^{+}$ CD8 T-cells in both the tumor and peripheral blood (**Figure 4.10C, D**). Also, as observed *in vitro*, *PRDM1* KO led to substantial increase in TCF1 (encoded by *TCF7*) expression in CAR T-cells *in vivo*. Both *PRDM1* single KO and *PRDM1/NR4A3* double KO CAR T-cells exhibited increased stem cell-like $TIM3^{-}TCF1^{+}$ CD8 T-cells[46] in the tumor and peripheral blood, although only *PRDM1/NR4A3* KO CAR T-cells showed a substantial decrease in the frequencies of $TIM3^{+}TCF1^{-}$ exhausted T-cells in the tumor (**Figure 4.10F-H)**.

To investigate whether *PRDM1/NR4A3* dual KO enhances CAR TIL effector function, we reactivated these TILs *ex vivo* and assessed intracellular cytokine production. Consistent with our *in vitro* results displayed in **Figure 4.3C, D**, *PRDM1* or *NR4A3* single KO failed to improve effector cytokine production, whereas *PRDM1/NR4A3* double KO CAR T-cells maintained higher polyfunctionality compared control CAR T-cells (**Figure 4.10 I-L**).

We also assessed the efficacy of *PRDM1* and *NR4A3* single KO or *PRDM1/NR4A3* double KO mesothelin-directed CAR T-cells in an *in vivo* model of highly resistant pancreatic adenocarcinoma, with AsPC1 tumor cells expressing endogenous levels of mesothelin (**Figure 4.11A**). In this study, only *PRDM1/NR4A3* double knockout anti-mesothelin CAR T-cells mediated a significant reduction in tumor burden over time (**Figure 4.11B**).

Further, we examined the antitumor activity of *PRDM1/NR4A3* KO CAR T-cells in the NALM-6 B-ALL model (**Figure 4.12A**). Similar to the results obtained from the PC3-PSMA model, *NR4A3* single KO CD19 CAR T-cells failed to suppress tumor growth. *PRDM1* single KO moderately enhanced tumor control and survival (**Figure 4.12B-D**). However, when *PRDM1* KO was combined with *NR4A3* KO, CAR T-cells induced rapid tumor clearance and durable antitumor efficacy (**Figure 4.12B-D**).

Additionally, in association with robust antitumor activity (**Figure 4.12D**), we found that *PRDM1/NR4A3* KO enhanced CD19 CAR T-cell expansion as well as central memory T-cell differentiation and reduced proportions of peripheral blood CAR T-cells co-expressing multiple inhibitory receptors (**Figure 4.12E-H**). To evaluate the durability of *PRDM1/NR4A3* double KO CAR T-cell therapeutic efficacy, we conducted a study in which CAR T-cell-treated NSG mice were rechallenged with NALM-6 cells 40 days after the initial leukemia cell transfer (**Figure 4.13A**). Because of the aggressive nature of this model, we administered a relatively high dose of CAR T-cells across all groups during the primary challenge to ensure initial tumor clearance. As shown in **Figure 4.13B**, PRDM1/NR4A3 dual KO CAR T-cells demonstrated better control of tumor growth than control CAR T-cells following rechallenge. These collective findings suggest that *PRDM1* depletion increases CAR T-cell expansion and mitigates dysfunction by increasing frequencies of $TCF7^{+}CD8^{+}$ T-cells and skewing fate away from the $TIM3^{+}CD8^{+}$ state. *NR4A3* KO rescues the *in vivo* potency-enhancing effect of *PRDM1* KO on CAR T-cell function by reducing exhaustion and inducing durable effector activity.

Discussion

Although single deletion of *PRDM1* favorably modulates CAR T-cell differentiation fate, antitumor effector activity is ultimately hampered by this modification in the setting of chronic antigen exposure. *PRDM1* regulates $CD8^+$ T-cell effector function and is required for granzyme B expression[108,109]. In acute LCMV infection, despite a significant reduction in cytotoxic molecule production, the cytolytic activity of virus-specific PRDM1 KO $CD8^+$ T-cells was marginally affected and both wild-type and *PRDM1* KO $CD8^+$ T-cells successfully cleared the infection[108]. However, in chronic LCMV infection, the killing activity of LCMV-directed *PRDM1* KO $CD8^+$ T-cells is significantly impaired, suggesting that loss of *PRDM1* can profoundly compromise cytotoxicity in the setting of exhaustion where the cytolytic potential of antigen-specific $CD8^+$ T-cells is relatively low[109]. Consistent with these previous studies, the cytotoxic capacity and effector cytokine production of *PRDM1* KO CAR T-cells were substantially compromised compared to conventional CAR T-cells after multiple rounds of tumor antigen exposure. In accordance with these findings, despite profound increase in expansion capacity, *PRDM1* KO CAR T-cells marginally enhanced antitumor activity over control CAR T-cells in xenogeneic murine models of prostate cancer and aggressive B-cell leukemia, and ultimately became progressively dysfunctional due to exacerbated loss of effector activity. The marginally enhanced tumor control observed with this single modification may be attributed to the large increase in the number of *PRDM1* KO CAR T-cells *in vivo*, despite upregulation of exhaustion pathways and concomitantly diminished effector function.

Until now, *PRDM1* was presumed to induce exhaustion modules in antigen-specific T-cells[109]. Lower frequencies of peripheral blood *PRDM1* KO PSMA CAR T-cells but not CAR TILs co-expressed multiple inhibitory receptors, suggesting that reduction of co-inhibitory receptor expression in *PRDM1*-deficient CAR T-cells was insufficient to promote effective antitumor immunity. We therefore examined whether other TFs may regulate the exhaustion module and compensate for the absence of *PRDM1*. Unexpectedly, we discovered for the first time to our knowledge that *PRDM1* KO CAR T-cells chronically challenged with tumor targets display upregulation of a battery of exhaustion-associated TFs, including those belonging to the NR4A and TOX families which are reported to drive a cell-intrinsic program of T-cell hyporesponsiveness[74]. These findings suggest that in the setting of *PRDM1* deletion, expression of certain inhibitory receptors and genes encoding exhaustion-related TFs are decoupled and the downregulation of specific inhibitor receptors may instead be reflective of changes to the activation or differentiation state of CAR T-cells.

T-cells in cancer and chronic viral infection differentiate into effector or exhausted T-cells, in association with global and site-specific changes to the epigenetic landscape, including TF binding sites[26,58,78]. Indeed, *PRDM1* KO increased accessibility of many exhaustion-related chromatin regions (e.g., NR4A3 TOX, TOX2) that normally become accessible in $CD8^+$ TILs[76], a number of these open regions colocalized with a *PRDM1* binding motif, suggesting that *PRDM1* may be acting as a transcriptional repressor. In addition to epigenetic regulation, *PRDM1* KO increased calcineurin/NFAT signaling, which is necessary and sufficient to induce exhaustion-related TF expression[129,130]. This increased NFAT signaling may be attributed to prolonged exposure

of *PRDM1* KO CAR T-cells to cancer cells in association with the delayed killing kinetics we demonstrated. Thus, our findings suggest that *PRDM1* can suppress expression of exhaustion TFs by directly or indirectly regulating transcriptional and epigenetic reprogramming as well as the killing activity of CAR T-cells.

In summary, this study provides a framework for developing the next-generation of 'best-in-class' CAR T-cells by identifying cellular and molecular characteristics associated with clinical response and engineering CAR T-cells to enrich desirable as well as reduce undesirable cell populations in infusion products. Our work also highlights the fundamental role of *PRDM1* in the regulation of human T-cell memory and provides a deeper understanding of how *PRDM1* mediates T-cell exhaustion (**Figure 4.14**). Additional experiments will be required to completely reveal the transcriptional networks involved. Combined disruption of *PRDM1* and *NR4A3* expression or activity has the direct potential to generate genetically reprogrammed T-cells capable of augmenting both immediate and long-term antitumor responses, since this strategy potentiates the formation of long-lived memory cells resistant to exhaustion imposed by tumors.

Materials and Methods

Primary human samples

Peripheral blood mononuclear cells (PBMC) were collected for small-scale CAR T-cell production via leukapheresis from healthy subjects. Study participants provided written informed consent according to the Declaration of Helsinki and the International Conference on Harmonization Guidelines for Good Clinical Practice.

Cell lines

PC3, PSMA-expressing PC3, and NALM-6 cells engineered to express click beetle green luciferase and green fluorescent protein (CBG-GFP), were kindly provided by Carl H. June and Marco Ruella (University of Pennsylvania), respectively. AsPC1 cells were obtained from the American Type Culture Collection (ATCC). PC3 and PC3-PSMA cells were cultured in Dulbecco's Modified Eagle Medium (DMEM) supplemented with 10% fetus bovine serum (FBS) and streptomycin/penicillin. NALM-6 and AsPC1 cells were maintained in Roswell Park Memorial Institute (RPMI) 1640 media supplemented with 10% fetus bovine serum (FBS) and streptomycin/penicillin (R10 media). HEK 293T-cells, used for lentivirus production, were obtained from ATCC and cultured in R10 media. Low-passage banks of cells were tested for mycoplasma with a MycoAlert kit (Lonza), according to the manufacturer’s instructions. Authentication of cell lines was carried out by the University of Arizona Genetics Core, based on criteria established by the International Cell Line Authentication Committee. Short-tandem-

repeat profiling revealed that these cell lines were above the 80% match threshold. Mycoplasma testing and authentication were routinely performed before and after molecular engineering.

Lentivirus production

Vector construction and lentiviral production were conducted as previously described[122]. In brief, CARs comprised of anti-PSMA[122], anti-CD19[123], or anti-Mesothelin[131] single-chain variable fragments (scFv) fused to 4-1BB and CD3ζ stimulatory endodomains were subcloned into the pTRPE vector. Lentivirus supernatant was collected from 293T-cells transfected with the pTRPE transfer vector and packaging plasmids using Lipofectamine 2000 (Thermo Fisher Scientific) and concentrated using ultracentrifugation.

Lentiviral transduction and T-cell culture

Healthy donor T-cells were isolated from peripheral blood mononuclear cells (PBMC) using the Pan T-cell Isolation Kit according to the manufacturer's instructions (Miltenyi Biotec). T-cells were activated with anti-CD3/CD28 antibody coated Dynabeads (Thermo Fisher Scientific) at 3:1 bead:cell ratio in T-cell media (OpTmizer CTS SFM media (Gibco) supplemented with 5% human AB serum and 100u/mL human IL-2). Following a 24-hour incubation, lentivirus encoding the PSMA CAR was added to

the culture at a multiplicity of infection (MOI) of 2.5. CAR T-cell expansion was carried out as previously described[122].

CRISPR/Cas9-mediated gene editing

Following T-cell activation as described above, beads were removed using a magnet on day 3 and electroporation was carried out with a P3 primary cell 4D-nucleofector kit (Lonza). 2×10^6 CAR T-cells were transfected with 12 μg TrueCut™ S. pyogenes Cas9 (Invitrogen) and 0.2nmol of chemically-modified tracrRNA and crRNA (Integrated DNA Technologies). Following electroporation, CAR T-cells were cultured in T-cell media. The crRNA sequences used in this study were: AAVS1: 5'-CCATCGTAAGCAAACCTTAG-3', PRDM1: 5'-CATCAGCACCAGAATCCCAG-3', NR4A3: 5'-CCTTGGCAGCACTGAGATCA-3'. The frequency of targeted mutations generated by double strand break were determined by Sanger sequencing and subsequent TIDE (tracking of indels by decomposition) analysis. Primers used for targeted amplification were: PRDM1-F1: tctcagaaggagccacaggaacgg, PRDM1-R1: cacccaccctatgctgcaagttgc, NR4A3-F1: gaggagaggatgacacttcctctctgtttc, NR4A3-R1: ctgcccagcacctccatgtacttcaagcag. Western blot and flow cytometric analysis were conducted to confirm KO at the protein level.

Western blot analysis

T-cells (1×10^6 cells) were suspended in a low-salt lysis buffer (10 mM HEPES, pH 7.9, 10 mM KCl, 0.1 mM EDTA, 0.1 mM EGTA, 1 mM DTT, 0.5 mM PMSF, 2 μg/ml aprotinin, 2 μg/ml leupeptin) and allowed to swell on ice for 30 minutes. After centrifugation (1000 × g), supernatants obtained from cells lysates (30 μg) were analyzed by 10% SDS-polyacrylamide gel electrophoresis and electrophoretically transferred to PVDF membranes (Millipore). The membranes were washed with PBS containing 0.1% Tween 20 (PBST), and then blocked for 1-hour in 5% skim milk in PBST. After washing with PBST, membranes were incubated overnight with one of the following antibodies: Mouse monoclonal anti-β-Tubulin (Sigma-Aldrich #T8318; 1:100) or rabbit monoclonal anti-Blimp1 (Cell Signaling #9115; 1:100) or mouse monoclonal anti-NR4A3 (Sigma-Aldrich #SAB1404566; 1:100). Membranes were washed with PBST and treated with 1:1000 diluted horseradish peroxidase-coupled goat anti-mouse or anti-rabbit secondary antibodies (Thermo Fisher Scientific) in PBST for 1-hour. After washing, the membranes were incubated in Pierce™ ECL western blotting substrate (Thermo Fisher Scientific) and visualized on X-ray film.

Flow cytometry

Cell surface anti-human antibodies were diluted in FACS buffer (PBS + 2% FBS). PSMA CAR expression was measured using an allophycocyanin (APC)-conjugated recombinant human PSMA protein (Sino Biological). T-cell immunophenotyping was carried out using the following antibodies: PD1-BV421

(Biolegend #329920), CD45-BV570 (Biolegend #304226), CD8-BV650 (Biolegend #301042), CD8-APC-H7 (BD Biosciences #560179), CD4-BV785 (Biolegend #317442), TIM3-PE (Biolegend #345006), CCR7-PE-CF594 (BD Biosciences #562381), CD62L-PE-Cy5 (Biolegend #304808), LAG3-PE-Cy7(eBioscience #25-2239-42), hCD45-APC (BD Biosciences #340943), murine CD45-PerCP-Cy5.5 (Biolegend #103132), CD127-BV570 (Biolegend #351307), HLA-DR-Alexa Fluor700 (Biolegend #307625), CD25-APC (ebioscience #17-0259-42). For intracellular staining, cells were first permeabilized and washed using the FoxP3 Transcription Factor Staining Buffer Kit (eBioscience) and subsequently stained with following antibodies: IL2-PE-CF594 (BD Biosciences #562384), IFNγ-BV570 (Biolegend #502534), TNFα- Alexa Fluor700 (Biolegend #502928), Perforin-BV421 (Biolegend # 353307), Perforin-APC (Biolegend #308112), GZMB-PE-Cy5.5 (Invitrogen #GRB18), TCF1- Alexa Fluor488 (Cell Signaling Technology #6444S), TOX-APC (Miltenyi Biotech #130-107-785), NFATC1-PE (Biolegend #649606) according to our previously published methods [22]. Samples were then analyzed using an LSRFortessa (BD Biosciences), FlowJo software (FlowJo, LLC) and/or FCS Express (De Novo Software).

CAR T-cell restimulation assay

CAR T-cell expansion capacity and effector function were assessed using a restimulation assay, as previously described [22,122,124]. Briefly, AAVS1 KO, PRDM1 KO, NR4A3 KO, PRDM1 + NR4A3 dKO PSMA CAR-positive T-cells were isolated using a Biotin-goat anti-mouse IgG F(ab)2 fragment (Jackson ImmunoResearch #115-065-072)

and anti-biotin kits (Miltenyi Biotech). Following isolation, CAR T-cell purity was confirmed by flow cytometric analysis and CAR T-cells were then serially exposed (i.e., every 2-5 days) to irradiated PC3-PSMA cells at an effector-to-target (E:T) ratio of 3:1 or 1:1. Restimulation assays were carried out for 25-30 days, since cell counts become largely unreliable beyond the fifth and sixth rounds of stimulation due to senescent proliferative arrest and a marked decrease in the viability of chronically stimulated CAR T-cells. Supernatants were collected 24-hours post-tumor challenge for cytokine analysis using the LEGENDplex™ human CD8 panel (Biolegend), and absolute numbers of T-cells in culture were monitored using a Luna automated cell counter (Logos Biosystems) during the assay.

Cytotoxicity assay

The longitudinal killing capacity of engineered CAR T-cells against PC3-PSMA cells was assessed using the xCELLigence system (ACEA Biosciences Inc.). CAR-expressing T-cells were magnetically enriched prior to the cytotoxicity assay. 2×10^4 PC3-PSMA cells were seeded in E-Plate VIEW 96 PET microwell plates. After 24-hours, PSMA CAR T-cells or control (untransduced) T-cells were added to wells containing tumor targets to achieve the desired E:T ratios. 20% Tween20 was added to separate wells consisting of PC3-PSMA cells alone as a full lysis control. Electrical impedance was monitored in 20-minute intervals over 7 days and cytotoxicity was assessed by calculating the normalized cell index and % cytolysis.

Quantitative real-time PCR

After 2-4 rounds of restimulation, $CD8^+$ CAR T-cells were isolated from culture using CD8 microbeads (Miltenyi Biotech) for qRT-PCR. First, total RNA was extracted from $CD8^+$ CAR T-cells using RNA Clean & Concentrator™ kits (Zymo Research). cDNA was then synthesized using the PrimeScript 1st strand cDNA Synthesis Kit (Takara Bio) as per the manufacturer's protocol and qRT-PCR was conducted using Applied Biosystems TaqMan Fast Advanced Master Mix (Thermo Fisher Scientific) on the QuantStudio3 (Applied Biosystems). The primer/probe sets used for these experiments were as follows: CD3E: Hs01062241_m1, NR4A2: Hs00428691_m1 and NR4A3: Hs00545009_g1 (Thermo Fisher Scientific).

Mouse xenograft studies

Mouse studies were performed with 6- to 8-week-old male NOD/SCID/IL-2Rγ-null (NSG) mice in compliance with a University of Pennsylvania Institutional Animal Care and Use Committee approved protocol. For the subcutaneous PC3-PSMA model, 10^6 or 5×10^6 PC3-PSMA-CBG-GFP tumor cells were premixed with Matrigel (Corning) and injected into the flanks of NSG mice. When the average tumor size reached 150-200 mm^3 or 500 mm^3, 3.5×10^5 PSMA CAR T-cells were injected intravenously. Tumor growth weekly monitored weekly by taking caliper measurements (tumor volume = (length × $width^2$)/2). Animals were sacrificed when tumor volume exceeded 1500 mm^3 or

2 cm in diameter. For the intraosseous PC3-PSMA model, male NSG mice were intrafemorally transplanted with 2×10^5 PC3-PSMA cells. On day 27, 1-2 $\times 10^5$ PSMA CAR T-cells were infused intravenously, and tumor burden was measured by bioluminescent imaging. To characterize CAR T-cell phenotype and function, peripheral blood and tumor tissues were isolated from mice. Blood samples were obtained at peak CAR T-cell expansion via cheek bleeding. Tumors isolated on day 13 post-CAR T-cell injection, were minced with a scalpel and treated with 100 U/mL collagenase IV and 0.25mg/mL DNase I for 1-hour at 37℃. The absolute number of human T-cells in the peripheral blood and tumors was quantified using 123count eBeads (Thermo Fisher Scientific). To assess the effector function of TILs, these ex vivo isolated T-cells were stimulated with 50 ng/mL phorbol 12-myristate 13-acetate (PMA) and 1mg/mL ionomycin in the presence of 5 ug/mL Brefeldin A for 6-hours and expression of IL-2, IFNγ and TNFα were assessed by intracellular staining. We used PMA/ionomycin stimulation to assess TIL effector function to eliminate potential confounding variables associated with antigen receptor expression and/or signaling.

To examine the antitumor efficacy of CAR T-cells in pancreatic cancer, 4×10^6 AsPC1 cells were premixed with Matrigel and subcutaneously injected into NSG mice. On day 30, when tumor volume reached 300-400 mm^3, mesothelin-directed CAR T-cells were intravenously injected, and tumor growth was monitored using caliper measurements.

For the B-cell acute lymphoblastic leukemia model, NSG mice were intravenously injected with 1×10^6 NALM-6-CBG cells. On day 7 post-tumor injection,

3×10^5 CD19 CAR T-cells were intravenously infused, and tumor growth was assessed twice weekly using bioluminescent imaging [22]. Peripheral blood was isolated on day 24 and flow cytometric T-cell immunophenotyping was carried out.

To assess the memory recall response of CAR T-cells, NSG mice were engrafted with 10^5 NALM-6-CBG cells. On day 6 post-tumor injection, 2×10^6 CD19 CAR T-cells were intravenously infused (n = 9-10). The mice that had exhibited initial control of NALM-6 cells and survived were rechallenged with 2×10^6 NALM-6 cells on day 40. Tumor growth was monitored using bioluminescent imaging.

Bulk RNA-seq

On days 0, 5 and 20 of the CAR T-cell restimulation assay, before stimulation and after the first and fourth tumor challenge respectively, $CD8^+$ CAR T-cells were isolated using CD8 microbeads (Miltenyi Biotec) and total mRNA was extracted with RNA Clean & Concentrator™ kits (Zymo Research). Bulk RNA-seq was conducted by Novogene using the Novaseq6000 system (paired-end 150bp) at 40×10^6 reads per sample. Reads were pseudoaligned to the human genome (GRCh38) transcriptomes using kallisto v0.46.0.

Differential expression analyses between *AAVS1* KO PSMA CAR T-cells and *PRDM1* KO PSMA CAR T-cells were performed using the edgeR v3.34.0 and limma v3.48.0 packages. Briefly, expression data were normalized using a trimmed mean of log expression ratios method and transformed into log2(counts per million). Linear models were used to assess differential expression, and P values were adjusted using the

Benjamini and Hochberg method. Gene set enrichment analysis was conducted using GSEABase v1.54.0, clusterProfiler v4.0.2, and msigdbr v7.4.1.

ATAC-seq analysis

On days 0 and 20 of the restimulation assay, dead cells were eliminated using the Dead Cell Removal Kit (Miltenyi Biotec) and $CD8^+$ CAR T-cells were isolated using CD8 microbeads (Miltenyi Biotec). 100,000 cells per sample were cryopreserved. Nuclei were isolated from $CD8^+$ T-cells for each replicate, followed by the transposition reaction in the presence of Tn5 transposase (Illumina, Inc.) for 45 minutes at 37°C. Purification of transposed DNA was then completed with the MinElute Kit (Qiagen) and fragments were barcoded with dual indexes (Illumina Nextra). Library preparation and sequencing were performed by Novogene using NovaSeq 6000 (paired-end 150bp reads) at a depth of 30×10^6 reads per sample.

FASTQ files for each sample were trimmed of adapter contamination using cutadapt (https://github.com/marcelm/cutadapt/). They were aligned to the hg19 reference genome using Bowtie2, restricting to properly aligned and properly paired reads between 10 and 1000 base pairs. Mitochondrial reads were removed (https://github.com/jsh58/harvard/blob/master/removeChrom.py). Files were sorted using samtools, and PCR duplicates were removed using Picard. BAM files were indexed using samtools in order to visualize tracks in IGV. Peak calling was performed with MACS2 with an FDR q-value of 0.01. The R package Diffbind was used to remove ENCODE blacklisted regions (https://sites.google.com/site/anshulkundaje/projects/blacklists), then

to identify peaks differentially opened between the control and the PRDM1 knockout. The findMotifsGenome script from HOMER was used to map the hg19 genome for occurrences of the PRDM1 motif (derived from ENCODE data accessible via GEO at GSE31477) and the NFACT1 motif[132].

Statistical analyses

Statistical analyses were conducted using Shapiro-Wilk test and D'Agostino & Pearson tests for normality. Pairwise comparisons were performed using the Mann Whitney U test and Student's t-test as appropriate. For nonparametric comparisons of three or more groups, the Kruskal-Wallis test with a post-hoc Dunn's multiple comparison test were used. Mouse survival was assessed using the Gehan-Breslow-Wilcoxon test. Statistical tests were performed in Prism 9 (GraphPad Software) and *P* values <0.05 were considered significant.

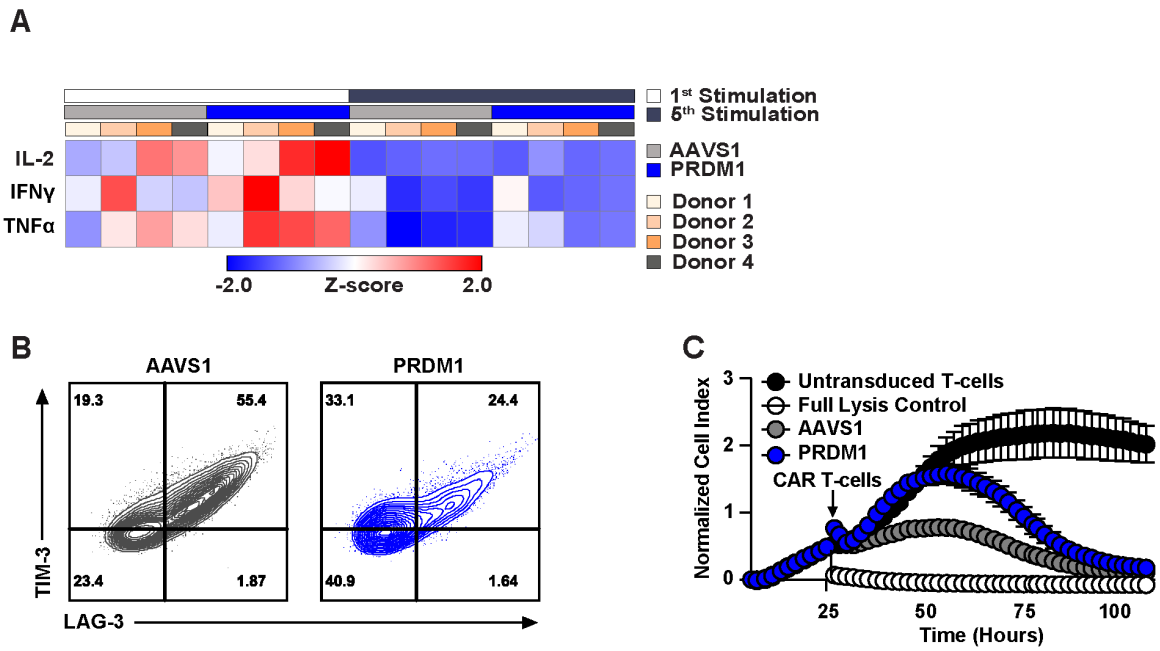

Figure 4.1 PRDM1 KO hampers CAR T-cell effector function during chronic CAR stimulation.

CAR T-cells were challenged five times with target-cell PC3-PSMA every 4-5 days at a ratio of E:T = 3:1. (**A**) Heat map showing effector cytokine secretion levels of AAVS1 KO and PRDM1 KO CAR T-cells after first and fifth tumor challenge. (**B**) Killing kinetics of AAVS1 KO and PRDM1 KO CAR T-cells. CAR T-cells were isolated after fifth tumor challenge and cocultured with PC3-PSMA at a ratio of E:T = 3:1. Cytotoxicity was monitored by real-time cellular impedance monitoring technology (xCELLigence). T-cells without CAR transduction were used as a negative control and 20% Tween20 treatment was served as a full lysis control. Data are mean ± S.D. from n = 6.

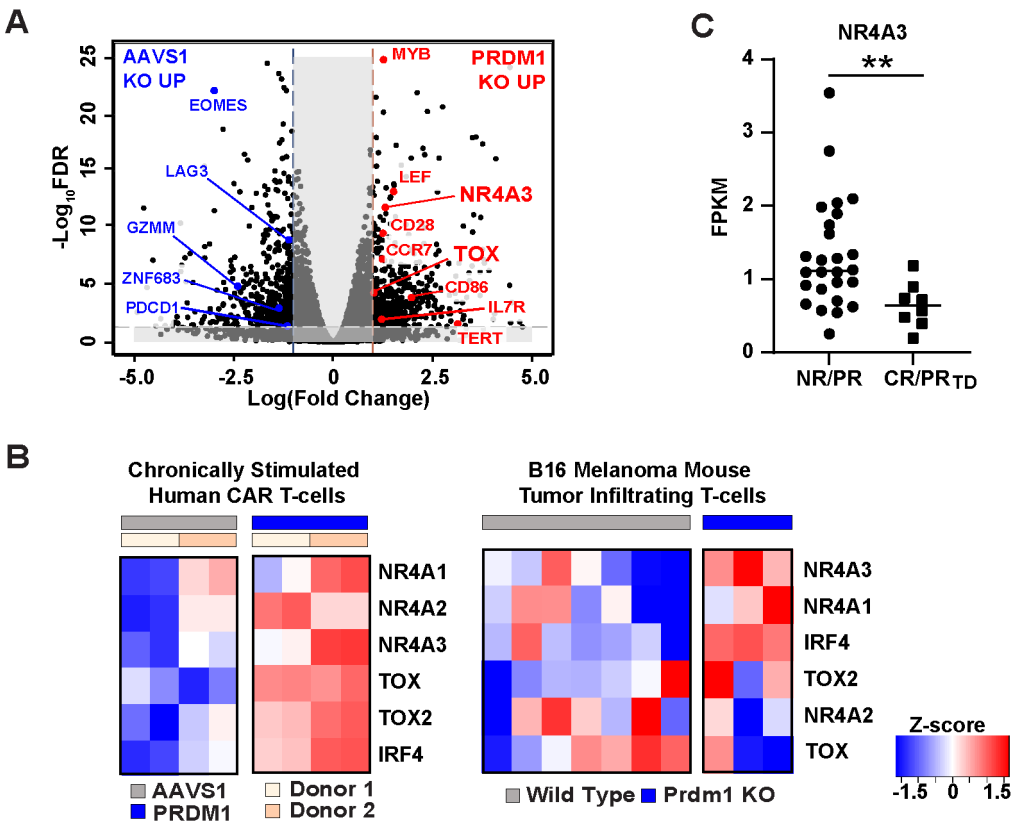

Figure 4.2 PRDM1 KO CAR T-cells fail to maintain a high degree of effector function due to upregulation of exhaustion-related transcription factors (TFs).

CD8+ CAR T-cells were isolated after fourth tumor challenge for bulk RNA sequencing. (**A**) Volcano plot illustrating differential gene expression analysis in PRDM1 KO compared to control AAVS1 KO CAR T-cells after the fourth consecutive tumor cell challenge. (**B**) Heat map showing expression levels of TF genes associated with T-cell exhaustion. RNA-seq experiments were conducted with CAR T-cells manufactured from 2 different subjects, each with replicates generated from two independent experiments. Exhaustion-related transcription factor expression profile in this study (left) and in a previous study (right: GSE113221). (**C**) Comparison of *NR4A3* expression levels in

CD19 CAR T-cell infusion products from CLL patients (CR: complete response; PR_{TD}: very good partial response; PR: partial response; no response) (FPKM: Fragments per kilo base of transcript per million mapped fragments). $*P < 0.05$, $*P < 0.01$, $***P < 0.001$, n.s.: not significant (two-tailed *t*-test).

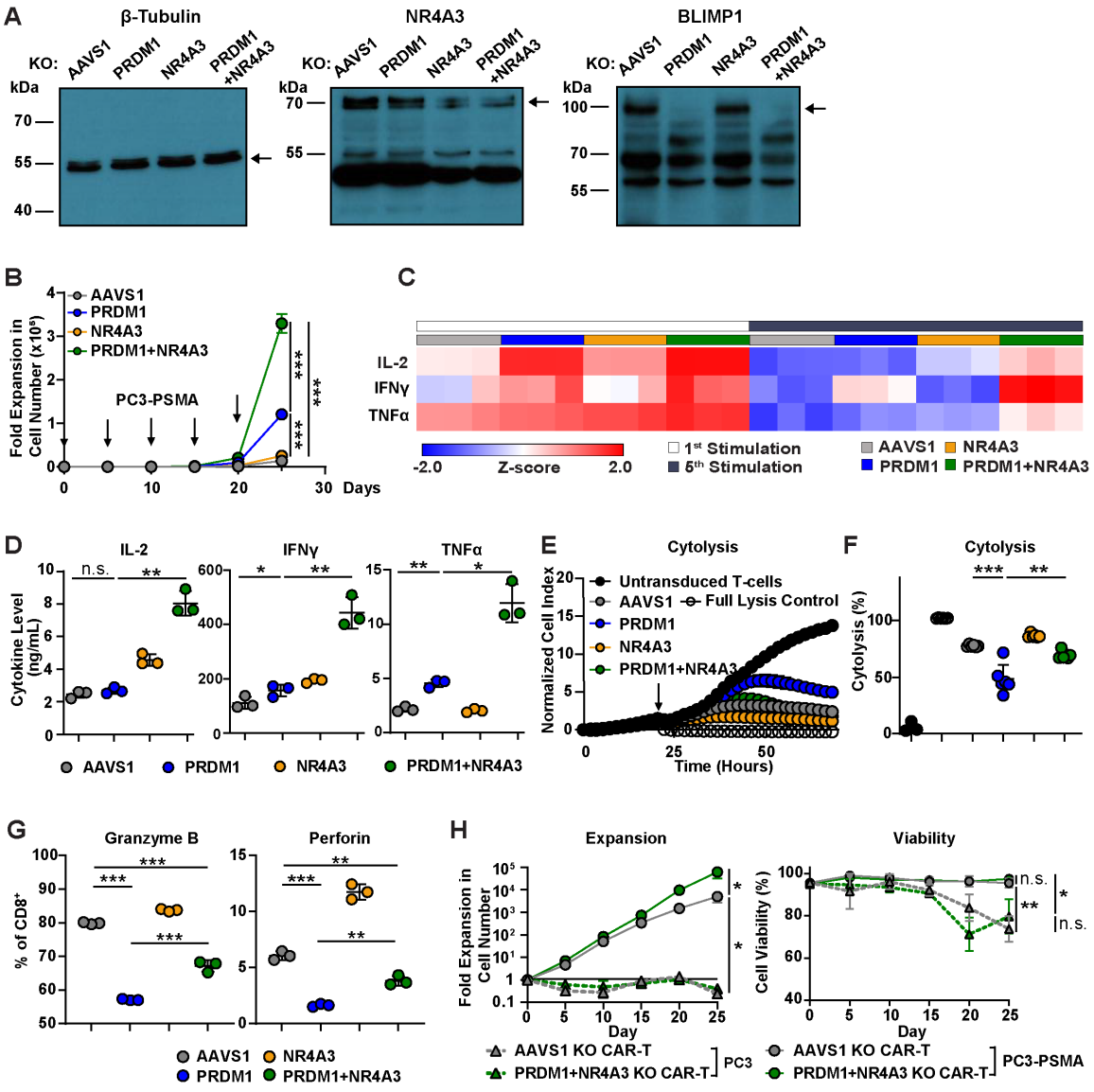

Figure 4.3 PRDM1/NR4A3 dual KO renders CAR T-cells resistant to exhaustion.

(**A**) Representative Western blots showing BLIMP1 and NR4A3 expression in gene-edited CAR T-cells. (**B**) Expansion kinetics of *PRDM1* and *NR4A3* knockout CAR T-cells during a restimulation assay. PSMA CAR T-cells were challenged with PC3-PSMA tumor cells every 5 days at an E:T ratio of 3:1. Arrow indicates the timing of PC3-PSMA challenge. Data are mean ± S.D. from n = 3. (**C, D**) Levels of effector cytokine

production by *AAVS1* KO, *PRDM1* KO, *NR4A3* KO and *PRDM1*/*NR4A3* dual KO CAR T-cells. (**C**) Heat map showing effector cytokine secretion levels 24-hours following the first and fifth tumor cell challenges. (**D**) Graphical summaries of effector cytokine production after the fifth CAR T-cell stimulation with tumor targets. Data are mean ± S.D. (n = 3). Killing kinetics (**E**) and cytolytic capacity at 36-hours post-CAR T-cell/tumor cell co-culture. (**F**) CAR T-cells were isolated after the fifth round of antigen stimulation and co-cultured with PC3-PSMA tumor cells at an E:T of 3:1 for a 'stressed' cytotoxicity assay. Data indicate mean ± S.D. (n = 6). (**B-F**) Data are representative of 3 independent experiments performed with engineered CAR T-cells manufactured from 3 different healthy subjects. (**G**) Granzyme B and Perforin expressions in $CD8^+$ CAR T-cells after fifth tumor challenge during restimulation assay. (**H**) CAR T-cells were repetitively challenged with PC3 or PC3-PSMA every 5 days at a ratio of E:T = 3:1. Expansion and viability of CAR T-cells were assessed over time. Data are mean ± S.D. from n = 3. Data are representative of 2 independent experiments performed with engineered CAR T-cells manufactured from 2 different subjects. *P < 0.05, *P < 0.01, ***P < 0.001, n.s.: not significant (two-tailed unpaired t-test).

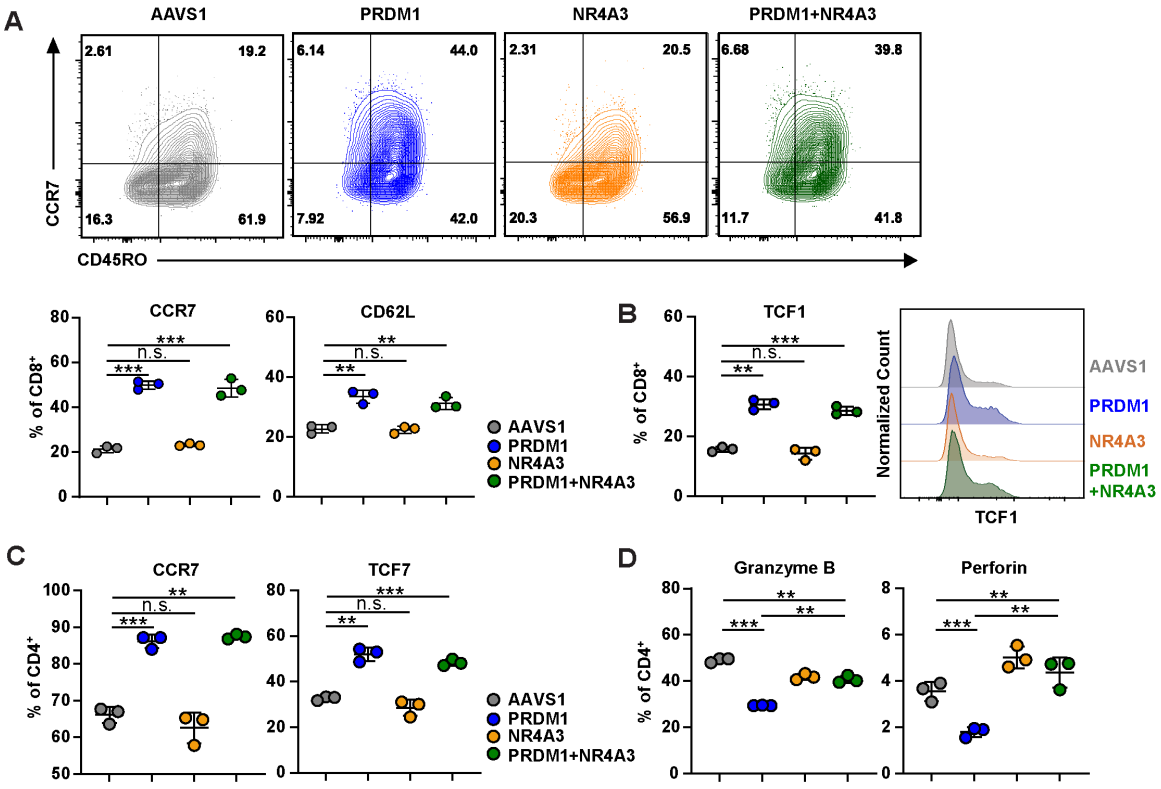

Figure 4.4 PRDM1/NR4A3 dual KO CAR T-cells exhibit early memory differentiation.

(**A**) Expression of early memory T-cell markers (CCR7 and CD62L) on gene-edited $CD8^+$ CAR T-cells 5 days post-tumor challenge. (**B**) Flow cytometric TCF1 expression at 5 days post-tumor challenge. (**C**) Expression of CCR7 and TCF1 in $CD4^+$ CAR T-cells 5 days post-tumor challenge. (**D**) Granzyme B and Perforin expressions in $CD4^+$ CAR T-cells after fifth tumor challenge. Data depict mean ± S.D. (n = 3). *P < 0.05, *P < 0.01, ***P < 0.001, n.s.: not significant (two-tailed t-test).

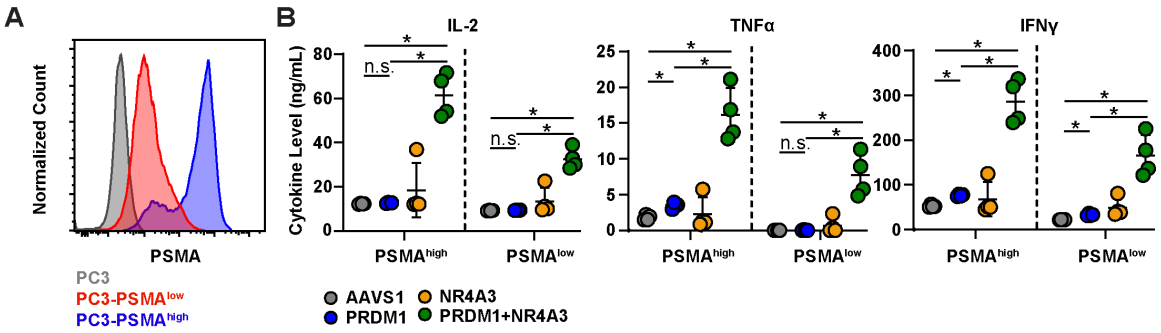

Figure 4.5 PRDM1/NR4A3 dual KO CAR T-cells show enhanced effector function against cancer cells expressing a low level of target antigen expression.

(**A**) PSMA expression levels of PC3 cell lines. (**B**) CAR T-cells were repetitively challenged with PC3-PSMA^{high} cell lines. After fifth tumor challenge, PSMA CAR T-cells were isolated and cocultured with PC3-PSMA^{high} or PC3-PSMA^{low} cell lines. Effector cytokines were measured 24hr post coculture. Data depict mean ± S.D. (n = 3). *P < 0.05, *P < 0.01, ***P < 0.001, n.s.: not significant (two-tailed t-test).

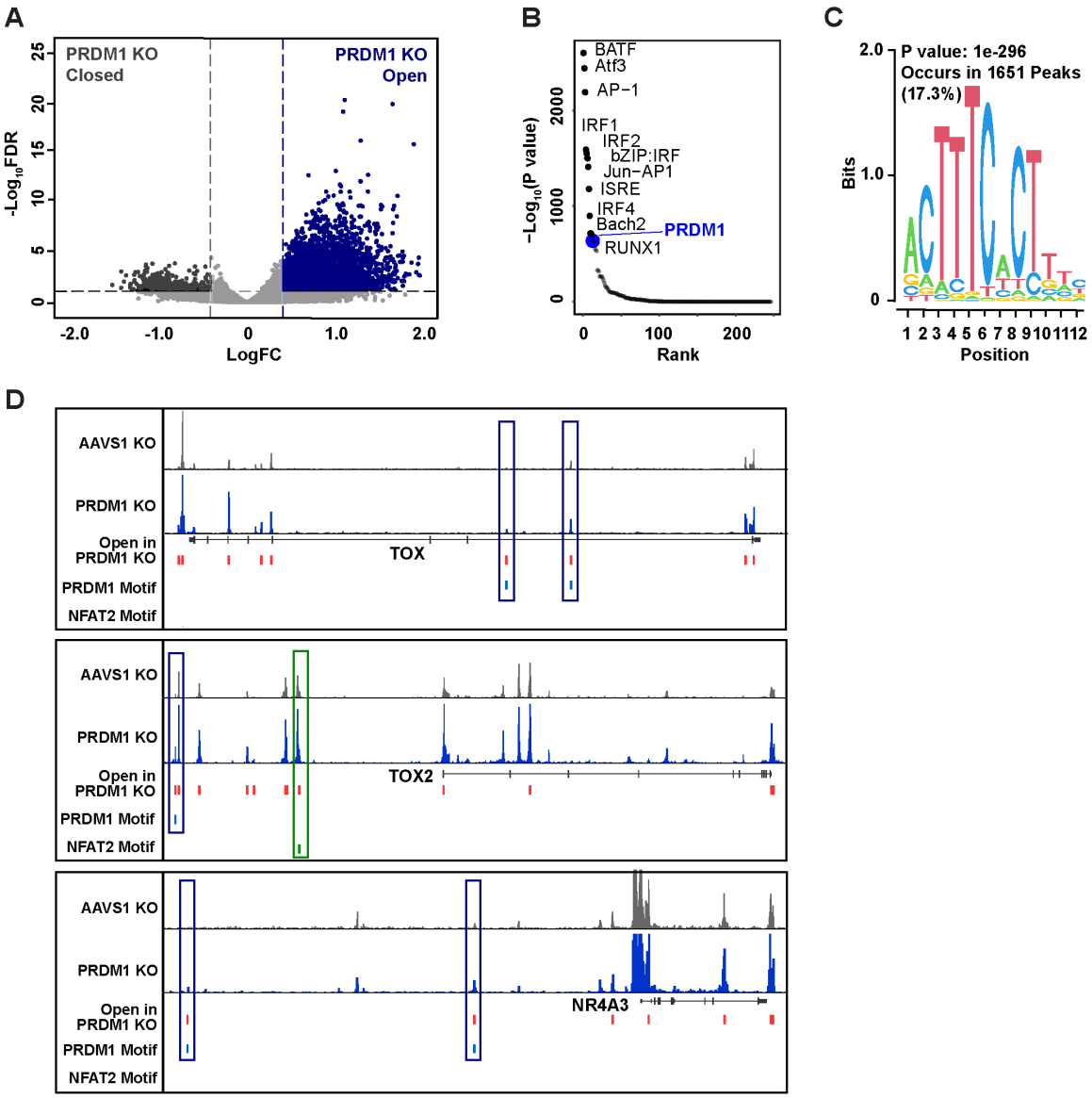

Figure 4.6 Upregulation of exhaustion-related TFs in PRDM1 KO CAR T-cells is attributed to increased chromatin accessibility.

ATAC-seq analysis of *AAVS1* KO and *PRDM1* KO CAR T-cells. At the end of manufacturing, CAR^+ T-cells were enriched and subjected to ATAC-seq analysis. (**A**) Volcano plot of differentially accessible chromatin regions. (**B**) Top TF motifs enriched in *PRDM1* KO compared to *AAVS1* KO CAR T-cells. (**C**) *PRDM1* binding motif

enriched in open chromatin regions of *PRDM1* KO CAR T-cells. (**D**) ATAC–seq tracks of TOX, TOX2, and NR4A3 loci. Opened chromatin regions in *PRDM1* KO CAR T-cells and the binding motifs of PRDM1 and NFAT2 are indicated. ATAC-seq experiments were conducted with CAR T-cells manufactured from 2 different subjects, each with replicates generated from two independent experiments.

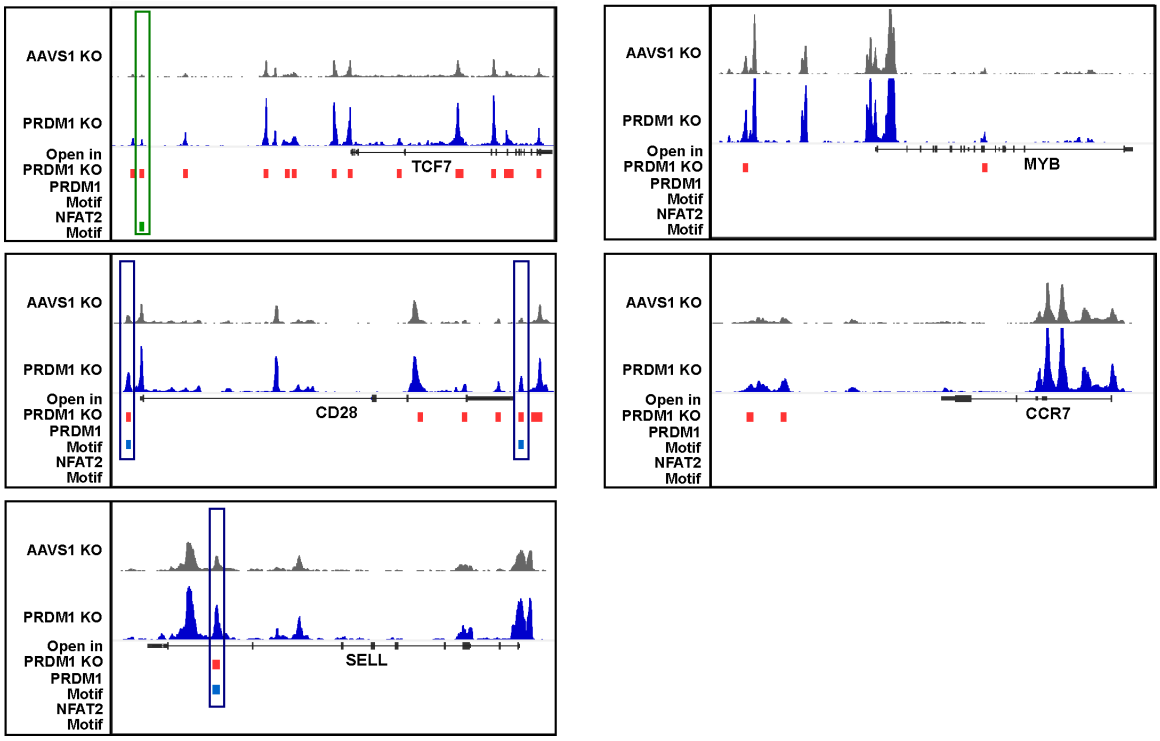

Figure 4.7 PRDM1 KO increases chromatin accessibility of T-cell memory-related genes.

ATAC–seq tracks of memory-related gene loci (*TCF7*, *MYB*, *CD28*, *CCR7*, *SELL*) in *AAVS1* and *PRDM1* KO CAR T-cells. Opened chromatin regions in *PRDM1* KO CAR T-cells and binding motifs of *PRDM1* and *NFAT2* are shown.

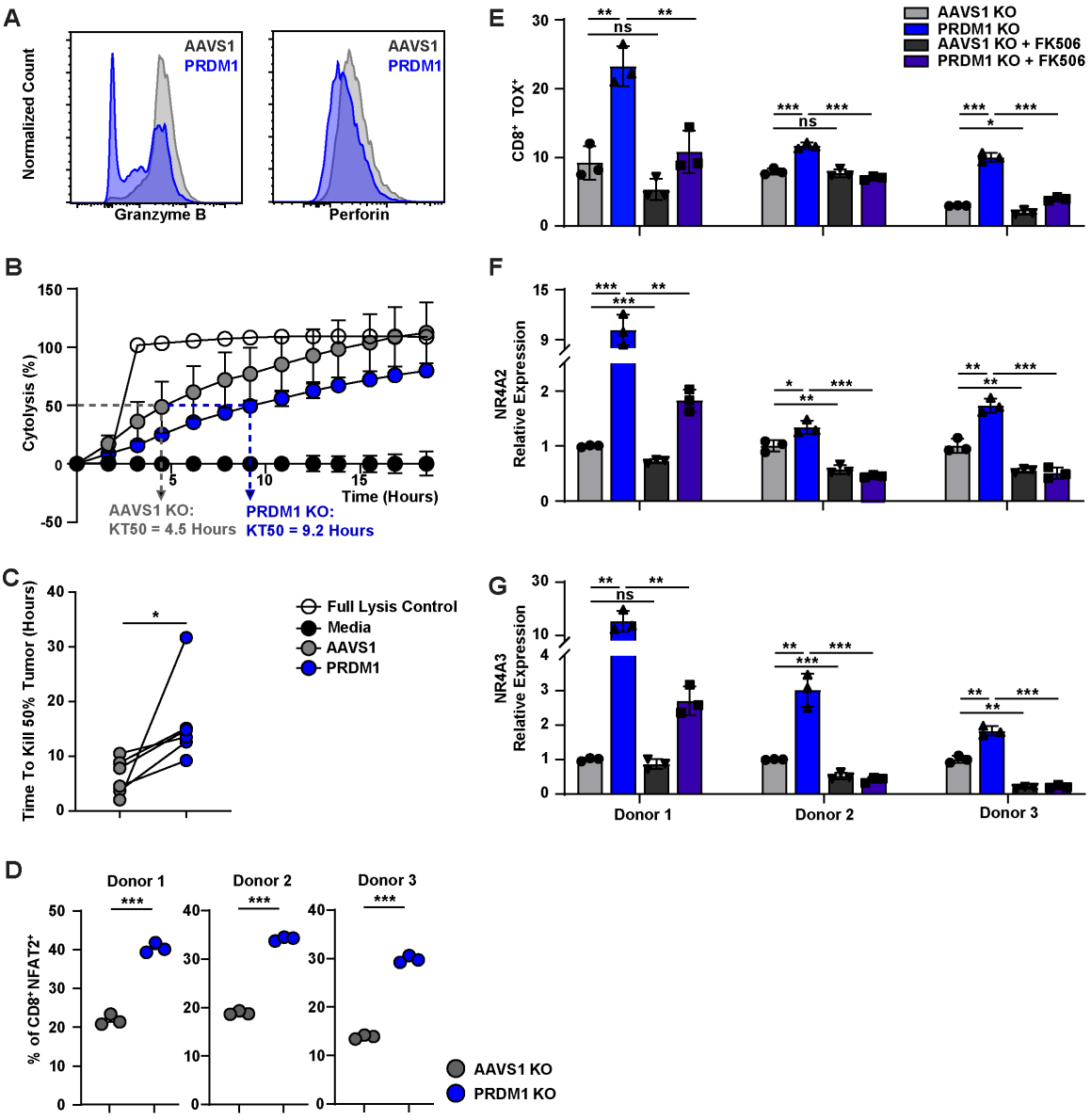

Figure 4.8 An increase in exhaustion-related transcription factor expression levels in PRDM1 KO CAR T-cells is mediated by elevated calcineurin-NFAT signaling.

(**A**) Expression of Granzyme B and perforin measured by flow cytometry. (**B-C**) Cytotoxicity assay to determine the time period needed to kill 50% of tumor target-cells (KT_{50}). (**B**) Representative killing kinetics of *AAVS1* and *PRDM1* KO CAR T-cells. Data show mean ± S.D. (n = 3). (**C**) Comparison of KT_{50} between *AAVS1* and *PRDM1* KO

CAR T-cells. Data were generated from 6 independent experiments with CAR T-cells manufactured from 4 different subjects. (**D**) Frequencies of NFAT2-expressing CD8+ CAR T-cells measured by flow cytometric analysis (n = 3) (**E-G**) Expression levels of exhaustion-related transcription factors following repetitive tumor cell challenges. *AAVS1* KO and *PRDM1* KO CAR T-cells were challenged with PC3-PSMA cells every 2-4 days at an E:T of 1:1 in the presence or absence of 100 nM FK506. Following two consecutive rounds of stimulation, CAR T-cells were isolated and expression levels of exhaustion-associated TFs were measured. (**E**) TOX expression measured by flow cytometric analysis. (**F**) *NR4A2* and (**G**) *NR4A3* expression measured by quantitative reverse transcription PCR (qRT-PCR). Data indicate mean ± S.D. (n = 3). *P < 0.05, *P < 0.01, ***P < 0.001, n.s.: not significant (two-tailed t-test).

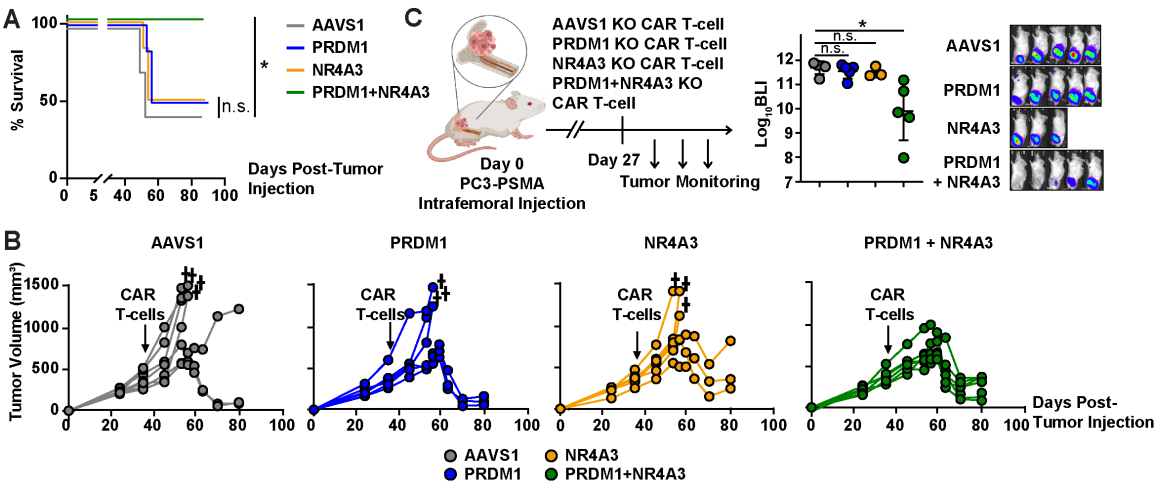

Figure 4.9 PRDM1/NR4A3 dual KO enhances CAR T-cell antitumor activity in prostate cancer xenograft models.

(**A-B**) Male NSG mice were subcutaneously engrafted with 5 × 10^6 PC3-PSMA tumor cells, and 3.5 × 10^5 PSMA CAR T-cells were given intravenously when tumor volume reached ~500 mm^3 (n = 6-7). (**A**) Kaplan–Meier curves showing overall survival in each group. The Gehan-Breslow-Wilcoxon test was used for statistical analysis. (**B**) Tumor growth monitored over time. (**C**) Male NSG mice were intrafemorally injected with 2 × 10^5 PC3-PSMA tumor cells. On day 27, 1-2 × 10^5 PSMA CAR T-cells were injected intravenously, and tumor burden was measured by bioluminescent imaging. (BLI: bioluminescence imaging (p/sec/cm2/sr)) *P < 0.05, *P < 0.01, ***P < 0.001, n.s.: not significant.

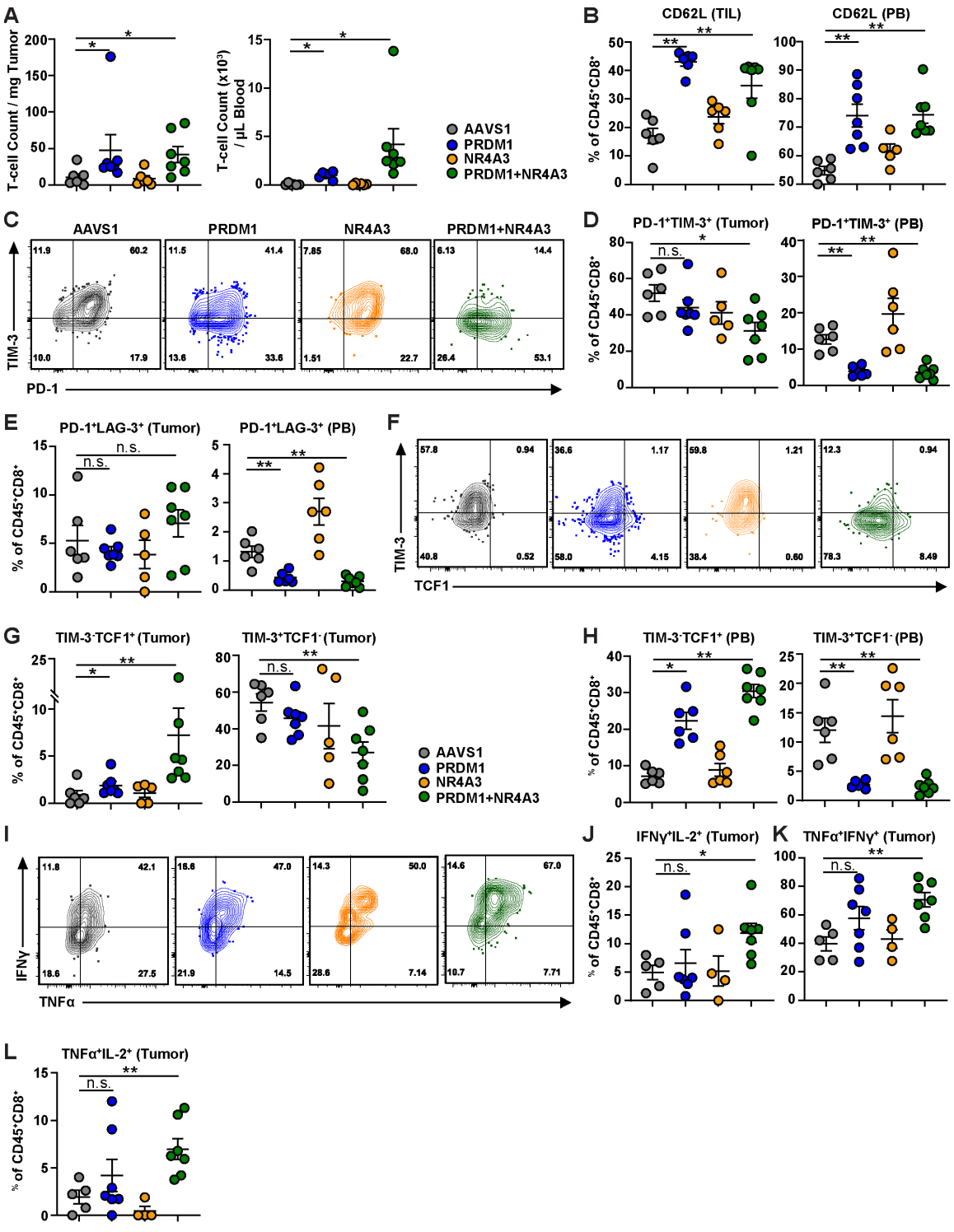
A
T-cell Count / mg Tumor
T-cell Count (x10³) / µL Blood
AAVS1
PRDM1
NR4A3
PRDM1+NR4A3
B
CD62L (TIL)
CD62L (PB)
% of CD45⁺CD8⁺
C
AAVS1
PRDM1
NR4A3
PRDM1+NR4A3
TIM-3
PD-1
D
PD-1⁺TIM-3⁺ (Tumor)
PD-1⁺TIM-3⁺ (PB)
n.s.
E
PD-1⁺LAG-3⁺ (Tumor)
PD-1⁺LAG-3⁺ (PB)
F
TIM-3
TCF1
G
TIM-3⁻TCF1⁺ (Tumor)
TIM-3⁺TCF1⁻ (Tumor)
H
TIM-3⁻TCF1⁺ (PB)
TIM-3⁺TCF1⁻ (PB)
I
IFNγ
TNFα
J
IFNγ⁺IL-2⁺ (Tumor)
K
TNFα⁺IFNγ⁺ (Tumor)
L
TNFα⁺IL-2⁺ (Tumor)

Figure 4.10 PRDM1/NR4A3 dual KO suppresses exhaustion and enhances effector function of tumor-infiltrating CAR T-cell.

AAVS1 KO, *PRDM1* KO, *NR4A3* KO, and *PRDM1*/*NR4A3* dual KO PSMA CAR T-cells were isolated from subcutaneous PC3-PSMA tumors and peripheral blood on day 45 post-tumor implantation when the tumor size was comparable between the groups. (**A**) Absolute numbers of human $CD45^+$ (hCD45) T-cells in tumors (left) and the peripheral blood (PB; right) are shown. Frequencies of gene-edited CAR T-cells isolated from the peripheral blood or tumors expressing (**B**) CD62L, (**C, D**) PD1 and TIM3, (**E**) PD1 and LAG3, (**F-H**) TIM3 and TCF1. (**I-L**) Effector cytokine expression levels measured by flow cytometry following *ex vivo* stimulation of CAR TILs. TILs were activated with 50 ng/mL phorbol 12-myristate 13-acetate (PMA) and 1 ug/mL ionomycin in presence of 5 ug/mL Brefeldin A for 6-hours, followed by staining IFNγ and TNFα staining (n = 4-7). (**I**) A representative flow cytometry plot and (**J-L**) graphical summary of IFNγ and TNFα expression is shown. Statistical analysis in panels **J**-**L** was conducted using a Mann Whitney U test; mean ± s.e.m shown. *$P < 0.05$, *$P < 0.01$, ***$P < 0.001$, n.s.: not significant.

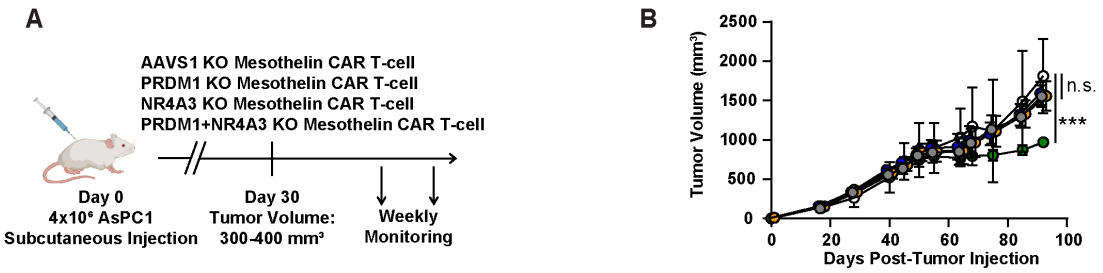

Figure 4.11 PRDM1/NR4A3 dual KO enhances CAR T-cell antitumor activity in a pancreatic cancer xenograft model.

(**A**) A schematic of the AsPC1 xenograft model. Briefly, NSG mice were subcutaneously injected with pancreatic cell line AsPC1. On day30, when tumor volume reached 300-400mm3, mesothelin-directed CAR T-cells were intravenously injected, and tumor growth was monitored. (**B**) AsPC1 tumor growth over time. *$P < 0.05$, *$P < 0.01$, ***$P <$ 0.001, n.s.: not significant (paired *t*-test).

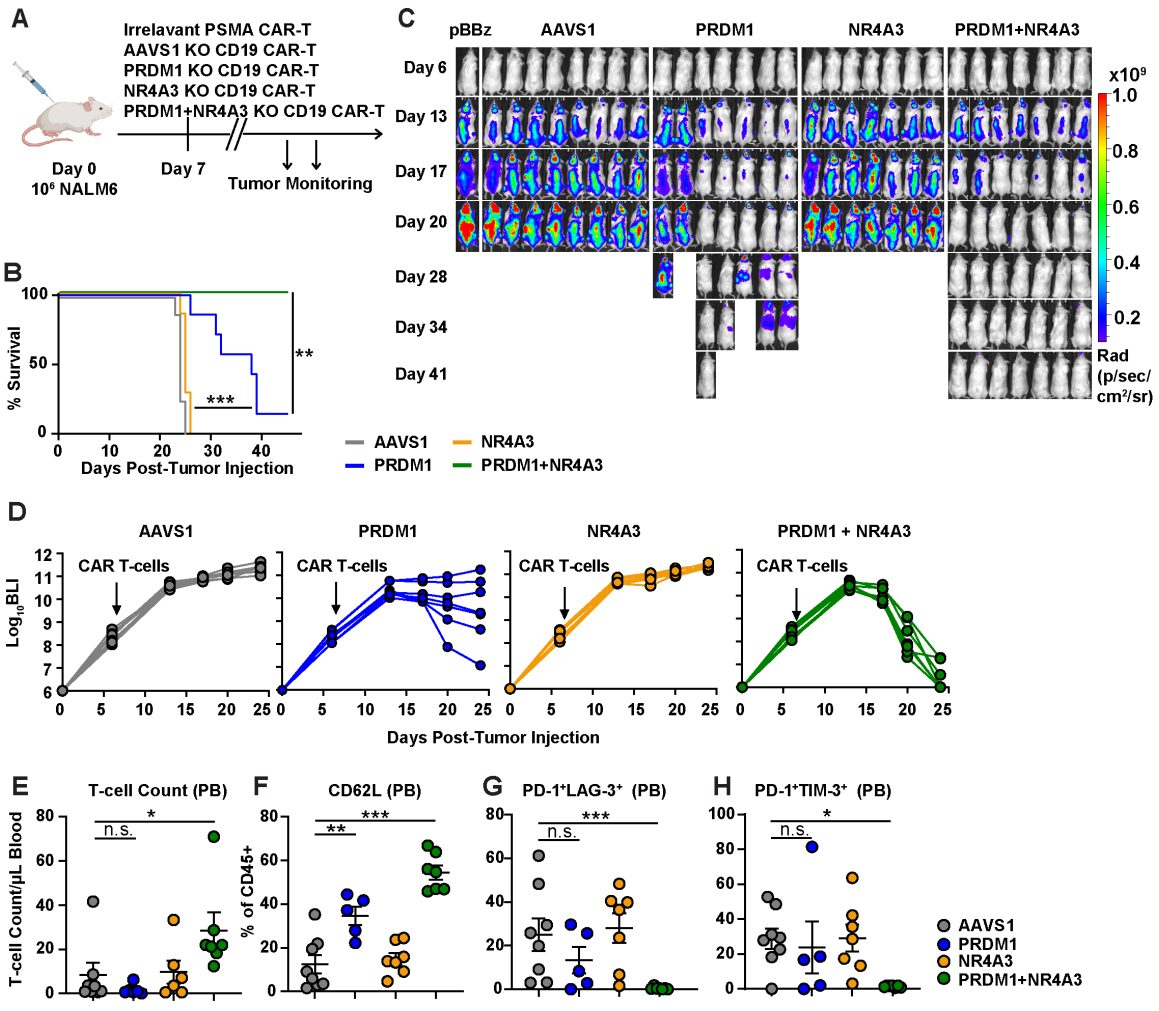

Figure 4.12 PRDM1/NR4A3 dual KO improves CAR T-cell antitumor activity in B-ALL cancer xenograft model by increasing early memory differentiation and reducing CAR T-cell exhaustion.

(**A**) A schematic of the NALM-6 xenograft model. Briefly, NSG mice were intravenously injected with 1 × 10^6 NALM6-CBG cells. On day 7 post tumor injection, 3 × 10^5 gene-edited CD19 or control CAR T-cells were treated (n = 7-8). (**B**) Survival and (**C-D**) graphical summaries of longitudinal bioluminescent tumor burden in NSG mice injected with 1 × 10^6 NALM-6 CBG cells, followed by treatment with 3 × 10^5 gene-edited CD19

or control CAR T-cells (n = 7-8) (BLI: bioluminescence imaging (p/sec/cm2/sr)). Data are representative of two independent experiments. (**E-H**) Immunophenotyping of CD19 CAR T-cells isolated from NALM-6 engrafted mice at day 24 post-tumor injection. (**E**) The CAR T-cell count in the peripheral blood is shown. (**F**) Frequencies of CD62L-positive CAR T-cells, (**G**) PD1 and LAG3 double-positive CAR T-cells and (**H**) PD1 and TIM3 double-positive T-cells. The Gehan-Breslow-Wilcoxon test was used for survival analysis shown in panel **B**. Statistical analysis in panels **E-H** was conducted using a Mann Whitney U test; mean ± s.e.m shown. *$P < 0.05$, *$P < 0.01$, ***$P < 0.001$, n.s.: not significant.

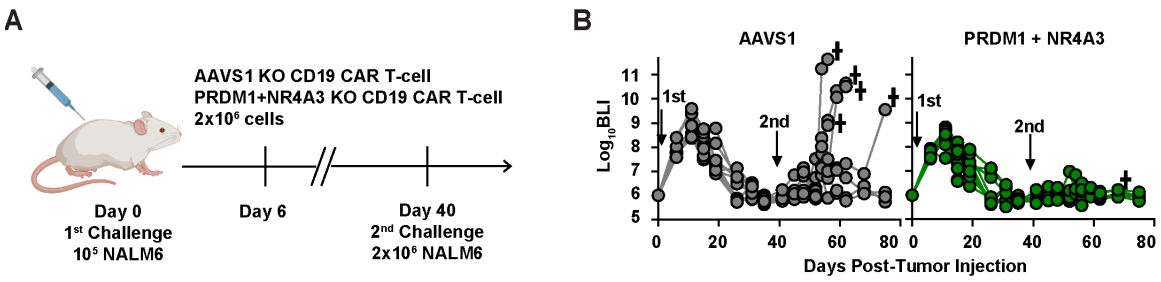

Figure 4.13 PRDM1/NR4A3 dual KO enhances memory recall response.

(**A**) A schematic of the NALM-6 rechallenge model. Briefly, NSG mice were intravenously injected with 1 × 10^5 NALM6-CBG cells. On day 6 post tumor injection, 2 × 10^6 CD19 CAR T-cells were treated (n = 9-10). The mice which had rejected initial NALM6 cells and had survived were treated with second dose of NALM6 cells on day 40. (**B**) The tumor growth was monitored over time. † = death.

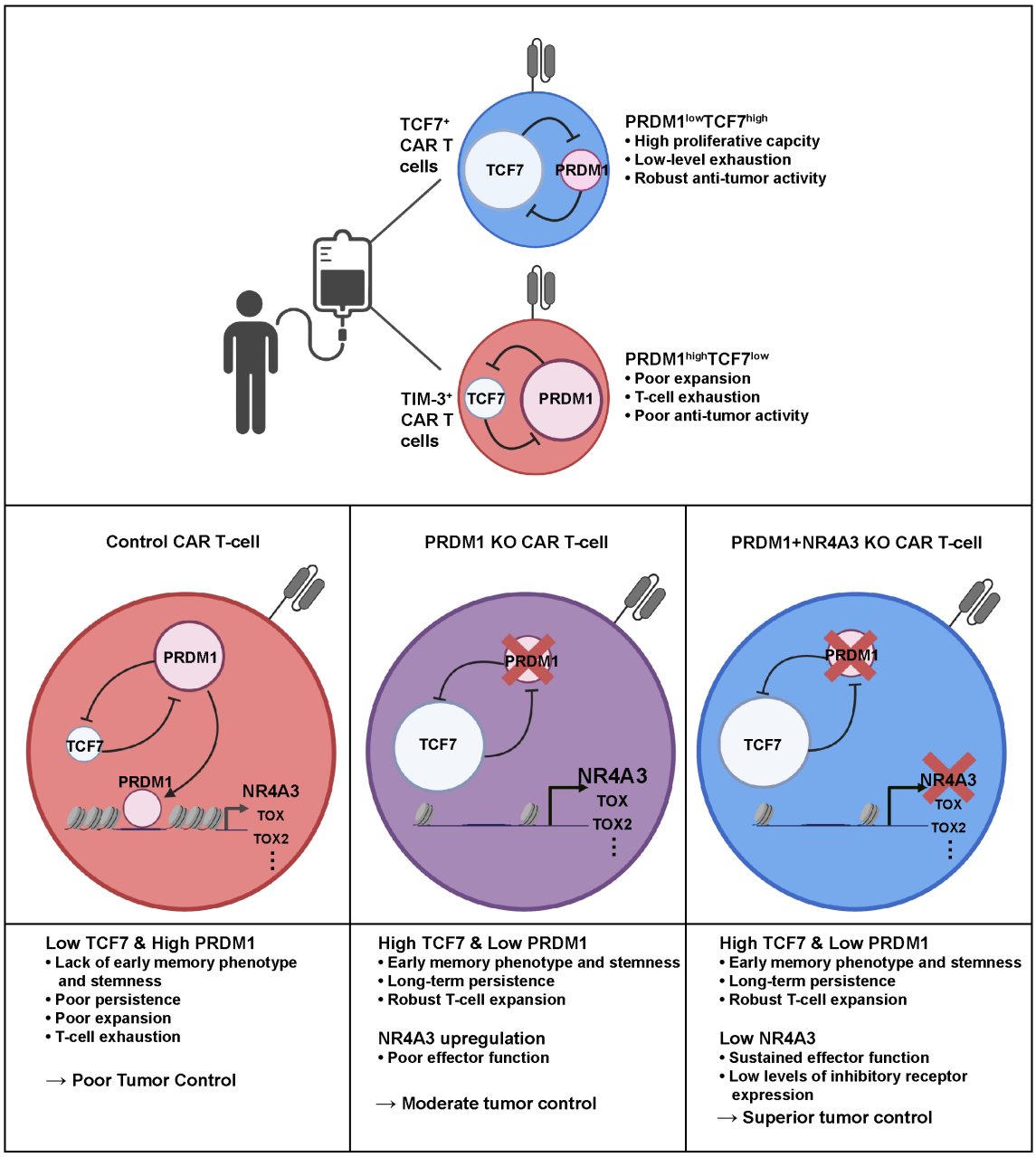
TCF7+ CAR T cells
TCF7
PRDM1
PRDM1lowTCF7high
• High proliferative capcity
• Low-level exhaustion
• Robust anti-tumor activity
TIM-3+ CAR T cells
TCF7
PRDM1
PRDM1highTCF7low
• Poor expansion
• T-cell exhaustion
• Poor anti-tumor activity
Control CAR T-cell
PRDM1
TCF7
PRDM1
NR4A3
TOX
TOX2
PRDM1 KO CAR T-cell
PRDM1
TCF7
NR4A3
TOX
TOX2
PRDM1+NR4A3 KO CAR T-cell
PRDM1
TCF7
NR4A3
TOX
TOX2
Low TCF7 & High PRDM1
• Lack of early memory phenotype and stemness
• Poor persistence
• Poor expansion
• T-cell exhaustion
→ Poor Tumor Control
High TCF7 & Low PRDM1
• Early memory phenotype and stemness
• Long-term persistence
• Robust T-cell expansion
NR4A3 upregulation
• Poor effector function
→ Moderate tumor control
High TCF7 & Low PRDM1
• Early memory phenotype and stemness
• Long-term persistence
• Robust T-cell expansion
Low NR4A3
• Sustained effector function
• Low levels of inhibitory receptor expression
→ Superior tumor control

Figure 4.14 Graphical summary of how PRDM1/NR4A3 dual ablation enhances CAR T-cell-mediated antitumor efficacy.

(**Top**) scRNA-sequencing analysis of CAR T-cells from a metastatic prostate cancer trial identified two distinct and independently validated cell states associated with antitumor potency or lack of efficacy. Low levels of the *PRDM1* gene encoding the BLIMP1 transcription factor defined highly potent $TCF7^{+}CD8^{+}$ CAR T-cells, while enrichment of $TIM3^{+}CD8^{+}$ T-cells with elevated *PRDM1* expression predicted poor outcome. (**Bottom**) *PRDM1* knockout promoted CAR T-cell stemness and proliferation. However, in the setting of *PRDM1* deficiency, a negative epigenetic feedback program of T-cell dysfunction characterized by upregulation of *NR4A3* and NFAT signaling hampered effector function. *PRDM1* and *NR4A3* dual-ablation skewed CAR T-cell phenotypes away from $TIM3^{+}CD8^{+}$ and toward $TCF7^{+}CD8^{+}$ to counter T-cell exhaustion and improve *in vivo* antitumor responses. Thus, disruption of *PRDM1* and *NR4A3* expression or activity is a promising strategy for cellular immunotherapy.

CHAPTER 5: DISCUSSION

Introduction

In the studies presented within this thesis, we show that deep profiling of CAR T-cells from a first-in-human trial in metastatic prostate cancer elucidates cell states and key transcription factors that reciprocally regulate the balance of T-cell stemness and exhaustion. Further, we present a novel multiplex gene-editing strategy to enrich stem-like CAR T-cells resistant to exhaustion in solid tumor models. Some top line messages for the field of cellular immunotherapy that we report for the first time are as follows: (i) heterogeneity in the cellular and molecular features of CAR T-cell infusion products in a solid tumor indication contributes to variation in therapeutic potency; (ii) low levels of the *PRDM1* gene encoding the BLIMP1 transcription factor characterized highly potent $TCF7^{+}CD8^{+}$ CAR T-cells, while enrichment of $TIM3^{+}CD8^{+}$ infusion product T-cells with elevated *PRDM1* expression predicts poor antitumor responses; (iii) *PRDM1* KO promotes CAR T-cell stemness, early memory differentiation and proliferation in a TCF7-dependent manner. This results in marginally enhanced leukemia control, which is consistent to some extent with previous work (see below). However, in the setting of *PRDM1* deficiency, a newly identified negative epigenetic feedback program of T-cell dysfunction characterized by reciprocal upregulation of NR4A3 and NFAT signaling hampered CAR TIL effector function in solid tumors; (iv) dual disruption of *PRDM1* and *NR4A3* not only enhances stemness and early memory differentiation, but also sustains a high degree of effector function by rendering T-cells resistant to exhaustion imposed by solid tumors. Importantly, this effect was not achieved with *PRDM1* or *NR4A3* single

disruption alone; and (v) combined inhibition of *PRDM1* and *NR4A3* expression or activity is a promising strategy for cellular immunotherapy. Accordingly, our findings elucidate the cellular and molecular basis of treatment resistance to CAR T-cell therapy with the goal expanding the use of immunotherapy to benefit more cancer patients - the cancer immunotherapy revolution.

Differentiation of this work from a previous *PRDM1* KO approach in antitumor T-cells

A recent study examined the effect of *PRDM1* KO alone on antitumor activity of human CAR T-cells[119]. There are key differences between some of our findings and those presented in this report. While we build on the observation that *TCF7* is a critical determinant of memory differentiation in the context of *PRDM1* deficiency using *TCF7* KO experiments, the suppression of long-term tumor control capacity and elicitation of robust antitumor effector function in *PRDM1* KO T-cells was not previously reported. Yoshikawa and colleagues[119] speculated that upregulation of *TOX* resulting from *PRDM1* deletion may diminish the antitumor response through upregulation of inhibitory receptors. Notably, we provide a mechanism by which *PRDM1* KO regulates a battery of genes encoding exhaustion-related TFs, which together regulate CAR T-cell phenotype and function. The decoupling of exhaustion-related TF upregulation, particularly NR4A3, and inhibitory receptor expression observed in our study and not by Yoshikawa et al. may be attributed to several reasons. These discrepancies may include differences in the *PRDM1* KO CAR- and TCR-transgenic T-cells used and the transfer of a fewer number of engineered T-cells in our study. Furthermore, we provide novel molecular and epigenetic mechanisms of how BLIMP1 regulates exhaustion transcription factors expression. Our findings underscore the need to balance a reciprocal upregulation of NR4A3 and NFAT signaling in the setting of BLIMP1 deficiency to generate effective CAR T- cell-mediated responses in a variety of tumor types. Further, we provide a novel

multiplex gene-editing strategy to enrich clinically-defined populations of stem-like CAR T-cells resistant to exhaustion.

Comparison of our novel approach with previous engineering strategies to overcome T-cell exhaustion

The antitumor efficacy of cellular immunotherapies has been limited in solid indications and blood cancers due in part to the T-cell exhaustion induced in the TME[133,134]. Currently there is growing interest in understanding underlying mechanisms of T-cell exhaustion in the context of T-cell therapies and a series of recent studies examined engineering strategies to mitigate T-cell exhaustion.

Disruption of inhibitory checkpoint signaling

Checkpoint blockade therapies including anti-PD1 have been shown to reinvigorate exhausted T-cells[58,135]. Accordingly, advances in gene-editing technology have enabled researchers to disrupt *PDCD1* (gene encoding PD-1) in T-cells to prevent T-cell exhaustion and improve effector function. Now there are 20 clinical trials world-wide using PD-1 knockout T-cells[136]. In various liquid and solid tumor models, PD-1 knockout improved the antitumor activity of CAR T-cells, mostly through enhancement of effector function[137-139]. However, it is still unclear whether PD-1 knockout renders T-cells resistant to exhaustion due to lack of appropriate *in vitro* and *in vivo* exhaustion models that incorporate human CAR T-cells. In a murine model of chronic LCMV infection, PD-1-deficient T-cells were more susceptible to exhaustion and demonstrated elevated frequencies of terminally differentiated effector populations, although effector function and proliferation were improved in the short-term[65,140].

Targeting exhaustion-related transcription factors

Inhibition of key transcription factors that drive T-cell exhaustion have shown promising outcomes in several preclinical studies. Chen et al. assessed the antitumor efficacy of *NR4A* knockout CD19 CAR T-cells against CD19-positive B16 melanoma[74]. While CAR T-cells with individual *NR4A1, NR4A2, or NR4A3* KO have shown marginal enhancement of tumor control, only *NR4A1, 2, 3* triple knockout CAR T-cells induced a significant improvement in tumor regression, by successfully suppressing multiple inhibitory receptors and generating polyfunctional CAR T-cell populations upon antigen restimulation[74]. In a subsequent study, the role of TOX and TOX2 transcription factors in exhaustion of CAR T-cells was investigated[73]. *TOX* and *TOX2* double knockout CD19 CAR T-cells downregulated exhaustion molecules and sustained effector function in a solid tumor mouse model[73]. Nevertheless, the question of whether TOX KO CAR T-cells can persist long-term and effect durable antitumor responses requires further investigation, since other studies have shown that TOX is essential for supporting T-cell persistence and survival [59,141].

Fine-tuning CAR signaling

To prevent constitutive tonic CAR signaling, a careful optimization of the ectodomain of CAR constructs is necessary to avoid antigen-independent scFv interactions or FcγR-binding[27,142]. The choice of transgene delivery methods is also important, as tonic CAR signaling is exacerbated in non-self-inactivating gammaretroviral vectors[142]. In addition, inclusion of co-stimulation domains such as 4-1BB rather than CD28 has been shown to ameliorate T-cell exhaustion induced by

antigen-independent CAR signalling[27]. In order to prevent T-cell exhaustion during antigen encounter, Feucht et al. have recently generated a novel anti-CD19 CAR with partially abrogated immunoreceptor tyrosine-based activation motif (ITAMs)[79]. As compared with conventional CAR constructs which typically contain three ITAMs in the CD3ζ domain, CARs encoding a single ITAM demonstrated improved antitumor T-cell potency through a mechanism involving decreased exhaustion[79].

A *PRDM1/NR4A3* dual-disruption approach: Filling the unmet needs

To achieve durable anti-tumor activity, it is critical to render CAR T-cells resistant to exhaustion and preserve T-cell stemness. Despite the recent advancements in the development of engineering strategies to overcome CAR T-cell exhaustion, the question of whether exhaustion-resistant CAR T-cells could persist and exert long-term tumor control was outstanding. For instance, despite the enhancement of CAR T-cell effector function, NR4A and TOX KO significantly decreased expression of memory-related genes, such as Ccr7, Sell, and Tcf7[73,74]. These results are consistent with the finding that Tox-deleted-tumor specific T-cells failed to persist in tumors and become susceptible to activation-induced cell death, suggesting that these exhaustion-related transcription factors may be required for T-cell survival and long-term persistence in the TME. A similar limitation is observed in the setting of PD-1 KO. In a recent study, PD-1-knockdown in CAR T-cells impaired proliferative capacity, which was associated with accelerated terminal differentiation of T-cells[143]. This result is concordant with a previous LCMV study showing that PD-1 supports the maintenance of $TCF1^+$ stem-like CD8 T-

cells during chronic infection[65]. In our study, we demonstrated that *PRDM1/NR4A3* KO not only renders CAR T-cells resistant to exhaustion, but also enhances T-cell stemness and early memory differentiation. Indeed, *PRDM1/NR4A3* KO CAR T-cells exhibited durable tumor control capacity in an antigen rechallenge mouse model. These results suggest that *PRDM1/NR4A3* KO may endow resistance to T-cell dysfunction without significantly compromising CAR T-cell stemness and proliferative capacity.

In addition to targeting T-cell intrinsic exhaustion pathways, CAR T-cell exhaustion can be mitigated through optimization of CAR signal strength. However, these engineering approaches can compromise the capacity of CAR T-cells to eliminate tumors expressing low levels of target antigens[144]. Robbie et al. demonstrated through use of a4-1BB costimulatory domain and reducing ITAM signaling impaired cytolytic activity of CAR T-cells against antigen-low tumors, compared to CARs incorporating a CD28 motif or multiple ITAMs[144]. In this study, we found that the *PRDM1/NR4A3* dual-KO approach enhanced antitumor activity in both antigen-high and -low expressing target tumor cells, implying that this double KO approach does not significantly impair CAR T-cell function against low antigen-expressing cancer cells (**Figure 4.5**). Further studies are required to investigate whether *PRDM1/NR4A3* KO CAR T-cells can eradicate low antigen-expressing tumors *in vivo*.

Safety considerations for the clinical application of *PRDM1/NR4A3 dual*-KO CAR T-cells

Cytokine release syndrome and neurotoxicity

"On-target, on-tumor" toxicity is one of the major concerns associated with CAR T-cells engineered to be resistant to T-cell dysfunction. Cytokine release syndrome (CRS) is a collection of systemic inflammatory responses following adoptive cell transfer therapies or administration of bispecific T-cell engagers[145,146]. CRS typically develops within 2 weeks after CAR T-cell infusion, with an incidence of 42-100% in patients treated with this therapy[147,148]. At the onset of CRS, mild flu-like symptoms such as fever, headache, tachypnea, and nausea can occur, and these could aggressively progress to severe toxicities including life-threatening pulmonary, cardiovascular, and renal failures[149]. Together with CRS, a spectrum of immune effector cell-associated neurotoxicity syndrome (ICANS) can develop, ranging from mild/moderate headaches, confusion, and language disturbances to severe seizures or cerebral edema[150]. IL-6, IL-1β, and other pro-inflammatory cytokines produced by activated macrophages are known to play critical role in endothelial activation, vascular leakage, and subsequent onset of CRS and ICANS[145,146,148,151]. The incidence and severity of CRS and ICANS are directly associated with increased CAR T-cell peak expansion, high baseline tumor burdens, administration of high intensity lympho-depletion regimens, and infusion of high CAR T-cell doses[146,147,151,152].

Our *in vitro* and *in vivo* studies demonstrate that disruption of the *PRDM1* and *NR4A3* substantially increased CAR T-cell expansion and production of effector

cytokines such as IFNγ IL-2, and TNFα, which may increase the risk of toxicity (**Figure 4.3C, D, Figure 4.10A, H-L**). Indeed, in an intraosseous PC3-PSMA xenograft mouse model, mice treated with *PRDM1/NR4A3* KO CAR T-cells lost around ~80% of body weight on day 11 post-CAR T-cell infusion, which may be indicative of the onset of cytokine-related toxicity (**Figure 5.1**). In contrast, mice treated with *AAVS1*, *PRDM1,* and *NR4A3* single knockout CAR T-cells did not show a significant change in body weight during the course of treatment. Although weight loss has not been observed in other *in vivo* tumor models used in our studies, further studies using a relevant mouse model of cytokine-related toxicity such as SCID-beige is required to thoroughly assess the effect of *PRDM1/NR4A3* double KO on the induction of CRS. Alternatively, the safety risk associated with this approach can be addressed in first-in-human dose-escalation studies using a more conservative dosing regimen as compared to the initial doses evaluated in our prior phase I dose-escalation study in mCRPC [97]. In this previous trial, three out of 13 patients developed grade≥3 CRS, including one patient who was treated with a high-dose PSMA CAR T-cells following cyclophosphamide/fludarabine lymphodepletion and experienced grade 4 CRS[97]. Given these uncertainties, first-in-human trials involving this strategy should test *PRDM1/NR4A3* dual KO CAR T-cell products at comparably lower dose levels, prior to incorporation of lymphodepletion, which we anticipated to enhance T-cell proliferation, antitumor activity, and treatment-related toxicity.

Safety concerns related to multi gene-editing approach

Gene-editing technologies have been actively incorporated into CAR T-cell manufacturing processes to generate allogeneic products, prevent CAR T-cell fratricide, and bolster antitumor activity[77,153-155]. A recent first-in-human phase I clinical trial demonstrated the safety and feasibility of triple gene-edited NY-ESO-1 TCR T-cells[153]. In this study, we simultaneously targeted two genes for KO, *PRDM1* and *NR4A3*, which significantly improved CAR T-cell stemness and antitumor efficacy. However, the safety profile of the gene-edited CAR T-cells should be carefully characterized to translate this approach into clinic.

One of the major concerns of gene-editing approaches is off-target editing. Unintended off-target editing of tumor suppressor genes can lead to development of malignant T-cells during manufacturing or following CAR T-cell infusion[153,154]. Off-target effects in gene-edited T-cells have been reported by several groups using different gene editing technologies, such as CRISPR/Cas9, MegaTAL, and Transcription activator-like effector nucleases (TALEN) [153,156,157]. The use of high-fidelity Cas9 variants or base editors that induce efficient KO without double-stranded DNA cleavage could minimize the frequency of off-target mutagenesis[158,159]. In addition, genome-wide unbiased off-target profiling analysis such as GUIDE-seq could be used to evaluate the safety of gRNAs used to target *PRDM1* and *NR4A3*[160,161].

Multiplex genome editing can also induce complex chromosomal rearrangements between double-strand break sites[153,156]. TALEN-mediated dual gene editing of *TRAC*

and *CD52* and CRISPR/Cas9-mediated triple editing of *TRAC*, *TRBC*, and *PDCD1* resulted in such chromosomal deletions and translocations[153,156]. However, the frequencies of chromosomal rearrangements decreased over time during cell product manufacturing and following infusion into patients, suggesting that these rearrangements may compromise the fitness of aberrantly-edited T-cells[153,156]. In this study, we confirmed that *PRDM1*/*NR4A3* KO CAR T-cells do not exhibit antigen-independent proliferation and show reduced viability in the absence of target antigen, suggesting the double KO strategy does not induce malignant transformation (**Figure 4.3H**). However long-term *in vivo* studies are required to thoroughly monitor the frequencies of chromosomal translocations in engineered cells over time to determine whether *PRDM1*/*NR4A3* KO CAR T-cells attain antigen-independent hyper-proliferative functions.

Mechanism of BLIMP1-mediated T-cell differentiation.

In this study, we demonstrated that *PRDM1* expression accelerates attrition of T-cell memory differentiation and stemness (**Figure 3.3 and 3.4**). The suppression of this early memory state is mediated by repression of *TCF7*, as *TCF7* double KO diminished expression of early memory marker expression, proliferative capacity, and the polyfunctionality of *PRDM1* KO CAR T-cells (**Figure 3.4**). However, it is still unclear whether *PRDM1* disruption can have similar memory-enhancing effect in terminally differentiated effector or exhausted T-cells. During progression of cancer, T-cells often lose stemness and proliferative capacity which can lead to CAR T-cell product manufacturing failure and poor clinical outcome following infusion[8,50,51]. Thus, there is huge unmet needs in the setting of re-differentiating effector or exhausted cells isolated from patients to highly potent naïve or memory-like T-cells. Previous acute LCMV infection studies used constitutive *Prdm1* knockout models, which make it challenging to determine which T-cell differentiation stage(s) *Prdm1* affects[40,82]. Recently, Yoshikawa *et al*. demonstrated that *PRDM1* disruption in human CAR T-cells which were continuously activated with target antigen increased expression of surface memory markers, including CCR7, CD62L, and CD28[121]. Consistent with this finding, when *PRDM1* is deleted in lung or gynecologic cancer-infiltrating T-cells, the frequencies of CD62L and CCR7-positive CD8 T-cells were increased, and *PRDM1* KO tumor-infiltrating T-cells showed higher polyfunctionality. These results suggest that *PRDM1* knockout may partially restore the memory phenotype of already differentiated effector cells. One caveat, however, is that T-cells used in these mechanistic studies were

comprised of a heterogeneous mixture of T-cells consisting of both memory and effector cells. Therefore, it is unclear whether *PRDM1* KO simply preserved the memory phenotype of less differentiated memory T-cells or rescued the memory phenotype of terminally differentiated T-cells. Investigation of immunophenotype after deletion of *PRDM1* in homogeneous effector or memory T-cell populations might reveal whether a *PRDM1* KO strategy can truly restore the early memory differentiation potential of terminally differentiated T-cells and in which development stage BLIMP1 is involved.

Mechanism of compensatory exhaustion induced by *PRDM1* knockout.

Herein, we found that *PRDM1* disruption in T-cells leads to upregulation of genes encoding multiple exhaustion-related transcription factors, including those belonging to the *TOX* and *NR4A* families (**Figure 4.2**). This compensatory exhaustion was accompanied by increased chromatin accessibility in exhaustion-related genes and co-localization of a BLIMP1 binding motif in these open chromatin regions (**Figure 4.6**). In addition, in **Figure 4.8**, we show that the impaired cytolytic activity of *PRDM1* KO CAR T-cells led to delayed tumor clearance. This increased exposure to target antigen subsequently induced an NFAT-mediated exhaustion pathway, and NFAT binding motifs were co-localized with an open chromatin region of TOX2 (**Figure 4.6D**). All together, these data suggest that BLIMP1 may be involves in the epigenetic regulation of a battery of exhaustion-associated genes, however, the precise molecular and epigenetic underpinnings of BLIMP1-mediated regulation of these gene targets requires further elucidation.

BLIMP1 contains five Krüppel-like zinc finger DNA binding domains at the C-terminus, which enables BLIMP1 binding to promoter regions (**Figure 5.2A**)[162-165]. BLIMP1 also recruits chromatin-modifying factors, such as G9a and HDAC2, to its target locus Il2ra and Cd27 through its proline-rich region located between PR and zinc finger domains. The recruitment of these enzymes increases repressive H3 deacetylation and H3-H9 trimethylation of target genes, which represses gene expression[166,167]. Similarly, BLIMP1 recruits LSD1 and EZH2 to regulate *Pdcd1*, *Spib*, *Tlr9*, *Klf2*, and *Btg1* in CD8 T-cells and B-cells[168,169]. These previous findings suggest that BLIMP1 is

not only a transcriptional repressor, but also a key epigenetic regulator which directly regulates immune cell differentiation (**Figure 5.2B**). Chromatin immunoprecipitation sequencing along with ATAC sequencing would determine whether BLIMP1 directly binds to exhaustion gene regions to repress gene expression. Furthermore, co-immunoprecipitation experiments will elucidate which transcription factors or epigenetic writers cooperate with BLIMP1 to regulate exhaustion genes during chronic stimulation.

Conclusion

In summary, the work presented in this thesis has helped to develop an innovative approach to address T-cell intrinsic resistance mechanisms in the setting of cellular immunotherapies for cancer. The reciprocal nature of BLIMP1 and NR4A3 regulation on T-cell fate and function is of great interest and, to our knowledge, unique. Prior gene editing approaches to improve the efficacy of CAR T-cell therapy have exclusively focused on disrupting targets to either prevent differentiation or ameliorate exhaustion. Continued work on the utility, safety and mechanism(s) of action of this new strategy will undoubtedly prove to be timely and important. Additionally, we provided further insight on how BLIMP1 regulates memory T-cell differentiation, stemness and adaptive exhaustion pathways. We made several novel findings through completion of these studies, including i) elucidation of the cellular and molecular features of CAR T-cell products associated with antitumor responses in both hematopoietic and non-hematopoietic malignancies , ii) development of a BLIMP1/NR4A3 dual-KO strategy which can enrich clinically favorable CAR T-cell populations by enhancing T-cell stemness and diminishing exhaustion, and iii) discovery of an epigenetically-programmed mechanism of compensatory exhaustion induced by *PRDM1* disruption. Collectively, our data present a new view on the reciprocal nature of T-cell stemness and exhaustion and highlight the need to carefully balance these cell states to generate 'best-in-class' CAR T-cell therapies for cancer and beyond.

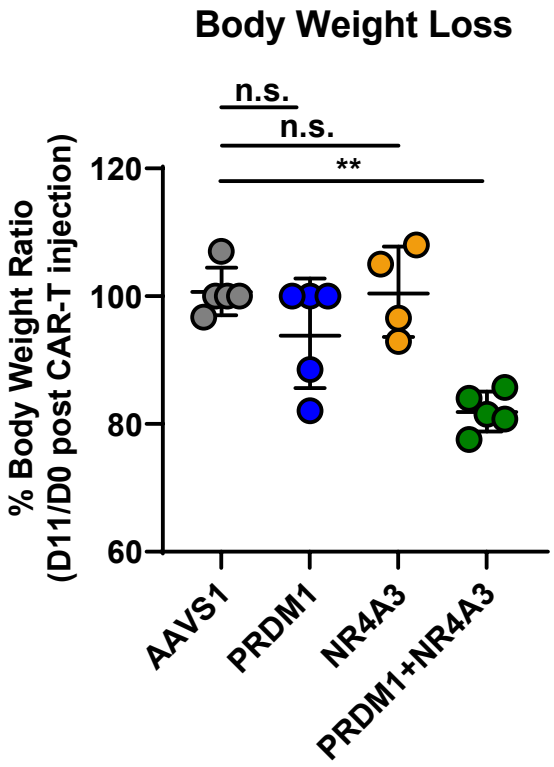

Figure 5.1. Body weight loss observed in PRDM1/NR4A3 dual-KO CAR T-cell-treated mice.

Male NSG mice were intrafemorally injected with 2×10^5 PC3-PSMA tumor cells. On day 27, 2×10^5 PSMA CAR T-cells were injected intravenously. Body weight was assessed before and after CAR T-cell injection. Statistical analysis was conducted using a Mann Whitney U test; mean ± s.e.m shown. *$P < 0.05$, *$P < 0.01$, ***$P < 0.001$, n.s.: not significant.

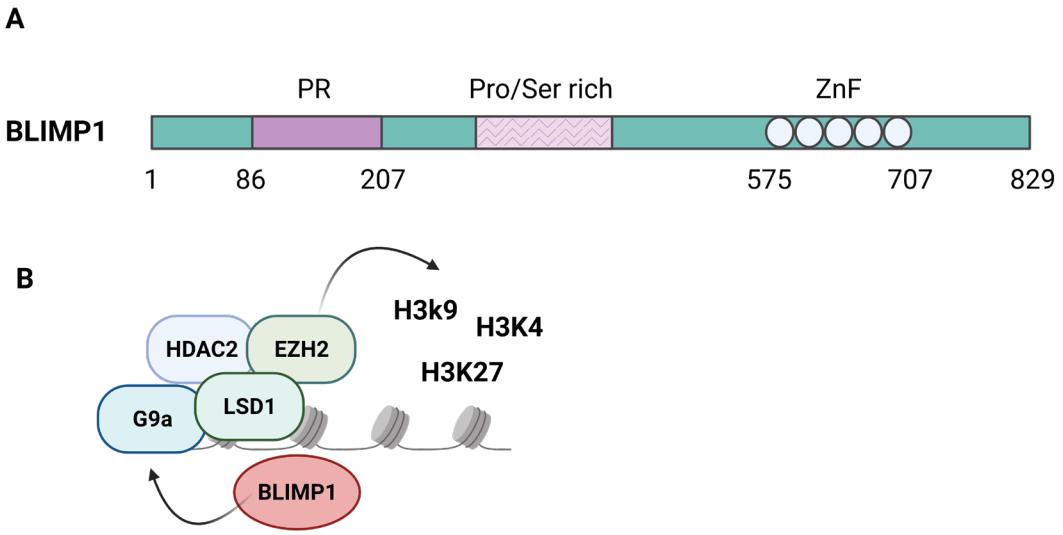

Figure 5.2 BLIMP1-mediated gene regulation.

A schematic demonstrating how BLIMP1 epigenetically regulates gene expression. (**A**) BLIMP1 has a PR domain at the N-terminal portion of the protein, which is homologous to the Su(var)3-9, Enhancer-of-zeste and Trithorax (SET) domain found in histone methyltransferase families. Unlike the conventional SET domain, however, the PR domain of BLIMP1 does not possess histone methyltransferase activity. Five Krüppel-like zinc finger DNA binding domains are located at the C-terminal of the protein. The first two zinc finger domains are required for BLIMP1 binding to promoters. Between PR and zinc finger domains is a proline-rich region, which presumably interacts with various histone modification enzymes. (**B**) BLIMP1 regulates target genes transcription by recruiting chromatin-modification proteins and transcription factors that form repressive histone modifications and chromatin structure, such as H3 deacetylation and H3-H9

trimethylation, and H3K4/H3K9 demethylation. The epigenetic regulators involved in this process include G9a, HDAC2, EZH2, and LSD1. Through these epigenetic regulatory mechanisms, BLIMP1 is known to modulate the differentiation of T-cells and B-cells.

BIBLIOGRAPHY

1 Gross, G., Waks, T. & Eshhar, Z. Expression of immunoglobulin-T-cell receptor chimeric molecules as functional receptors with antibody-type specificity. *Proc Natl Acad Sci U S A* **86**, 10024-10028, doi:10.1073/pnas.86.24.10024 (1989).

2 Till, B. G. *et al.* Adoptive immunotherapy for indolent non-Hodgkin lymphoma and mantle cell lymphoma using genetically modified autologous CD20-specific T cells. *Blood* **112**, 2261-2271, doi:10.1182/blood-2007-12-128843 (2008).

3 Eshhar, Z., Waks, T., Gross, G. & Schindler, D. G. Specific activation and targeting of cytotoxic lymphocytes through chimeric single chains consisting of antibody-binding domains and the gamma or zeta subunits of the immunoglobulin and T-cell receptors. *Proc Natl Acad Sci U S A* **90**, 720-724, doi:10.1073/pnas.90.2.720 (1993).

4 Zhao, Z. *et al.* Structural Design of Engineered Costimulation Determines Tumor Rejection Kinetics and Persistence of CAR T Cells. *Cancer Cell* **28**, 415-428, doi:10.1016/j.ccell.2015.09.004 (2015).

5 Maude, S. L. *et al.* Tisagenlecleucel in Children and Young Adults with B-Cell Lymphoblastic Leukemia. *N Engl J Med* **378**, 439-448, doi:10.1056/NEJMoa1709866 (2018).

6 Neelapu, S. S. *et al.* Axicabtagene Ciloleucel CAR T-Cell Therapy in Refractory Large B-Cell Lymphoma. *N Engl J Med* **377**, 2531-2544, doi:10.1056/NEJMoa1707447 (2017).

7 Peters, F. S., Strefford, J. C., Eldering, E. & Kater, A. P. T-cell dysfunction in chronic lymphocytic leukemia from an epigenetic perspective. *Haematologica* **106**, 1234-1243, doi:10.3324/haematol.2020.267914 (2021).

8 van Bruggen, J. A. C. *et al.* Chronic lymphocytic leukemia cells impair mitochondrial fitness in CD8(+) T cells and impede CAR T-cell efficacy. *Blood* **134**, 44-58, doi:10.1182/blood.2018885863 (2019).

9 Porter, D. L. *et al.* Chimeric antigen receptor T cells persist and induce sustained remissions in relapsed refractory chronic lymphocytic leukemia. *Sci Transl Med* **7**, 303ra139, doi:10.1126/scitranslmed.aac5415 (2015).

10 Fraietta, J. A. *et al.* Determinants of response and resistance to CD19 chimeric antigen receptor (CAR) T cell therapy of chronic lymphocytic leukemia. *Nat Med* **24**, 563-571, doi:10.1038/s41591-018-0010-1 (2018).

11 Porter, D. L. *et al.* Chimeric antigen receptor T cells persist and induce sustained remissions in relapsed refractory chronic lymphocytic leukemia. *Science Translational Medicine* **7**, 303ra139-303ra139, doi:10.1126/scitranslmed.aac5415 (2015).

12 Neelapu, S. S. *et al.* Axicabtagene Ciloleucel CAR T-Cell Therapy in Refractory Large B-Cell Lymphoma. *The New England Journal of Medicine* **377**, 2531-2544, doi:10.1056/NEJMoa1707447 (2017).

13 Maude, S. L. *et al.* Tisagenlecleucel in Children and Young Adults with B-Cell Lymphoblastic Leukemia. *The New England Journal of Medicine* **378**, 439-448, doi:10.1056/NEJMoa1709866 (2018).

14 Raje, N. *et al.* Anti-BCMA CAR T-Cell Therapy bb2121 in Relapsed or Refractory Multiple Myeloma. *N Engl J Med* **380**, 1726-1737, doi:10.1056/NEJMoa1817226 (2019).

15 Cohen, A. D. *et al.* B cell maturation antigen-specific CAR T cells are clinically active in multiple myeloma. *J Clin Invest* **129**, 2210-2221, doi:10.1172/JCI126397 (2019).

16 Frey, N. V. *et al.* Long-Term Outcomes From a Randomized Dose Optimization Study of Chimeric Antigen Receptor Modified T Cells in Relapsed Chronic Lymphocytic Leukemia. *J Clin Oncol* **38**, 2862-2871, doi:10.1200/JCO.19.03237 (2020).

17 Chong, E. A., Ruella, M., Schuster, S. J. & Lymphoma Program Investigators at the University of, P. Five-Year Outcomes for Refractory B-Cell Lymphomas with CAR T-Cell Therapy. *N Engl J Med* **384**, 673-674, doi:10.1056/NEJMc2030164 (2021).

18 Maude, S. L. *et al.* Chimeric antigen receptor T cells for sustained remissions in leukemia. *N Engl J Med* **371**, 1507-1517, doi:10.1056/NEJMoa1407222 (2014).

19 Finney, O. C. *et al.* CD19 CAR T cell product and disease attributes predict leukemia remission durability. *J Clin Invest* **129**, 2123-2132, doi:10.1172/JCI125423 (2019).

20 Chen, G. M. *et al.* Integrative Bulk and Single-Cell Profiling of Premanufacture T-cell Populations Reveals Factors Mediating Long-Term Persistence of CAR T-cell Therapy. *Cancer Discov* **11**, 2186-2199, doi:10.1158/2159-8290.CD-20-1677 (2021).

21 Deng, Q. *et al.* Characteristics of anti-CD19 CAR T cell infusion products associated with efficacy and toxicity in patients with large B cell lymphomas. *Nat Med* **26**, 1878-1887, doi:10.1038/s41591-020-1061-7 (2020).

22 Long, K. B. *et al.* CAR T Cell Therapy of Non-hematopoietic Malignancies: Detours on the Road to Clinical Success. *Front Immunol* **9**, 2740, doi:10.3389/fimmu.2018.02740 (2018).

23 Yong, C. S. M. *et al.* CAR T-cell therapy of solid tumors. *Immunol Cell Biol* **95**, 356-363, doi:10.1038/icb.2016.128 (2017).

24 Newick, K., O'Brien, S., Moon, E. & Albelda, S. M. CAR T Cell Therapy for Solid Tumors. *Annu Rev Med* **68**, 139-152, doi:10.1146/annurev-med-062315-120245 (2017).

25 Hou, A. J., Chen, L. C. & Chen, Y. Y. Navigating CAR-T cells through the solid-tumour microenvironment. *Nat Rev Drug Discov* **20**, 531-550, doi:10.1038/s41573-021-00189-2 (2021).

26 Sen, D. R. *et al.* The epigenetic landscape of T cell exhaustion. *Science* **354**, 1165-1169, doi:10.1126/science.aae0491 (2016).

27 Long, A. H. *et al.* 4-1BB costimulation ameliorates T cell exhaustion induced by tonic signaling of chimeric antigen receptors. *Nat Med* **21**, 581-590, doi:10.1038/nm.3838 (2015).

28 Wen, S. *et al.* TCF-1 maintains CD8(+) T cell stemness in tumor microenvironment. *J Leukoc Biol* **110**, 585-590, doi:10.1002/JLB.5MR1120-778R (2021).

29 Martin, M. D. & Badovinac, V. P. Defining Memory CD8 T Cell. *Front Immunol* **9**, 2692, doi:10.3389/fimmu.2018.02692 (2018).

30 Caccamo, N., Joosten, S. A., Ottenhoff, T. H. M. & Dieli, F. Atypical Human Effector/Memory CD4(+) T Cells With a Naive-Like Phenotype. *Front Immunol* **9**, 2832, doi:10.3389/fimmu.2018.02832 (2018).

31 Golubovskaya, V. & Wu, L. Different Subsets of T Cells, Memory, Effector Functions, and CAR-T Immunotherapy. *Cancers (Basel)* **8**, doi:10.3390/cancers8030036 (2016).

32 Sallusto, F., Lenig, D., Forster, R., Lipp, M. & Lanzavecchia, A. Two subsets of memory T lymphocytes with distinct homing potentials and effector functions. *Nature* **401**, 708-712, doi:10.1038/44385 (1999).

33 Bachmann, M. F., Wolint, P., Schwarz, K., Jager, P. & Oxenius, A. Functional properties and lineage relationship of CD8+ T cell subsets identified by expression of IL-7 receptor alpha and CD62L. *J Immunol* **175**, 4686-4696, doi:10.4049/jimmunol.175.7.4686 (2005).

34 Slutter, B., Pewe, L. L., Kaech, S. M. & Harty, J. T. Lung airway-surveilling CXCR3(hi) memory CD8(+) T cells are critical for protection against influenza A virus. *Immunity* **39**, 939-948, doi:10.1016/j.immuni.2013.09.013 (2013).

35 Cui, W., Liu, Y., Weinstein, J. S., Craft, J. & Kaech, S. M. An interleukin-21-interleukin-10-STAT3 pathway is critical for functional maturation of memory CD8+ T cells. *Immunity* **35**, 792-805, doi:10.1016/j.immuni.2011.09.017 (2011).

36 Ichii, H., Sakamoto, A., Kuroda, Y. & Tokuhisa, T. Bcl6 acts as an amplifier for the generation and proliferative capacity of central memory CD8+ T cells. *J Immunol* **173**, 883-891, doi:10.4049/jimmunol.173.2.883 (2004).

37 Yang, C. Y. *et al.* The transcriptional regulators Id2 and Id3 control the formation of distinct memory CD8+ T cell subsets. *Nat Immunol* **12**, 1221-1229, doi:10.1038/ni.2158 (2011).

38 Intlekofer, A. M. *et al.* Effector and memory CD8+ T cell fate coupled by T-bet and eomesodermin. *Nat Immunol* **6**, 1236-1244, doi:10.1038/ni1268 (2005).

39 Cannarile, M. A. *et al.* Transcriptional regulator Id2 mediates CD8+ T cell immunity. *Nat Immunol* **7**, 1317-1325, doi:10.1038/ni1403 (2006).

40 Rutishauser, R. L. *et al.* Transcriptional repressor Blimp-1 promotes CD8(+) T cell terminal differentiation and represses the acquisition of central memory T cell properties. *Immunity* **31**, 296-308, doi:10.1016/j.immuni.2009.05.014 (2009).

41 Joshi, N. S. *et al.* Inflammation directs memory precursor and short-lived effector CD8(+) T cell fates via the graded expression of T-bet transcription factor. *Immunity* **27**, 281-295, doi:10.1016/j.immuni.2007.07.010 (2007).

42 Kishton, R. J., Vodnala, S. K., Vizcardo, R. & Restifo, N. P. Next generation immunotherapy: enhancing stemness of polyclonal T cells to improve anti-tumor activity. *Curr Opin Immunol* **74**, 39-45, doi:10.1016/j.coi.2021.10.001 (2022).

43 Gautam, S. *et al.* The transcription factor c-Myb regulates CD8(+) T cell stemness and antitumor immunity. *Nat Immunol* **20**, 337-349, doi:10.1038/s41590-018-0311-z (2019).

44 Jeannet, G. *et al.* Essential role of the Wnt pathway effector Tcf-1 for the establishment of functional CD8 T cell memory. *Proc Natl Acad Sci U S A* **107**, 9777-9782, doi:10.1073/pnas.0914127107 (2010).

45 Im, S. J. *et al.* Defining CD8+ T cells that provide the proliferative burst after PD-1 therapy. *Nature* **537**, 417-421, doi:10.1038/nature19330 (2016).

46 Siddiqui, I. *et al.* Intratumoral Tcf1(+)PD-1(+)CD8(+) T Cells with Stem-like Properties Promote Tumor Control in Response to Vaccination and Checkpoint Blockade Immunotherapy. *Immunity* **50**, 195-211 e110, doi:10.1016/j.immuni.2018.12.021 (2019).

47 Sade-Feldman, M. *et al.* Defining T Cell States Associated with Response to Checkpoint Immunotherapy in Melanoma. *Cell* **175**, 998-1013 e1020, doi:10.1016/j.cell.2018.10.038 (2018).

48 Gattinoni, L. *et al.* A human memory T cell subset with stem cell-like properties. *Nat Med* **17**, 1290-1297, doi:10.1038/nm.2446 (2011).

49 Vodnala, S. K. *et al.* T cell stemness and dysfunction in tumors are triggered by a common mechanism. *Science* **363**, doi:10.1126/science.aau0135 (2019).

50 Riches, J. C. *et al.* T cells from CLL patients exhibit features of T-cell exhaustion but retain capacity for cytokine production. *Blood* **121**, 1612-1621, doi:10.1182/blood-2012-09-457531 (2013).

51 Funk, C. R. *et al.* PI3Kdelta/gamma inhibition promotes human CART cell epigenetic and metabolic reprogramming to enhance antitumor cytotoxicity. *Blood* **139**, 523-537, doi:10.1182/blood.2021011597 (2022).

52 Blaeschke, F. *et al.* Induction of a central memory and stem cell memory phenotype in functionally active CD4(+) and CD8(+) CAR T cells produced in an automated good manufacturing practice system for the treatment of CD19(+) acute lymphoblastic leukemia. *Cancer Immunol Immunother* **67**, 1053-1066, doi:10.1007/s00262-018-2155-7 (2018).

53 Ghassemi, S. *et al.* Reducing Ex Vivo Culture Improves the Antileukemic Activity of Chimeric Antigen Receptor (CAR) T Cells. *Cancer Immunol Res* **6**, 1100-1109, doi:10.1158/2326-6066.CIR-17-0405 (2018).

54 Ghassemi, S. *et al.* Rapid manufacturing of non-activated potent CAR T cells. *Nat Biomed Eng* **6**, 118-128, doi:10.1038/s41551-021-00842-6 (2022).

55 Shin, H., Blackburn, S. D., Blattman, J. N. & Wherry, E. J. Viral antigen and extensive division maintain virus-specific CD8 T cells during chronic infection. *J Exp Med* **204**, 941-949, doi:10.1084/jem.20061937 (2007).

56 Blackburn, S. D. *et al.* Coregulation of CD8+ T cell exhaustion by multiple inhibitory receptors during chronic viral infection. *Nat Immunol* **10**, 29-37, doi:10.1038/ni.1679 (2009).

57 Wherry, E. J., Blattman, J. N., Murali-Krishna, K., van der Most, R. & Ahmed, R. Viral persistence alters CD8 T-cell immunodominance and tissue distribution and results in distinct stages of functional impairment. *J Virol* **77**, 4911-4927, doi:10.1128/jvi.77.8.4911-4927.2003 (2003).

58 Pauken, K. E. *et al.* Epigenetic stability of exhausted T cells limits durability of reinvigoration by PD-1 blockade. *Science* **354**, 1160-1165, doi:10.1126/science.aaf2807 (2016).

59 Khan, O. *et al.* TOX transcriptionally and epigenetically programs CD8(+) T cell exhaustion. *Nature* **571**, 211-218, doi:10.1038/s41586-019-1325-x (2019).

60 Terakura, S. *et al.* Generation of CD19-chimeric antigen receptor modified CD8+ T cells derived from virus-specific central memory T cells. *Blood* **119**, 72-82, doi:10.1182/blood-2011-07-366419 (2012).

61 Wherry, E. J., Blattman, J. N., Murali-Krishna, K., van der Most, R. & Ahmed, R. Viral Persistence Alters CD8 T-Cell Immunodominance and Tissue Distribution and Results in Distinct Stages of Functional Impairment. *Journal of Virology* **77**, 4911-4927, doi:10.1128/JVI.77.8.4911-4927.2003 (2003).

62 Yao, C. *et al.* Single-cell RNA-seq reveals TOX as a key regulator of CD8(+) T cell persistence in chronic infection. *Nat Immunol* **20**, 890-901, doi:10.1038/s41590-019-0403-4 (2019).

63 Pellegrini, M. *et al.* Adjuvant IL-7 antagonizes multiple cellular and molecular inhibitory networks to enhance immunotherapies. *Nat Med* **15**, 528-536, doi:10.1038/nm.1953 (2009).

64 Kurtulus, S. *et al.* Checkpoint Blockade Immunotherapy Induces Dynamic Changes in PD-1(-)CD8(+) Tumor-Infiltrating T Cells. *Immunity* **50**, 181-194 e186, doi:10.1016/j.immuni.2018.11.014 (2019).

65 Chen, Z. *et al.* TCF-1-Centered Transcriptional Network Drives an Effector versus Exhausted CD8 T Cell-Fate Decision. *Immunity* **51**, 840-855 e845, doi:10.1016/j.immuni.2019.09.013 (2019).

66 Miller, B. C. *et al.* Subsets of exhausted CD8(+) T cells differentially mediate tumor control and respond to checkpoint blockade. *Nat Immunol* **20**, 326-336, doi:10.1038/s41590-019-0312-6 (2019).

67 Sommermeyer, D. *et al.* Chimeric antigen receptor-modified T cells derived from defined CD8+ and CD4+ subsets confer superior antitumor reactivity in vivo. *Leukemia* **30**, 492-500, doi:10.1038/leu.2015.247 (2016).

68 Singh, N., Perazzelli, J., Grupp, S. A. & Barrett, D. M. Early memory phenotypes drive T cell proliferation in patients with pediatric malignancies. *Sci Transl Med* **8**, 320ra323, doi:10.1126/scitranslmed.aad5222 (2016).

69 Chen, Z. *et al.* TCF-1-Centered Transcriptional Network Drives an Effector versus Exhausted CD8 T Cell-Fate Decision. *Immunity* **51**, 840-855.e845, doi:10.1016/j.immuni.2019.09.013 (2019).

70 Kurtulus, S. *et al.* Checkpoint Blockade Immunotherapy Induces Dynamic Changes in PD-1-CD8+ Tumor-Infiltrating T Cells. *Immunity* **50**, 181-194.e186, doi:10.1016/j.immuni.2018.11.014 (2019).

71 Martinez, G. J. *et al.* The transcription factor NFAT promotes exhaustion of activated CD8(+) T cells. *Immunity* **42**, 265-278, doi:10.1016/j.immuni.2015.01.006 (2015).

72 Lynn, R. C. *et al.* c-Jun overexpression in CAR T cells induces exhaustion resistance. *Nature* **576**, 293-300, doi:10.1038/s41586-019-1805-z (2019).

73 Seo, H. *et al.* TOX and TOX2 transcription factors cooperate with NR4A transcription factors to impose CD8(+) T cell exhaustion. *Proc Natl Acad Sci U S A* **116**, 12410-12415, doi:10.1073/pnas.1905675116 (2019).

74 Chen, J. *et al.* NR4A transcription factors limit CAR T cell function in solid tumours. *Nature* **567**, 530-534, doi:10.1038/s41586-019-0985-x (2019).

75 Liu, X. *et al.* Genome-wide analysis identifies NR4A1 as a key mediator of T cell dysfunction. *Nature* **567**, 525-529, doi:10.1038/s41586-019-0979-8 (2019).

76 Seo, H. *et al.* BATF and IRF4 cooperate to counter exhaustion in tumor-infiltrating CAR T cells. *Nat Immunol* **22**, 983-995, doi:10.1038/s41590-021-00964-8 (2021).

77 Eyquem, J. *et al.* Targeting a CAR to the TRAC locus with CRISPR/Cas9 enhances tumour rejection. *Nature* **543**, 113-117, doi:10.1038/nature21405 (2017).

78 Weber, E. W. *et al.* Transient rest restores functionality in exhausted CAR-T cells through epigenetic remodeling. *Science* **372**, doi:10.1126/science.aba1786 (2021).

79 Feucht, J. *et al.* Calibration of CAR activation potential directs alternative T cell fates and therapeutic potency. *Nat Med* **25**, 82-88, doi:10.1038/s41591-018-0290-5 (2019).

80 Wu, T. *et al.* TCF1 Is Required for the T Follicular Helper Cell Response to Viral Infection. *Cell Rep* **12**, 2099-2110, doi:10.1016/j.celrep.2015.08.049 (2015).

81 Shin, H. *et al.* A role for the transcriptional repressor Blimp-1 in CD8(+) T cell exhaustion during chronic viral infection. *Immunity* **31**, 309-320, doi:10.1016/j.immuni.2009.06.019 (2009).

82 Shin, H. M. *et al.* Epigenetic modifications induced by Blimp-1 Regulate CD8(+) T cell memory progression during acute virus infection. *Immunity* **39**, 661-675, doi:10.1016/j.immuni.2013.08.032 (2013).

83 Smith, M. *et al.* Gut microbiome correlates of response and toxicity following anti-CD19 CAR T cell therapy. *Nat Med* **28**, 713-723, doi:10.1038/s41591-022-01702-9 (2022).

84 Singh, N. *et al.* Impaired Death Receptor Signaling in Leukemia Causes Antigen-Independent Resistance by Inducing CAR T-cell Dysfunction. *Cancer Discov* **10**, 552-567, doi:10.1158/2159-8290.CD-19-0813 (2020).

85 Li, M. *et al.* The differential effects of tumor burdens on predicting the net benefits of ssCART-19 cell treatment on r/r B-ALL patients. *Sci Rep* **12**, 378, doi:10.1038/s41598-021-04296-3 (2022).

86 Deng, Q. *et al.* Characteristics of anti-CD19 CAR T cell infusion products associated with efficacy and toxicity in patients with large B cell lymphomas. *Nature Medicine* **26**, 1878-1887, doi:10.1038/s41591-020-1061-7 (2020).

87 Jiang, Y. *et al.* Prospect of Prostate Cancer Treatment: Armed CAR-T or Combination Therapy. *Cancers (Basel)* **14**, doi:10.3390/cancers14040967 (2022).

88 Schepisi, G. *et al.* CAR-T cell therapy: a potential new strategy against prostate cancer. *J Immunother Cancer* **7**, 258, doi:10.1186/s40425-019-0741-7 (2019).

89 Smith, M. R. *et al.* Natural history of rising serum prostate-specific antigen in men with castrate nonmetastatic prostate cancer. *J Clin Oncol* **23**, 2918-2925, doi:10.1200/JCO.2005.01.529 (2005).

90 Beer, T. M. *et al.* Enzalutamide in metastatic prostate cancer before chemotherapy. *N Engl J Med* **371**, 424-433, doi:10.1056/NEJMoa1405095 (2014).

91 Ryan, C. J. *et al.* Abiraterone in metastatic prostate cancer without previous chemotherapy. *N Engl J Med* **368**, 138-148, doi:10.1056/NEJMoa1209096 (2013).

92 de Bono, J. S. *et al.* Abiraterone and increased survival in metastatic prostate cancer. *N Engl J Med* **364**, 1995-2005, doi:10.1056/NEJMoa1014618 (2011).

93 Antonarakis, E. S. *et al.* AR-V7 and resistance to enzalutamide and abiraterone in prostate cancer. *N Engl J Med* **371**, 1028-1038, doi:10.1056/NEJMoa1315815 (2014).

94 Kantoff, P. W. *et al.* Sipuleucel-T immunotherapy for castration-resistant prostate cancer. *N Engl J Med* **363**, 411-422, doi:10.1056/NEJMoa1001294 (2010).

95 Hafron, J. M. *et al.* Real-World Effectiveness of Sipuleucel-T on Overall Survival in Men with Advanced Prostate Cancer Treated with Androgen Receptor-Targeting Agents. *Adv Ther* **39**, 2515-2532, doi:10.1007/s12325-022-02085-6 (2022).

96 Hansen, A. R. *et al.* Pembrolizumab for advanced prostate adenocarcinoma: findings of the KEYNOTE-028 study. *Ann Oncol* **29**, 1807-1813, doi:10.1093/annonc/mdy232 (2018).

97 Narayan, V. *et al.* PSMA-targeting TGFbeta-insensitive armored CAR T cells in metastatic castration-resistant prostate cancer: a phase 1 trial. *Nat Med* **28**, 724-734, doi:10.1038/s41591-022-01726-1 (2022).

98 Ahel, J., Hudorovic, N., Vicic-Hudorovic, V. & Nikles, H. Tgf-Beta in the Natural History of Prostate Cancer. *Acta Clin Croat* **58**, 128-138, doi:10.20471/acc.2019.58.01.17 (2019).

99 Junghans, R. P. *et al.* Phase I Trial of Anti-PSMA Designer CAR-T Cells in Prostate Cancer: Possible Role for Interacting Interleukin 2-T Cell Pharmacodynamics as a Determinant of Clinical Response. *Prostate* **76**, 1257-1270, doi:10.1002/pros.23214 (2016).

100 Fedorov, V. D., Themeli, M. & Sadelain, M. PD-1- and CTLA-4-based inhibitory chimeric antigen receptors (iCARs) divert off-target immunotherapy responses. *Science translational medicine* **5**, 215ra172, doi:10.1126/scitranslmed.3006597 (2013).

101 Kasakovski, D., Xu, L. & Li, Y. T cell senescence and CAR-T cell exhaustion in hematological malignancies. *Journal of hematology & oncology* **11**, 91, doi:10.1186/s13045-018-0629-x (2018).

102 Xu, Y. *et al.* Closely related T-memory stem cells correlate with in vivo expansion of CAR.CD19-T cells and are preserved by IL-7 and IL-15. *Blood* **123**, 3750-3759, doi:10.1182/blood-2014-01-552174 (2014).

103 Hurton, L. V. *et al.* Tethered IL-15 augments antitumor activity and promotes a stem-cell memory subset in tumor-specific T cells. *Proc Natl Acad Sci U S A* **113**, E7788-e7797, doi:10.1073/pnas.1610544113 (2016).

104 Long, A. H. *et al.* 4-1BB costimulation ameliorates T cell exhaustion induced by tonic signaling of chimeric antigen receptors. *Nature Medicine* **21**, 581-590, doi:10.1038/nm.3838 (2015).

105 Pais Ferreira, D. *et al.* Central memory CD8(+) T cells derive from stem-like Tcf7(hi) effector cells in the absence of cytotoxic differentiation. *Immunity* **53**, 985-1000 e1011, doi:10.1016/j.immuni.2020.09.005 (2020).

106 Utzschneider, D. T. *et al.* T Cell Factor 1-Expressing Memory-like CD8(+) T Cells Sustain the Immune Response to Chronic Viral Infections. *Immunity* **45**, 415-427, doi:10.1016/j.immuni.2016.07.021 (2016).

107 Chen, G. M. *et al.* Integrative Bulk and Single-Cell Profiling of Premanufacture T-cell Populations Reveals Factors Mediating Long-Term Persistence of CAR T-cell Therapy. *Cancer Discovery* **11**, 2186-2199, doi:10.1158/2159-8290.Cd-20-1677 (2021).

108 Rutishauser, R. L. *et al.* Blimp-1 promotes terminal differentiation of virus-specific CD8 T cells and represses the acquisition of central memory T cell properties. *Immunity* **31**, 296-308, doi:10.1016/j.immuni.2009.05.014 (2009).

109 Shin, H. *et al.* A role for the transcriptional repressor Blimp-1 in CD8(+) T cell exhaustion during chronic viral infection. *Immunity* **31**, 309-320, doi:10.1016/j.immuni.2009.06.019 (2009).

110 Chihara, N. *et al.* Induction and transcriptional regulation of the co-inhibitory gene module in T cells. *Nature* **558**, 454-459, doi:10.1038/s41586-018-0206-z (2018).

111 Wu, T. *et al.* TCF1 Is Required for the T Follicular Helper Cell Response to Viral Infection. *Cell Reports* **12**, 2099-2110, doi:10.1016/j.celrep.2015.08.049 (2015).

112 Differentiation and Persistence of Memory CD8+ T Cells Depend on T Cell Factor 1. *Immunity* **33**, 229-240, doi:10.1016/j.immuni.2010.08.002 (2010).

113 Melenhorst, J. J. *et al.* Decade-long leukaemia remissions with persistence of CD4(+) CAR T cells. *Nature* **602**, 503-509, doi:10.1038/s41586-021-04390-6 (2022).

114 Jackson, Z. *et al.* Sequential single cell transcriptional and protein marker profiling reveals TIGIT as a marker of CD19 CAR-T cell dysfunction in patients with non-Hodgkin's lymphoma. *Cancer Discov*, doi:10.1158/2159-8290.CD-21-1586 (2022).

115 Chen, Y. *et al.* Engineering Human Stem Cell Lines with Inducible Gene Knockout using CRISPR/Cas9. *Cell Stem Cell* **17**, 233-244, doi:10.1016/j.stem.2015.06.001 (2015).

116 Ji, Y. *et al.* Repression of the DNA-binding inhibitor Id3 by Blimp-1 limits CD8+ T cell memory formation. *Nature immunology* **12**, 1230-1237, doi:10.1038/ni.2153 (2011).

117 Wu, T. *et al.* The TCF1-Bcl6 axis counteracts type I interferon to repress exhaustion and maintain T cell stemness. *Science Immunology* **1**, eaai8593, doi:10.1126/sciimmunol.aai8593 (2016).

118 Gautam, S. *et al.* The transcription factor c-Myb regulates CD8+ T cell stemness and antitumor immunity. *Nature Immunology* **20**, 337-349, doi:10.1038/s41590-018-0311-z (2019).

119 Yoshikawa, T. *et al.* Genetic ablation of PRDM1 in antitumor T cells enhances therapeutic efficacy of adoptive immunotherapy. *Blood*, doi:10.1182/blood.2021012714 (2021).

120 Leong, Y. A. *et al.* CXCR5(+) follicular cytotoxic T cells control viral infection in B cell follicles. *Nat Immunol* **17**, 1187-1196, doi:10.1038/ni.3543 (2016).

121 Yoshikawa, T. *et al.* Genetic ablation of PRDM1 in antitumor T cells enhances therapeutic efficacy of adoptive immunotherapy. *Blood* **139**, 2156-2172, doi:10.1182/blood.2021012714 (2022).

122 Kloss, C. C. *et al.* Dominant-Negative TGF-β Receptor Enhances PSMA-Targeted Human CAR T Cell Proliferation And Augments Prostate Cancer Eradication. *Molecular Therapy* **26**, 1855-1866, doi:10.1016/j.ymthe.2018.05.003 (2018).

123 Milone, M. C. *et al.* Chimeric receptors containing CD137 signal transduction domains mediate enhanced survival of T cells and increased antileukemic efficacy in vivo. *Mol Ther* **17**, 1453-1464, doi:10.1038/mt.2009.83 (2009).

124 Fraietta, J. A. *et al.* Ibrutinib enhances chimeric antigen receptor T-cell engraftment and efficacy in leukemia. *Blood* **127**, 1117-1127, doi:10.1182/blood-2015-11-679134 (2016).

125 Miggelbrink, A. M. *et al.* CD4 T-Cell Exhaustion: Does It Exist and What Are Its Roles in Cancer? *Clin Cancer Res* **27**, 5742-5752, doi:10.1158/1078-0432.CCR-21-0206 (2021).

126 Tay, R. E., Richardson, E. K. & Toh, H. C. Revisiting the role of CD4(+) T cells in cancer immunotherapy-new insights into old paradigms. *Cancer Gene Ther* **28**, 5-17, doi:10.1038/s41417-020-0183-x (2021).

127 Shin, Hyun M. *et al.* Epigenetic Modifications Induced by Blimp-1 Regulate CD8+ T Cell Memory Progression during Acute Virus Infection. *Immunity* **39**, 661-675, doi:10.1016/j.immuni.2013.08.032 (2013).

128 Singh, N. *et al.* Impaired Death Receptor Signaling in Leukemia Causes Antigen-Independent Resistance by Inducing CAR T-cell Dysfunction. *Cancer Discovery* **10**, 552-567, doi:10.1158/2159-8290.CD-19-0813 (2020).

129 Khan, O. *et al.* TOX transcriptionally and epigenetically programs CD8+ T cell exhaustion. *Nature* **571**, 211-218, doi:10.1038/s41586-019-1325-x (2019).

130 Seo, H. *et al.* TOX and TOX2 transcription factors cooperate with NR4A transcription factors to impose CD8+ T cell exhaustion. *Proceedings of the National Academy of Sciences of the United States of America* **116**, 12410-12415, doi:10.1073/pnas.1905675116 (2019).

131 Haas, A. R. *et al.* Phase I Study of Lentiviral-Transduced Chimeric Antigen Receptor-Modified T Cells Recognizing Mesothelin in Advanced Solid Cancers. *Mol Ther* **27**, 1919-1929, doi:10.1016/j.ymthe.2019.07.015 (2019).

132 Jolma, A. *et al.* Multiplexed massively parallel SELEX for characterization of human transcription factor binding specificities. *Genome Research* **20**, 861-873, doi:10.1101/gr.100552.109 (2010).

133 Gumber, D. & Wang, L. D. Improving CAR-T immunotherapy: Overcoming the challenges of T cell exhaustion. *EBioMedicine* **77**, 103941, doi:10.1016/j.ebiom.2022.103941 (2022).

134 Rodriguez-Garcia, A., Palazon, A., Noguera-Ortega, E., Powell, D. J., Jr. & Guedan, S. CAR-T Cells Hit the Tumor Microenvironment: Strategies to Overcome Tumor Escape. *Front Immunol* **11**, 1109, doi:10.3389/fimmu.2020.01109 (2020).

135 Wherry, E. J. & Kurachi, M. Molecular and cellular insights into T cell exhaustion. *Nat Rev Immunol* **15**, 486-499, doi:10.1038/nri3862 (2015).

136 McGowan, E. *et al.* PD-1 disrupted CAR-T cells in the treatment of solid tumors: Promises and challenges. *Biomed Pharmacother* **121**, 109625, doi:10.1016/j.biopha.2019.109625 (2020).

137 Hu, W. *et al.* CRISPR/Cas9-mediated PD-1 disruption enhances human mesothelin-targeted CAR T cell effector functions. *Cancer Immunol Immunother* **68**, 365-377, doi:10.1007/s00262-018-2281-2 (2019).

138 Rupp, L. J. *et al.* CRISPR/Cas9-mediated PD-1 disruption enhances anti-tumor efficacy of human chimeric antigen receptor T cells. *Sci Rep* **7**, 737, doi:10.1038/s41598-017-00462-8 (2017).

139 Liu, X. *et al.* CRISPR-Cas9-mediated multiplex gene editing in CAR-T cells. *Cell Res* **27**, 154-157, doi:10.1038/cr.2016.142 (2017).

140 Odorizzi, P. M., Pauken, K. E., Paley, M. A., Sharpe, A. & Wherry, E. J. Genetic absence of PD-1 promotes accumulation of terminally differentiated exhausted CD8+ T cells. *J Exp Med* **212**, 1125-1137, doi:10.1084/jem.20142237 (2015).

141 Scott, A. C. *et al.* TOX is a critical regulator of tumour-specific T cell differentiation. *Nature* **571**, 270-274, doi:10.1038/s41586-019-1324-y (2019).

142 Watanabe, N. *et al.* Fine-tuning the CAR spacer improves T-cell potency. *Oncoimmunology* **5**, e1253656, doi:10.1080/2162402X.2016.1253656 (2016).

143 Wei, J. *et al.* PD-1 silencing impairs the anti-tumor function of chimeric antigen receptor modified T cells by inhibiting proliferation activity. *J Immunother Cancer* **7**, 209, doi:10.1186/s40425-019-0685-y (2019).

144 Majzner, R. G. *et al.* Tuning the Antigen Density Requirement for CAR T-cell Activity. *Cancer Discov* **10**, 702-723, doi:10.1158/2159-8290.CD-19-0945 (2020).

145 Li, J. *et al.* CD3 bispecific antibody-induced cytokine release is dispensable for cytotoxic T cell activity. *Sci Transl Med* **11**, doi:10.1126/scitranslmed.aax8861 (2019).

146 Hirayama, A. V. & Turtle, C. J. Toxicities of CD19 CAR-T cell immunotherapy. *Am J Hematol* **94**, S42-S49, doi:10.1002/ajh.25445 (2019).

147 Santomasso, B., Bachier, C., Westin, J., Rezvani, K. & Shpall, E. J. The Other Side of CAR T-Cell Therapy: Cytokine Release Syndrome, Neurologic Toxicity, and Financial Burden. *Am Soc Clin Oncol Educ Book* **39**, 433-444, doi:10.1200/EDBK_238691 (2019).

148 Xiao, X. *et al.* Mechanisms of cytokine release syndrome and neurotoxicity of CAR T-cell therapy and associated prevention and management strategies. *J Exp Clin Cancer Res* **40**, 367, doi:10.1186/s13046-021-02148-6 (2021).

149 Shimabukuro-Vornhagen, A. *et al.* Cytokine release syndrome. *J Immunother Cancer* **6**, 56, doi:10.1186/s40425-018-0343-9 (2018).

150 Lee, D. W. *et al.* ASTCT Consensus Grading for Cytokine Release Syndrome and Neurologic Toxicity Associated with Immune Effector Cells. *Biol Blood Marrow Transplant* **25**, 625-638, doi:10.1016/j.bbmt.2018.12.758 (2019).

151 Gust, J. *et al.* Endothelial Activation and Blood-Brain Barrier Disruption in Neurotoxicity after Adoptive Immunotherapy with CD19 CAR-T Cells. *Cancer Discov* **7**, 1404-1419, doi:10.1158/2159-8290.CD-17-0698 (2017).

152 Hay, K. A. *et al.* Factors associated with durable EFS in adult B-cell ALL patients achieving MRD-negative CR after CD19 CAR T-cell therapy. *Blood* **133**, 1652-1663, doi:10.1182/blood-2018-11-883710 (2019).

153 Stadtmauer, E. A. *et al.* CRISPR-engineered T cells in patients with refractory cancer. *Science* **367**, doi:10.1126/science.aba7365 (2020).

154 Jung, I. Y. & Lee, J. Unleashing the Therapeutic Potential of CAR-T Cell Therapy Using Gene-Editing Technologies. *Mol Cells* **41**, 717-723, doi:10.14348/molcells.2018.0242 (2018).

155 Cooper, M. L. *et al.* An "off-the-shelf" fratricide-resistant CAR-T for the treatment of T cell hematologic malignancies. *Leukemia* **32**, 1970-1983, doi:10.1038/s41375-018-0065-5 (2018).

156 Poirot, L. *et al.* Multiplex Genome-Edited T-cell Manufacturing Platform for "Off-the-Shelf" Adoptive T-cell Immunotherapies. *Cancer Res* **75**, 3853-3864, doi:10.1158/0008-5472.CAN-14-3321 (2015).

157 Osborn, M. J. *et al.* Evaluation of TCR Gene Editing Achieved by TALENs, CRISPR/Cas9, and megaTAL Nucleases. *Mol Ther* **24**, 570-581, doi:10.1038/mt.2015.197 (2016).

158 Komor, A. C., Kim, Y. B., Packer, M. S., Zuris, J. A. & Liu, D. R. Programmable editing of a target base in genomic DNA without double-stranded DNA cleavage. *Nature* **533**, 420-424, doi:10.1038/nature17946 (2016).

159 Slaymaker, I. M. *et al.* Rationally engineered Cas9 nucleases with improved specificity. *Science* **351**, 84-88, doi:10.1126/science.aad5227 (2016).

160 Tsai, S. Q. *et al.* GUIDE-seq enables genome-wide profiling of off-target cleavage by CRISPR-Cas nucleases. *Nat Biotechnol* **33**, 187-197, doi:10.1038/nbt.3117 (2015).

161 Nobles, C. L. *et al.* iGUIDE: an improved pipeline for analyzing CRISPR cleavage specificity. *Genome Biol* **20**, 14, doi:10.1186/s13059-019-1625-3 (2019).

162 Keller, A. D. & Maniatis, T. Only two of the five zinc fingers of the eukaryotic transcriptional repressor PRDI-BF1 are required for sequence-specific DNA binding. *Mol Cell Biol* **12**, 1940-1949, doi:10.1128/mcb.12.5.1940-1949.1992 (1992).

163 Turner, C. A., Jr., Mack, D. H. & Davis, M. M. Blimp-1, a novel zinc finger-containing protein that can drive the maturation of B lymphocytes into immunoglobulin-secreting cells. *Cell* **77**, 297-306, doi:10.1016/0092-8674(94)90321-2 (1994).

164 Keller, A. D. & Maniatis, T. Identification and characterization of a novel repressor of beta-interferon gene expression. *Genes Dev* **5**, 868-879, doi:10.1101/gad.5.5.868 (1991).

165 Nadeau, S. & Martins, G. A. Conserved and Unique Functions of Blimp1 in Immune Cells. *Front Immunol* **12**, 805260, doi:10.3389/fimmu.2021.805260 (2021).

166 Kubicek, S. *et al.* Reversal of H3K9me2 by a small-molecule inhibitor for the G9a histone methyltransferase. *Mol Cell* **25**, 473-481, doi:10.1016/j.molcel.2007.01.017 (2007).

167 Gyory, I., Wu, J., Fejer, G., Seto, E. & Wright, K. L. PRDI-BF1 recruits the histone H3 methyltransferase G9a in transcriptional silencing. *Nat Immunol* **5**, 299-308, doi:10.1038/ni1046 (2004).

168 Bally, A. P. R. *et al.* PD-1 Expression during Acute Infection Is Repressed through an LSD1-Blimp-1 Axis. *J Immunol* **204**, 449-458, doi:10.4049/jimmunol.1900601 (2020).

169 Guo, M. *et al.* EZH2 Represses the B Cell Transcriptional Program and Regulates Antibody-Secreting Cell Metabolism and Antibody Production. *J Immunol* **200**, 1039-1052, doi:10.4049/jimmunol.1701470 (2018).